Performance Analysis of Indoor Wireless Communications in Dense Cellular Networks

Hui Zheng

Department of Electronic and Electrical Engineering

University of Sheffield

Supervisors: Prof. Jie Zhang, Dr. Wei Liu

This thesis is submitted for the approval of the

Doctor of Philosophy

February 2019

This thesis is dedicated to my beloved parents. Without their unconditional love, encouragement and support, I would not be the person I am today.

Acknowledgements

First and foremost, I am sincerely grateful to my supervisor, Professor Jie Zhang for his trust and great support during my Ph.D studies. His optimism and confidence towards to life and work truly have a positive impact on me.

I am very grateful to Dr. Jiliang Zhang who most importantly helped me from a beginner to an independent researcher. I could never accomplish my Ph.D studies without his guidance and persistent help.

A very special gratitude to Dr. Peng Wu who has encouraged me through emotional difficulties during my Ph.D studies.

Last but not least, I would like to express my heartfelt appreciation for my parents who always encourage and support me with patience and love.

Abstract

The current decades have witnessed the explosive increase of traffic-data demand. It is predicted that indoor wireless communications will be one of the fastest growing markets, since the vast majority (over 80%) of data demand occurs in indoors. Facing such a huge data demand, the dense deployment of small cells (SCs) in indoor environments is boosted, which brings breakthroughs of throughput for in-building communications. However, the densification of indoor small-cell (SC) networks also poses new challenges, such as complex propagating environments, severe blockage effects and short link distances, which significantly influence the evaluation of network performance. This thesis mainly investigates the performance analysis of indoor dense SC networks.

Firstly, the probability of Line-of-Sight (LOS) propagation is crucial to model the real signal propagation channels and to evaluate the performance of cellular networks. However, existing LOS probability models are oversimplified to provide the exact LOS probability in indoor scenarios. By considering the realistic layout of building structures, this thesis proposes a novel and analytical LOS probability model for downlink radio propagations in typical indoor scenarios, which have rectangular rooms and corridors. Through the proposed model, the LOS probability can be calculated directly without the measurement and simulation.

Next, in terms of the impact of LOS and Non-Line-of-Sight (NLOS) transmissions, the traditional works do not distinguish them, which is not practical for dense cellular networks. Thus, a tractable path loss model considering both LOS and NLOS propagations is proposed for the performance analysis of indoor dense SC networks. Based on the theory of stochastic geometry, the performance metrics, such as coverage probability, spectral efficiency (SE)

and area spectral efficiency (ASE), are analytically derived. The analytical results provide insights into the design of indoor dense SC networks in the future.

Thirdly, regarding the severe effects of blockages in indoor environments, the traditional approach that simply considers it as a log-normal shadowing is too simple. Therefore, a wall blockage model is developed to characterize the impact of blockages based on the stochastic geometry. Furthermore, the mathematical expression of coverage probability for the case of impenetrable blockages is derived, which employs a path loss model incorporating both the blockage-based and distance-based path loss.

List of Publications

Published

1. **H. Zheng**, J. Zhang, H. Li, Q. Hong, H. Hu, and J. Zhang, "Exact Line-of-Sight Probability for Channel Modelling in Typical Indoor Environments," *IEEE Antennas and Wireless Propagation Letters*, vol. 17, pp. 1359 -1362, Jul. 2018.

2. **H. Zheng**, J. Zhang, H. Hu, and J. Zhang, "The Analysis of Indoor Wireless Communications by a Blockage Model in Ultra-dense Networks," in *Proc. 2018 IEEE 88th Vehicular Technology Conference (VTC2018-Fall)*, accepted, 2018.

3. H. Li, J. Zhang, Q. Hong, **H. Zheng**, and J. Zhang, "QoS-aware channel-width adaptation in wireless mesh networks," in *Proc. 2016 IEEE International Conference on Communications (ICC)*, pp. 1-6, 2016.

4. H. Li, J. Zhang, Q. Hong, **H. Zheng**, and J. Zhang, "Digraph-based joint routing and resource allocation in software-de ned backhaul networks," in *Proc. IEEE 22nd International Workshop on Computer Aided Modeling and Design of Communication Links and Networks (CAMAD)*, pp. 1-5, 2017.

5. Q. Hong, J. Zhang, **H. Zheng**, H. Li, H. Hu, B. Zhang, Z. Lai, and J. Zhang, "The impact of antenna height on 3D-MIMO channel: A ray launching based analysis," *Electronics*, vol. 7, 2018

Table of contents

List of figures

List of tables

Chapter 1

Introduction

Overview

In recent decades, the data traffic is experiencing the explosive growth, most of which is generated by mobile smart devices in indoor environments. In order to satisfy this huge data demand occurring indoors, some researches have been carried out on the development of indoor dense small-cell (SC) networks. Nevertheless, facing the evolution of indoor network densification, new challenges are also unavoidable for researchers and network operators. This motivates the thesis to investigate indoor wireless communications in dense cellular networks.

In this chapter, the background and motivation of this thesis will be introduced firstly. Then, the research objectives will be presented. Finally, the organization of this thesis will be illustrated.

1.1 Background and Motivation

1.1.1 Requirements of Indoor Wireless Communications

In the last decades, with the rapid development of mobile smart devices, such as mobile phones, tablets, and portable laptops, the amount of required data traffic has emerged an

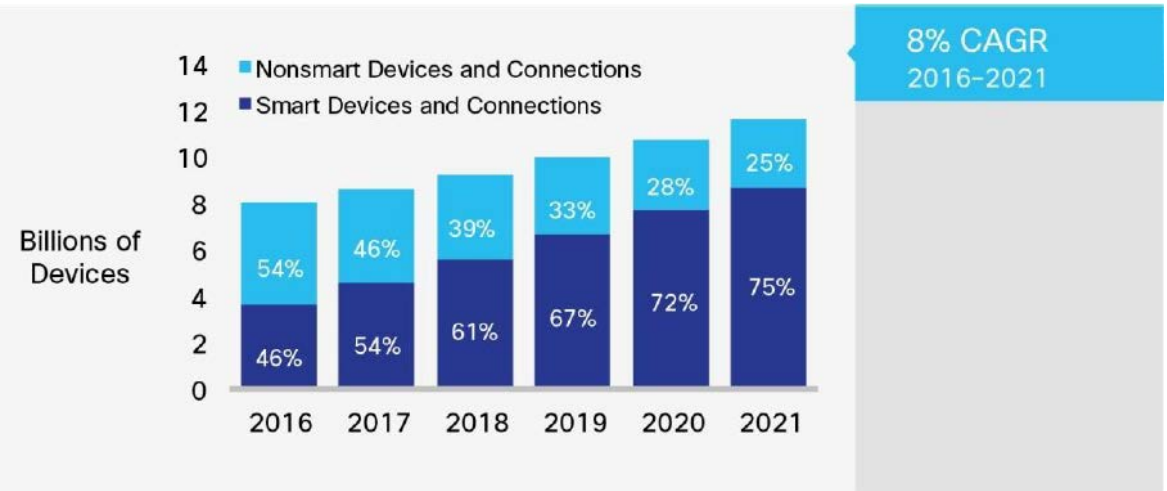

Fig. 1.1 Global increase of Mobile Devices from 2016 to 2021 forecasted by Cisco [Source: Cisco VNI Mobile, 2017]

explosive growth. Fig. 1.1 and Fig. 1.2 indicate that the mobile devices and data traffic will continue to grow at a surprising speed, respectively [1]. Actually, a majority (80%) of voice services and multimedia services occur indoors, since the people usually spend most of the time on the home life and working in the office. It is certain that the capacity demand of indoor communications will keep the horrendous increasing trend, since more advanced applications are desired to be implemented. For example, in the future smart city, people will study and work at home through the virtual reality and augmented reality techniques; besides, people at home can control the autonomous vehicle remotely so as to realize the safe and efficient driving. These instances necessarily require the more advanced indoor communication networks in support of the vast data traffic.

As is known to all, stimulated by the above application demands, the wireless communication networks have experienced the rapid evolutions, from 3G to 4G LTE, and further to 5G era. Herein, the indoor wireless communication is predicted to be one of markets with the fastest growth [1]. Therefore, providing better coverage and higher capacity for indoor environments is an urgent issue, especially facing the increasing subscribers' data demand. However, there exists a question that whether 5G can satisfy the data transmission demand in the next decades? We guess no one can give the doubtless answers. So the academia and

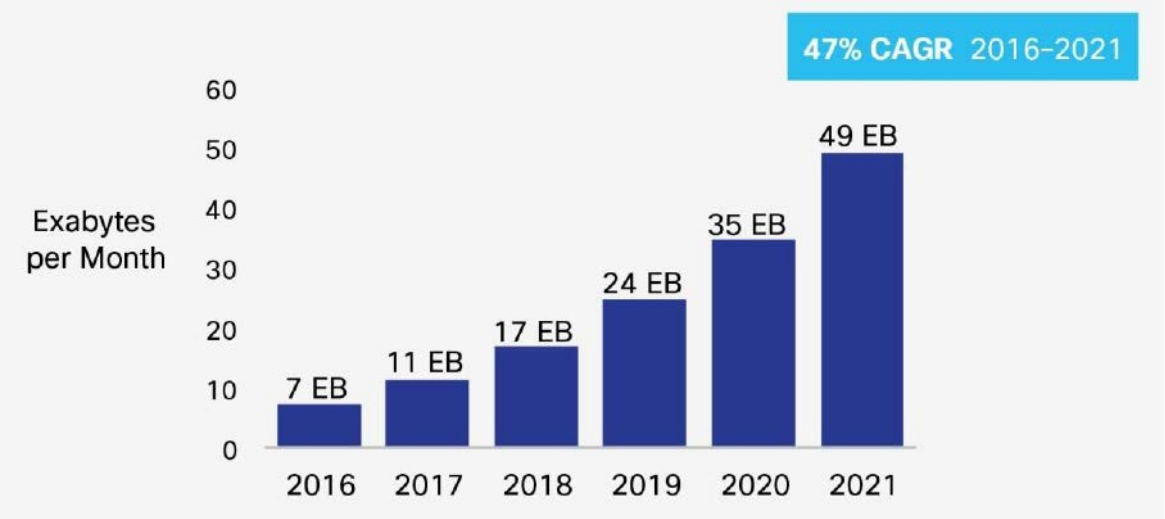

Fig. 1.2 Global Mobile Data Traffic from 2016 to 2021 forecasted by Cisco [Source: Cisco VNI Mobile, 2017]

industry should pay more attention to the critical technologies to realize the higher capacity of indoor communication networks than the current expectations.

1.1.2 Dense Small-Cell Networks

In order to satisfy such an immense data demand, network operators and academic researchers represent the concept of dense SC network [2], of which the structure is shown in Fig. 1.3. The network densification is a key mechanism for the traffic-demand evolution, which can be realized by deploying the increased number of small cells (SCs). With the closer distance between base stations (BSs) and users, the propagation loss on channels will be smaller. Thus the coverage probability and throughput can be improved. In addition, the employment of dense SCs can boost the frequency reuse ratio greatly, which leads to the huge capacity gain for communication networks and improves the spectrum efficiency (SE) with lower power and lower cost.

However, although dense SC deployment could bring network performance improvement, some technical challenges are also brought in, such as inter-cell interference, in-device interference, unplanned deployment, and performance analysis difficulties. Therein, cell deployment planning is one of the fundamental problems we are considering for indoor SC

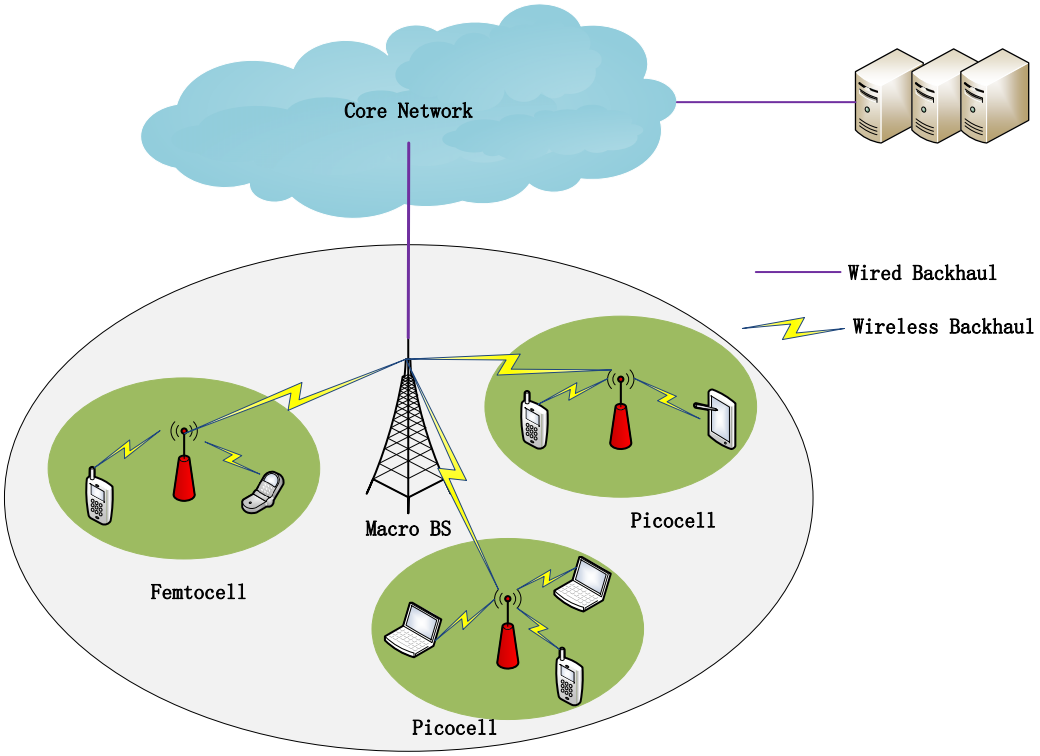

Fig. 1.3 Multi-tier dense SC network

networks. It aims to deploy the network access nodes in optimal densities and locations to provide guaranteed quality of network services. Fortunately, up to now, there are some emerged technologies to solve the above difficulties. For the severe interference problem, massive multiple-input multiple-output (MIMO) and millimeter wave (mmWave) can alleviate the inter-cell interference, because of the beamforming of multi-antennas and the short transmission distance of mmWave. In addition, for the performance analysis of dense SC networks, Stochastic Geometry is a mathematically tractable tool, which can reveal the relationship between the dense cell networks and the major performance-impacting parameters. In summary, the dense SC network has been widely accepted by academia and industry for improving the network coverage and capacity.

1.1.3 Motivation

As presented above, inspired by the concept of dense SC deployment, the architecture of in-building SC network is investigated recently and in the future. It is a good compromise

of the conventional approach, in which the indoor communication service is provided by outdoor macrocells.

Nevertheless, there still exists some challenges brought by the differences between outdoor and indoor dense SC networks, which are inevitable and worthy of attention by academia and industries. By considering the unique features of indoor propagations, such as shorter links and more complex obstacles, some of the main challenges are summarized as follows.

Challenges

• The accurate propagation model for indoor communications is a necessity. The indoor environments are very complicated because of the dense and various obstacles, such as wall blockages, furnitures and moving human bodies. In order to capture the effects of these influential factors, exact Line-of-Sight (LOS) models are required for network performance evaluation.

• Existing path loss models are too simplified to accurately analyse the performance of indoor dense small networks, which do not differentiate LOS and Non-Line-of-Sight (NLOS) propagation. With the increase of SC density and the transition from macrocells to indoor SCs, some NLOS transmissions are transformed into LOS transmissions caused by the shorter link distance. It implies that the indoor propagation has a higher LOS probability compared with the outdoor transmission given the same BS numbers [3–5]. The network performance is certainly influenced by the transformation.

• The effects of obstacles on signal propagations become dominant. Indoor scenarios usually have more complex and dense obstacles, such as wall blockages and moving human bodies. The wall blockages significantly attenuate the signal strength, especially for higher frequencies. Thus, the performance of indoor networks is largely characterized by blockages.

1.2 Contributions of the Thesis

This main research contributions of this thesis are summarised as follows:

• To propose an analytical and accurate LOS probability model by considering the realistic building structures for downlink radio propagations in indoor scenarios. The main content is corresponded to Chapter 4.

•To develop a tractable approach to evaluate the network performance metrics, such as coverage probability, spectral efficiency (SE) and area spectral efficiency (ASE) of indoor communications, which is comprised of a practical path loss model by considering the LOS and NLOS transmissions based on the proposed LOS probability model in Chapter 4. The main content is corresponded to Chapter 5.

• To develop a mathematical model of interior wall blockages based on the stochastic geometry, which is employed to analyse the coverage probability of indoor wireless communications by incorporating both the blockage-based and distance-based path loss. The main content is corresponded to Chapter 6.

1.3 Structure of the Thesis

The structure of this thesis will be presented in this section, which are introduced as follows:

Chapter2: State of the Art and Research Challenges

This chapter firstly presents the development and related research works of indoor wireless communications, from the traditional network architecture to the indoor dense SC network. Then, the stochastic geometry analysis for dense network performance and its related works are presented.

Chapter3: Fundamentals of Stochastic Geometry

This chapter focuses on the introduction of stochastic geometry fundamentals, including the properties and key mathematical techniques. This lays the foundation for its application in dense cellular networks.

Chapter 4: Exact Line-of-Sight (LOS) Probability for Channel Modelling in Typical Indoor Environments

The model of LOS probability is essential for channel modelling and network performance evaluation. The existing LOS models are too simplified to exactly capture the characterizations of indoor propagations. This chapter proposes an exact and analytical LOS probability model for downlink radio propagations in typical indoor environments, by considering the realistic building layout.

Main contributions

• The proposed model is developed by considering realistic building structure, which is more practical for channel modelling.

• The proposed model analytically constructs the mapping from a building's layout (structure) to the LOS probability distribution. With this model, we can directly obtain the LOS probability of propagation links inside a given building without simulations or measurements.

• The proposed method is tractable and can be generalized to indoor scenarios with similar properties.

Chapter 5: Performance Analysis for Indoor Dense Small-Cell Networks with LOS and NLOS Transmissions

In order to meet the huge demand of indoor data traffic, indoor cellular networks are becoming denser. The network densification introduces problems for network performance analysis. Traditionally, the performance evaluation of indoor networks is usually based on simplified path loss models, which fails to distinguish the LOS and NLOS transmission. This drawback is obviously for the indoor dense network. The reason is that some transmissions are transformed into LOS cases with the increase of BS density and the shorter distance between users ans BSs. This chapter presents a practical path loss model, and builds a mathematical framework to analyse the effect of the path loss model on the indoor dense network performance. The analytical results of performance metrics are derived. This work provides a certain guidance for the design of indoor dense SC networks.

Main contributions

• A practical path loss model is proposed for indoor dense cellular networks, by considering the LOS and NLOS propagations. The effects of different path loss models are analytically investigated.

• Performance metrics, i.e., the coverage probability, SE and ASE, are derived for both a general path loss model and a special linear path loss model.

Chapter 6: Analysis of Indoor Wireless Communications by a Blockage Model

The effects of blockages on signals become dominant for in-building wireless communications, since obstacles are more dense and complex and the link distances are shorter. The traditional pathloss model deals with it as a log-normal fading along with the reflection, scattering and diffraction, which cannot accurately reflect the blockage effects. This chapter aims to investigate the indoor blockage effects. Then a complex path loss model is built by combining both the blockage-based and distance-based path loss. Finally, a mathematical framework is obtained to evaluate the performance of indoor networks.

Main contributions

• The indoor blockages are built as a model by abstracting the walls as a random process, which makes it possible to analytically investigate the effects of indoor wall blockages.

• The path loss model is developed by incorporating both the blockage-based and distance-based path loss for indoor dense networks.

• The analytical result of coverage probability is obtained for analysing the performance of indoor dense networks, by using the sophisticated path loss model.

Chapter 7: Conclusions and Future work

This chapter summarises the works of this thesis and presents the future work.

Chapter 2

State of the Art and Research Challenges

Overview

In this chapter, the topics related to indoor wireless communications are reviewed. Specifically, state of the art in indoor dense SC networks is presented. Then the application of stochastic geometry analysis in cellular networks is illustrated.

2.1 Reviews of Indoor Wireless Communications

With the exponentially increasing demand of mobile data in indoor scenarios, the dense deployment of indoor SC networks has been widely accepted and practised by academia and industries. The traditional architecture for providing indoor communications by outdoor macrocells is gradually replaced. However, challenges are being brought in the meantime, because of the increased density of indoor SCs. By considering the unique features of indoor environments, the challenges can be mainly concluded as follows.

Firstly, by considering the complex and dense obstacles in indoor environments, an exact LOS probability model is needed to accurately distinguish between LOS and NLOS propagations. It is crucial to model the real signal propagation channels and evaluate the performance of networks.

Next, with the network becoming denser, the transition from NLOS tansmissions to LOS transmissions occurs because of the shorter distances between transmitters and users. The effects of LOS and NLOS propagations are significant for the accurate performance evaluation of indoor dense cellular networks. Therefore, how to tractably analyse the network performance with the practical indoor path loss model is desired to be solved.

Thirdly, in indoor environments, the effects of interior wall blockages on signal propagations become dominant, since the interior wall blockages are densely located and the link length is shorter compared to outdoor environments. It is meaningful to analytically investigate the influence of wall blockages on the network performance.

2.1.1 LOS Probability Model

The LOS or NLOS propagation is a characteristic of signals, which implies that the signals propagate in direct or indirect paths. This characteristic is essentially to describe propagation channels and build a path loss model for wireless communications [6].

Particularly, in indoor environments, the LOS (or NLOS) probability is seriously influenced by the complex obstacles including stationary obstacles (e.g. building structure, furniture) and moving obstacles (e.g. moving human bodies) [7] [8]. Traditionally, the available works [6–10] incorporated obstacle effects into a log-normal shadowing fading, which is independent of the distance-dependant path loss. However, the LOS and NLOS transmissions are not distinguished.

Recently, some works presented that the signal strength is attenuated significantly by NLOS channels, especially in mmWave networks [11]. Although the signal to noise ratio (SNR) can be improved by using the MIMO system, it is still hard to overcome the attenuation caused by NLOS channels [12]. Moreover, the attenuation translates to the inaccurate evaluation of system performance, e.g. coverage probability [11, 13].

For the accuracy of performance evaluation, previous works seek to develop LOS distribution models. Traditionally, the Fresnel clearance is an important and meaningful method for distinguishing between the LOS and NLOS propagation. The LOS is defined by that the obstacle(s) is clear of the 60% of the first Fresnel zone [14]. However, in indoor environments,

due to the complex and ultra-dense obstacles and users, it is very hard to obtain an analytical LOS and NLOS probability model through the Fresnel clearance method.

In terms of the standards of the 3rd Generation Partnership Project (3GPP) [15], the LOS probability was expressed as a function of the link distance by the measurement. On this basis, the work [16] improved LOS models in 3GPP to apply them to the three-dimensional (3D) channels. Authors in [17] improved the LOS models proposed in 3GPP to best fit specific scenarios.

In work [18], the authors proposed an analytical framework to derive the LOS probability model, by assuming random blockages as a random process based on the stochastic geometry theory. However, it is developed in outdoor scenarios.

To conclude, the LOS probability is modelled by the measurement or by random shape theory. However, the former cannot capture the specific characterizations of environments and is not efficient. The latter sacrifices the information of the realistic building layout, although the random shape theory provides a tractable approach. In reality, blockages in a given indoor environment are fixed when the building layout is given. Therefore, an analytical and accurate LOS model is needed by considering the realistic building layout.

2.1.2 Effects of LOS and NLOS Propagations

As described in [19], the path loss model distinguishing the LOS and NLOS path is more practical in the in-building dense SC networks. Therefore, a tractable method of the performance analysis for indoor dense networks with LOS and NLOS transmissions is needed to be addressed, which evaluates the dense network performance more accurately and conveniently.

For the conventional performance analysis of cellular networks, most prior works considered the standard power-law path loss models [20–22] which do not distinguish LOS and NLOS transmissions. They modeled BSs as a homogeneous (Poisson point process) PPP, and employed the standard path loss models and the Rayleigh fading as the channel model. Moreover, the works [20] with the nearest association and [21] with the strongest association showed that the coverage probability and SE are independent of the BS density, when the BS density is large enough. It also showed the ASE increases linearly with the BS density.

However, such conclusions were drawn under the considerable simplifications in the channel model. It would be of interest to explore whether these conclusions still hold in the more practical propagation environments.

A few valuable works were carried out to solve this problem [19, 23, 24]. In [23], the authors considered the effects of the multi-slope path loss model on the dense networks. Herein, the path loss exponents are different for various distance ranges. In [24], a piece-wise path loss model and two LOS probability functions were considered. However, its results are less tractable than those of [23], due to the more complicated exponential LOS probability functions used in [24]. Similarly, the authors of [19] also used the piece-wise path loss model, but they obtained the more tractable results since the linear LOS propagation function was introduced. Unlike previous works, [26–28] considered the more realistic parameters in the dense network performance analysis. In [26], the authors assumed the Rician fading for the LOS transmission and the Rayleigh fading for the NLOS transmission. In [27, 28], the authors considered the influence of BS antenna heights and the BS idle mode on the dense network performance. Except for the downlink, the uplink performance with power control under LOS and NLOS transmissions was also analysed in [25].

In the above new works, they all studied the piece-wise path loss model considering LOS and NLOS propagations, and derived the tractable methods for analysing the coverage probability and ASE with the BS density. The results of them showed that the coverage probability increases firstly then decreases for the BS density being denser than a value of threshold. In addition, the ASE does not increases linearly with the BS density.

However, the above studies focus on the outdoor SC network There are still few researches for the indoor dense SC network with LOS and NLOS propagations. The authors in [29] presented that the increase of the throughput is not linearly with the BS density, which considered a path loss model with the impact of blockages as an exponential function of the distance. Nevertheless, it's based on the scaling law rather than the tractable method.

Therefore, a tractable approach for analysing the indoor dense network performance, considering LOS and NLOS propagations, is urgent to be put forward.

2.1.3 Effects of Blockages

In indoor SC networks, the performance is characterized in large part by obstacles, such as walls. The effects caused by wall blockages make the performance analysis difficult, particularly for high-frequency cellular networks. This section will introduce related works to describe the blockage impact.

Traditionally, the approach that involves the effects of blockages on signal transmission is the ray tracing [30, 31]. This method was employed to investigate the characterizations of indoor scenarios [32–34]. The ray tracing requires the specific environmental information to generate results, while it cannot provide a general result such as ensemble average for scenarios with similar characteristics. The computational complexity of the ray tracing also makes it inefficient.

Recently, an analytical approach from the random shape theory was investigated to establish a statistic model that represents the wall blockages' statistics without the need of terrain data. The random shape theory models the blockages as randomly distributed by the segment line process in a wireless cellular network [35]. In [18], the authors provided a more general model by assuming that buildings are presented as a random project process in urban scenarios. The buildings were abstracted as rectangles with random orientations and sizes, whose centres form a PPP. The mathematical technique makes it possible to analyse the impact of blockages in general networks.

Owing to the tractability and efficiency of the random blockage model, some research works extended the application of the random shape theory to analyse indoor blockages. The authors in [36, 37] established the indoor wall blockage model with the horizontal or vertical orientations, and random locations. The work [37] compared different blockage generating methods, including random shaper theory and semi-deterministic methods. However, these two works only applied the proposed model to networks with a specific arrangement of transmitters, which is not suitable for general networks.

The works [38, 39] presented a general mathematical approach by modelling wall blockages as a Poisson line process. In the method, a building was modelled as a grid consisting of multiple rectangular rooms, which are randomly distributed in space. However, for analytical

simplicity, the distance-based path loss was ignored in this work. This may result in an inaccurate estimation of the network performance, despite the work's general application of analysing indoor networks.

In summary, there are two main methods to investigate blockages in indoor environments. The ray tracing method requires the site-specific information, which is time and cost consuming. The stochastic geometry theory presents a tractable approach to model wall blockages as random processes, which has been utilized to efficiently analyse blockage effects on urban scenarios.

2.2 Review of Stochastic Geometry in Dense Cellular Networks

With the development of dense cellular network, the stochastic geometry analysis in wireless networks has been one of the most important mathematical method to model and analyse the performance of cellular networks. Related works mainly focus on how the stochastic geometry evaluates and predicts the performance of wireless networks, including coverage probability, SE and etc.

This section will simply introduce the fundamental thought of the application of stochastic geometry in wireless networks. Then, the related works in this research field will be illustrated and discussed.

2.2.1 Overview of Stochastic Geometry Analysis

Stochastic geometry provides a tractable and rigorous mathematical framework, which has been successfully to model a variety of cellular networks and analyse their performance [40–44]. The analysis based on stochastic geometry not only can capture the spatial randomness of wireless networks, but also can incorporate some uncertain sources, such as shadowing and fading.

Now we first present a broad view of the thought of stochastic geometry analysis. In reality, cellular networks are already known and deployed for a given scenario. However, the stochastic geometry is not used to investigate a specific cellular network with a certain geographical layout. Instead, it provides a general mathematical model, which gives us a view of the average of all cellular networks [45]. Through the work [20], transmitters at different locations form random layouts over a very big space. Therefore, the analytical method by stochastic geometry is on the basis of the probabilistic spatial distribution of transmitters, instead of a deterministic network implementation. Stochastic geometry models the cellular networks by a stochastic point process (mostly by PPP), which models transmitter locations as points in the Euclidean space [46]. Thus, transmitters are abstracted to random spatial patterns formed by points.

The main focus of stochastic geometry analysis is the average performance over all network implementations, which provides statistically characteristics of cellular networks. Such metrics mainly include the coverage probability (outage probability), ergodic capacity, ASE, system error probability and etc. [45]. Stochastic geometry builds a bridge between expressions of the aforementioned metrics and the parameters of cellular networks. The analytical results are helpful to provide insights into the operation and design of cellular networks.

As described above, the analytical expressions of performance metrics can be obtained by stochastic geometry. One key problem is how the cellular networks are analysed by the approach. Now, the analysis procedure based on the thought of stochastic geometry is concluded as the followed by taking PPP as an example.

A. System modelling

The first step is to choose the system model for the research object, such as scenario, path loss model, transmitting power, user position(s). This is the basis for analysing a wireless network.

B. Abstracting networks

The next step is to abstract elements of cellular networks (transmitters and/or users) by employing a point process, mostly PPP. Locations of transmitters are realized by each point of PPP in a finite space, which reflects some important characterizations of transmitters [45]. Without loss of generality, the performance analysis is executed for a typical user, of which the position can be an arbitrary reference point. Usually, the typical user is assumed at the origin for simplicity. The obtained results are location-independent since the PPP is stationary.

Then, by choosing a connectivity policy, the interference I at typical user can be calculated as the aggregate of signals from interfering transmitters, which have been equivalently abstracted as random points of PPP. Thus, the interference function involves random and uncertain signal sources because of the randomness of transmitters. The following step will provide the mathematical tools for handing the randomness of interference, and further evaluate performance metrics statistically.

C. Analysing network performance

By following the network abstraction, the interested performance metrics can be analytically presented. Then mathematical techniques from stochastic geometry are utilized to assess the network performance. Two of most important techniques are the probability generating functional (PGFL) and Campbell's theorem, which handle the randomness by integrating functions over the point space.

The utilization of these two main techniques requires the function with a certain expression. For the PGFL, an expectation of a random product is mandatory. For Campbell's theorem, an expectation of a random sum is needed.

In conclusion, The procedure of stochastic geometry analysis can be summarised as in Fig. 2.1. The technical details will be introduced in next chapter.

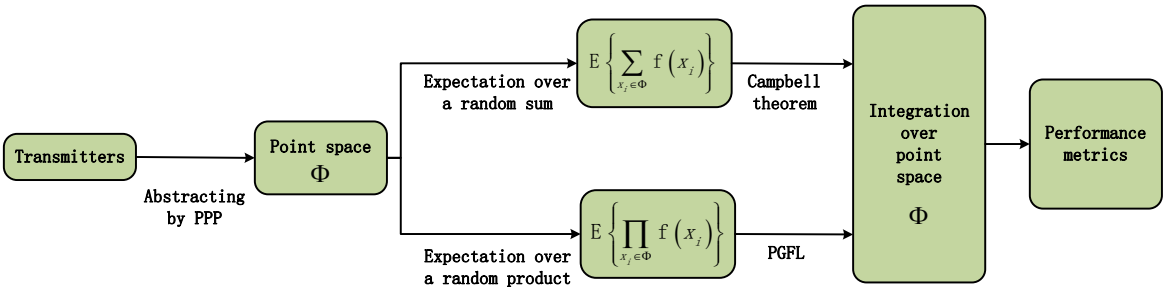

Fig. 2.1 Performance analysis of cellular networks by PPP

2.2.2 Related Works

Stochastic geometry has been widely utilized by academia since it successfully provides a mathematical framework for modelling and analysing wireless networks. The research works mainly focus on evaluating and predicting key metrics of network performance by stochastic geometry theory.

Due to the strength of capturing the randomness by stochastic geometry, it was mostly used to the ad hoc networks. The attempts of modelling cellular networks by stochastic geometry began from the late 90's [47, 48]. While it was not successfully until the works published [20, 49, 50], which revealed the irrationality of hexagonal grid model, and the randomness of realistic cellular networks. The work [20] firstly derived simple analytical expressions of performance metrics experienced by users. The PPP network model was validated by comparing with the hexagonal grid model and actual networks. Furthermore, the simulation results also showed that the PPP network model provides the tight lower bound for network performance, while the traditional hexagonal grid model provides the upper bound. Due to the tractability of PPP network, it launched a new research field of modelling and analysing cellular networks. In [49], the authors further proofed the rationality of PPP network model by the comparison of realistic transmitter layouts in different locations, and again confirmed the tight lower bound provided by PPP network. The work [50] presented the convergence results of PPP networks with respect to the environments with variant shadowing.

By the employment of PPP for cellular networks, some extraordinary results have been achieved. The downlink system of cellular networks was characterized in the following

works. At first, single-layer cases were investigated in [20, 50, 51], which were considered as the most basic and simplistic cellular network for analysing. Then, the researchers of works [52–55] extended the tractable approach to downlink multi-tier cases, which introduced the interference from different tiers and exposed the effects of the number of tiers and BSs on the network performance. Different from the prior references on the assumption of the single-antenna BS, the authors of [56–60] investigated MIMO technology in cellular networks, which explored the influence of antenna numbers and beamformimg schemes on the network performance, further expanded to the cellular networks analysis with massive MIMO [61, 62]. Similarly, as one of most critical technique of 5G era, the mmWave in cellular networks was also analysed by Stochastic geometry in [63–65], which took the propagation characteristics of the mmWave and the blockage model into account. Meantime, due to the densification of networks, some researchers came up with the corresponding analytical interference management methods and BS cooperation schemes [66–70]. In order to enhance the coverage probability, some works considered the relaying nodes in the cellular networks [71–74], which not only modeled the BSs and mobile users as PPP processes, but also assumed relay nodes as PPP processes. Additionally, the cognitive radio used in cellular networks was studied by means of stochastic geometry, so as to take a full advantage of spectrum resources [75–79]. Since the future 5G communication networks would contain a large number of small BSs, the energy efficiency (EE) is a critical performance metrics, which was as well investigated in works [80–84]. Moreover, as an effective way to enhance the network EE, nodes with energy harvesting function were also modeled by PPP to analyse the network energy utilization [85–87]. In summary, by making use of these analytical methods and thoughts, it will contribute to modelling the downlink performance of indoor dense networks and giving deep insights into the design.

By the way, stochastic geometry has also been broadly employed for the performance analysis of the uplink performance of cellular networks such as [88–90] and device-to-device communications [91–93]. These works will not be elaborated since this thesis does not focus on them.

Chapter 3

Fundamentals of Stochastic Geometry

Overview

The performance of cellular networks is tightly related to the positions of users and service nodes. However, the positions are usually uncertain. Hence, they can be modelled as the random process of points on a two-dimensional (2D) or 3D space. In the field of mathematics, the mathematical framework of this random model and its analytical approach are defined as stochastic geometry, especially the random point process. The modelling and analysis of wireless cellular networks is a direct application of stochastic geometry. Thus, this chapter will introduce some preliminary background knowledge of stochastic geometry according to the work [43].

3.1 Basic Concepts of Stochastic Geometry

This section will illustrate the basic concepts of stochastic geometry, which can be used to deal with the random spatial pattern. Generally, as the basic object of stochastic geometry, point process theory is of great importance. The point processes can be used to model the distributions of transceivers in a wireless network where positions of them are with uncertainty. Thus, the transmitters or receivers can be described by the characterizations of points in the point process.

3.1.1 Properties of Point Process

This section introduces important properties of the point process, which are presented as follows:

Translated point process: If we define $\Phi = \{x_1,\ x_2,\ ...\}$ as a point process, then $\Phi \triangleq \{x_1 + x,\ x_2 + x,\ ...\}$ is considered as the point process by translating $x \in \mathbb{R}^d$.

Stationarity: Given a point process on $\mathbb{R}^d$, if its distribution is translation-invariant, then this point process is stationary, i.e., $\Phi \stackrel{d}{=} \Phi_x$.

Isotropy: Given a point process on $\mathbb{R}^d$, if its distribution is rotationally invariant in regard of the original point o, then this point process is named isotropy, i.e., $\Phi \stackrel{d}{=} r\Phi_x$, where r is an arbitrary rotation about o.

Motion-invariance: Given a point process, if it is stationary and isotropic, then it is defined motion-invariant.

Thinning of point process: Generally, thinning is the removing certain points from a point process according to a rule. If the removal operation is independent for all points, in other words, the removal point is independent for other points, then the thinning is named independent thinning. Otherwise, the thinning is called dependent thinning.

3.1.2 Distances

In this section, we will introduce several basic but important distances of point process, and characteristic functions of distances.

Firstly, we introduce a definition of the nearest-neighbour operator. If a point set ϕ is with two points at least, the nearest-neighbour operator is presented as

$$NN_\phi(x) \triangleq \underset{y \in \phi \setminus \{x\}}{\arg\min} \{||y - x||\}, \quad x \in \phi. \tag{3.1}$$

If there are several nearest neighbours, the operator randomly chooses one of them. This operator can also be applied to an arbitrary location $u \in \mathbb{R}^d$. In this case, the nearest-neighbour operator is a more appropriate appellation. Moreover, the expression $||u - B||,\ B \in \mathbb{R}^d$ is the

notation of the minimum distance from the point x to the set B:

$$||u-B|| \triangleq min\{||u-y||\}, \quad u \in \mathbb{R}^d, B \in \mathbb{R}^d, y \in B. \tag{3.2}$$

Definition 3.1.1. *(Contact distance) Given a point process Φ, its contact distance at position u is defined as $||u-\Phi||$.*

Definition 3.1.2. *(Contact distribution function) The function of the contact distribution F^u is the CDF of contact distance $||u-\Phi||$, which is presented as:*

$$F^u(r) \triangleq \mathbb{P}(||u-\Phi|| \leq r) = \mathbb{P}(N(b(u,r)) > 0). \tag{3.3}$$

If a point process Φ is stationary, then the function F^u does not depend on the location u, and can be denoted as F. This function is widely used in cellular networks, e.g., the function of the nearest distance from the typical user to the designated(nearest) transmitter.

Definition 3.1.3. *(Nearest-neighbour distance) The distance between a point of the point process to its nearest neighbour is called nearest-neighbour distance, as presented:*

$$||x-NN_\Phi(x)|| = ||x-\Phi\setminus\{x\}||, x \in \Phi. \tag{3.4}$$

Definition 3.1.4. *(Nearest-neighbour distance distribution function) The function describes the distribution of the nearest-neighbour distance, as presented:*

$$G^x(r) = \mathbb{P}(||x-NN_\Phi(x)|| \leq r). \tag{3.5}$$

Similarly, if the point process Φ is stationary, G^x does not depend on x and is denoted by G. For the PPP, the contact distribution function is identical on the nearest-neighbour distance distribution, we just write as:

$$F^u(r) \triangleq G^u_{\Phi\cup\{u\}}(r), \tag{3.6}$$

where $G^{u}_{\Phi\cup\{u\}}(r)$ is the nearest-neighbour distance distribution at location u of the point process $\Phi\cup\{u\}$. This follows that all points of a PPP are independent. Additionally, if the PPP is uniform, the two distance distribution functions are independent of the location x.

3.2 Moment Measures

For numerical random variables, there are statistical properties existing, such as the mean, variance and high-order statistics. Similarly, the point process theory also provides useful analogues, which are called moment measures. This section will give an illustration.

3.2.1 The First-Order Moment Measure

The first-order moment of a point process is its intensity measure, presented as

$$\Lambda(B) = \mathbb{E}[\Phi(B)], \tag{3.7}$$

which is corresponded to the mean of a random variable. If the stationary point process Φ is given, and then the property:$\Lambda(B) = \Lambda(B+v),$ for $v \in \mathbb{R}^d$, which indicates the intensity measure is translation-invariant.

3.2.2 The Second Moment Measures

In point processes, the simple examples of second moments are variance and covariance, which are presented respectively as:

$$\text{var}\,\Phi(B) = \mathbb{E}(\Phi(B)^2) - (\mathbb{E}\Phi(B))^2 \tag{3.8}$$

$$\text{cov}\,(\Phi(A),\Phi(B)) = \mathbb{E}\,(\Phi(A)\Phi(B)) - \mathbb{E}\Phi(A)\mathbb{E}\Phi(B) \tag{3.9}$$

Then there are two measures derived from the following definitions.

Definition 3.2.1. *(Second moment measure) Given a point process Φ on $\mathbb{R}^d$, then $\Phi^{(2)} \triangleq \Phi \times \Phi$ can be called a point process on the space $\mathbb{R}^d \times \mathbb{R}^d$, which is consisted of all ordered pairs of points x, $x' \in \Phi$. The notation $\mu^{(2)}$ is the intensity measure for the point process $\Phi \times \Phi$. Then*

$$\mu^{(2)}(A \times B) \triangleq \mathbb{E}\left(\Phi(A)\Phi(B)\right), \tag{3.10}$$

which is also called the second moment measure.

Hence, we can obtain the variance and covariance respectively:

$$\text{var}\left(\Phi(A)\right) = \mu^{(2)}\left(A^2\right) - \left(\Lambda(A)\right)^2 \tag{3.11}$$

$$\text{cov}\left(\Phi(A), \Phi(B)\right) = \mu^{(2)}(A \times B) - \Lambda(A)\Lambda(B) \tag{3.12}$$

Employ the Campbell theorem on then point process $\Phi \times \Phi$, we can obtain that

$$\mathbb{E}\left(\sum_{x \in \Phi} \sum_{y \in \Phi} f(x,y)\right) = \int_{\mathbb{R}^d} \int_{\mathbb{R}^d} f(x,y)\mu^{(2)}(\mathrm{d}x, \mathrm{d}y) \tag{3.13}$$

Straightforwardly, the second moment measure can be generalised to the higher-order moment measure, where the nth- order moment measure is presented as

$$\mu^{(n)}\left(B_1 \times B_2 \times \ldots B_n\right) = E\left(\Phi(B_1)\Phi(B_2)\ldots\Phi(B_n)\right) \tag{3.14}$$

Definition 3.2.2. *(Second moment factorial measure) Let a point process $\Phi * \Phi \triangleq \{(x,x') \in \Phi \times \Phi : x \neq x'\}$, its intensity measure is called second moment factorial measure:*

$$\alpha^{(2)}(A \times B) \triangleq \mathbb{E}\left(\Phi(A)\Phi(B)\right) - E\left(\Phi(A \cap B)\right) \tag{3.15}$$

Assume the set A and set B are disjoint, then we can get $\mu^{(2)}(A \times B)$. In generality, it is written as

$$\mu^{(2)}(A \times B) = \alpha^{(2)}(A \times B) + \Lambda(A \cap B) \tag{3.16}$$

From equation (3.16), we can observe that the difference between $\alpha^{(2)}(A \times B)$ and $\mu^{(2)}(A \times B)$ is the expectation of $A \cap B$.

3.2.3 Second Moment Density

Definition 3.2.3. *(Second moment density) Given an compact set $C = A \times B$ in $\mathbb{R} \times \mathbb{R}^d$, if we have*

$$\alpha^{(2)}(C) = \alpha^{(2)}(A \times B) = \int_A \int_B \rho^{(2)}(x,y)dxdy = \int_C \rho^{(2)}(x,y)dydx, \tag{3.17}$$

then it is said the point process Φ has second moment density $\rho^{(2)}$.

Written as the form of differentiation

$$\alpha^{(2)}(\mathrm{d}x, \mathrm{d}y) = \rho^{(2)}(x,y)\mathrm{d}x\mathrm{d}y \tag{3.18}$$

In simplicity, $\rho^{(2)}(x,y)$ denotes the disjoint probability that there are two points of Φ located at x and y in the infinitesimal volumes $\mathrm{d}x$ and $\mathrm{d}y$, namely

$$\mathbb{P}(\Phi(\mathrm{d}x) > 0, \Phi(\mathrm{d}y) > 0) \sim \mathbb{E}(\Phi(\mathrm{d}x)\Phi(\mathrm{d}y)) = \rho^{(2)}(x,y)\mathrm{d}y\mathrm{d}x \tag{3.19}$$

The second moment density can be extended to higher-order moment density, then the nth moment density is presented as

$$\alpha^{(n)}(B_1 \times B_2 \times \cdots \times B_n) = \int_{B_1} \int_{B_2} \cdots \int_{B_n} \rho^{(n)}(x_1, x_2, \ldots, x_n)\mathrm{d}x_1\mathrm{d}x_2 \ldots \mathrm{d}x_n \tag{3.20}$$

3.3 Sums and Products Based on Point Processes

The operations of sums and products of a point process are important and widely applied on wireless cellular networks. For instance, we formulate the transmitters as a point process. Then the interference at a receiver is the sum of signals from all interfering transmitters,

which are at random locations. The coverage at a receiver is considered as the product of the point process.

In this section, in order to introduce the sums and products of point processes, we will first present important definitions of random fields. Based on the definitions, the useful theorems are obtained.

A. Shot-noise random fields

The shot-noise random field is a random variable of geometrical structure. It is obtained from the superposition of random impulses that are generated by the points of a point process. These impulses are only determined by the difference $y-x$, where y implies the location of the measure random field, and x is $x \in \Phi$. Assume the function $g(y)$ denotes the contribution of the origin point to the random field, then the function $g(y-x)$ is considered as the contribution from the point x.

Definition 3.3.1. *(Shot noise) If a point process si given, its shot-noise random field is presented as*

$$\varsigma(y) \triangleq \sum_{x\in\Phi} g(y-x), \quad y \in \mathbb{R}^d \tag{3.21}$$

where $g : \mathbb{R}^d \to \mathbb{R}$. If the point process Φ is PPP, the random field is defined as Poisson shot noise.

In wireless networks, one of important applications is the interference field. The point process Φ models the distribution of transmitters, and the function g denotes the path loss model.

B. The mean of the sum of shot-noise random fields

Given a point process $\Phi = \{x_i\} = \{x_1, x_2, \dots\} \in \mathbb{R}^d$, and the function $f : \mathbb{R}^d \to \mathbb{R}$ is measurable. The sum of $f(x)$ over Φ can be presented as

$$\sum_{x\in\Phi} f(x) = \int_{\mathbb{R}^d} f(x)\Phi(\mathrm{d}x) = \int_{\mathbb{R}^d} f(x)p(x)\mathrm{d}x \tag{3.22}$$

where

$$p(x) = \sum_{y \in \Phi} \delta(x-y), \tag{3.23}$$

where δ is the Dirac delta function. As described above, the sum over Φ is a shot-noise random field.

$$\mathbb{E}\left(\sum_{x \in \Phi} f(x)\right) = \int_N \sum_{x \in \phi} f(x) \mathrm{P}(\mathrm{d}\varphi) = \int_N \int_{\mathbb{R}^d} f(x) \varphi(\mathrm{d}x) \mathrm{P}(\mathrm{d}\varphi). \tag{3.24}$$

Theorem 3.1. *(Campbell's theorem for sums) Given a point process $\Phi \in \mathbb{R}^d$, and $f : \mathbb{R}^d \to R$ is defined as a measurable function. The calculation of its random sum is*

$$S = \sum_{x \in \Phi} f(x), \tag{3.25}$$

which is still a random variable, of which the mean

$$\mathbb{E}(S) = \int_{\mathbb{R}^d} f(x) \Lambda(\mathrm{d}x). \tag{3.26}$$

If Φ has an intensity function, then

$$\mathbb{E}(S) = \int_{\mathbb{R}^d} f(x) \lambda(x) \mathrm{d}x. \tag{3.27}$$

Proof. Assume f is a step function, present as $f = \sum_{k=1}^{K} c_k 1_{B_k}$, where $B_k \subset \mathbb{R}^d$ and $c_k \in \mathbb{R}$. 1_{B_k} is the indicator function of the set B_k. The function $1_{B_k}(x)$ is defined as 1 for $x \in B_k$, otherwise it is 0. Then the sum of $f(x)$ is written as

$$S = \sum_{x \in \Phi} f(x) = \sum_{x \in \Phi} \sum_{k=1}^{K} c_k 1_{B_k}(x) = \sum_{k=1}^{K} c_k \Phi(B_k) \tag{3.28}$$

Hence, its mean is

$$\mathbb{E}(S) = \mathbb{E}\left(\sum_{k=1}^{N} c_k \Phi(B_i)\right) = \sum_{k=1}^{K} c_k \mathbb{E}\left(\Phi(B_k)\right) = \sum_{k=1}^{K} c_k \Lambda(B_k) = \int_{\mathbb{R}^d} f(x) \Lambda(\mathrm{d}x). \tag{3.29}$$

□

Corollary 3.1. *(Campbell's theorem for sums over stationary point process) If a stationary point process $\Phi \subset \mathbb{R}^d$ is set with an intensity λ, then the sum , denoted by $S = \sum_{x\in\Phi} f(x)$ is a variable with random distribution. Its parameter of mean is*

$$\mathbb{E}(S) = \lambda \int_{\mathbb{R}^d} f(x)\mathrm{d}x. \tag{3.30}$$

C. The probability of generating functional

Followed by the above, we will give the definition of products, namely the probability of generating functional. Given a non-negative integer random variable X, the generating function G_X of X is provided by

$$G_X(t) \triangleq \mathbb{E}(t^X) = \sum_{n=0}^{\inf} t^n \mathbb{P}(X = n) \quad t \in [0,1]. \tag{3.31}$$

Though differentiating G_X, we can obtain

$$G'_X(1) = \frac{\mathrm{d}G_X(t)}{\mathrm{d}t}\Big|_{t=1} \text{ and } G''_X(1) = \frac{\mathrm{d}^2 G_X(t)}{\mathrm{d}t^2}\Big|_{t=1} \tag{3.32}$$

Therefore, the variance and mean of X are calculated as

$$\mathbb{E}(X) = G'(1) \text{ and } \operatorname{var}(X) = G''_x(1) + G'_x(1)(1 - G'_x(1)). \tag{3.33}$$

Definition 3.3.2. *(Probability generating functional of a point process) Let a measurable function $v : \mathbb{R}^d \to [0,1]$, such that the function $1 - v$ is bounded. The PGFL is given as*

$$G[v] \triangleq \mathbb{E}\left(\prod_{x\in\Phi} v(x)\right) = \int_N \prod_{x\in\phi} v(x) P(\mathrm{d}\phi) \tag{3.34}$$

Due to

$$G[v] = \mathbb{E}\left[\exp\left(\sum_{x\in\Phi} \log v(x)\right)\right], \tag{3.35}$$

the PGFL is alternatively written as the below according to equation (3.22)

$$G[v] \triangleq \mathbb{E}\left[\exp\left(\int_{\mathbb{R}^d} \log v(x)\Phi(\mathrm{d}x)\right)\right]. \tag{3.36}$$

3.4 Poisson Point Process

This section introduces the Poisson point process (PPP), a basic and very important point process, which has been widely utilized for analysing wireless cellular networks.

A. One-dimensional poisson point process

Definition 3.4.1. *(One-dimensional Poisson process) The point process with the uniform intensity is named one-dimensional Poisson point process, which satisfies the following conditions*

• *for an arbitrary bounded interval* $[c,d)$, $N([c,d))$ *is a Poisson distribution with mean* $\lambda(d-c)$, *and*

$$\mathbb{P}(N([c,d)) = k) = e^{-\lambda(d-c)}\frac{(\lambda(d-c))^k}{k!}; \tag{3.37}$$

• *if the intervals* $[c_1,d_1),[c_2,d_2),\ldots,(c_m,d_m]$ *are disjoint, then* $N[c_1,d_1),N[c_2,d_2),\ldots,N(c_m,d_m]$ *are independent random variables.*

In terms of the point process in Definition 3.4.1, the intensity λ is independent of the location, hence the point process is also named homogeneous (or uniform). The inhomogeneous PPP can be defined that its intensity depends on the location, presented as $\lambda(t) \geq 0,\ for\, t \in \Phi$. Accordingly, the expected number of points in an arbitrary interval $[c,d)$ is calculated as

$$\mathbb{E}N([c,d)) = \int_c^d \lambda(t)\mathrm{d}t, \tag{3.38}$$

where the number $N([c,d))$ in the disjoint bounded intervals is also independendt random variables.

B. General poisson point process

Now we give a general definition of PPP on $\mathbb{R}^d$.

Definition 3.4.2. *(General Poisson point process) For a PPP defined on $\mathbb{R}^d$, it is assumed to be with the intensity measure Λ. Then it satisfies the following conditions:*

• *given an arbitrary compact set $C \cap \mathbb{R}^d$, the number operator of points is a Poisson distribution with expectd value $\Lambda(C)$. If Λ is denoted by a density λ, then the distribution of points' number $N(C)$ is presented as*

$$\mathbb{P}(N(C)=k) = \exp\left(-\int_C \lambda(x)\mathrm{d}x\right) \frac{\left(\int_C \lambda(x)\mathrm{d}x\right)^k}{k!}; \tag{3.39}$$

• *given disjoint compact sets $C_1, C_2, \ldots, C_m$, then $N(C_1), N(C_2), \ldots, N(C_m)$ are independent.*

Remark 1. *The intensity measure varaible, denoted by Λ, is defined on $\mathbb{R}^d$. Then the number of all points is finite, i.e. $\int_{\mathbb{R}^d} dx = \Lambda(\mathbb{R}^d)$ is a finite value.*

In terms of the homogeneous PPP, it is a special case with $\Lambda(C) = \lambda|C|$, which is widely employed to model transmitters in wireless networks.

C. The moment-generating function of sums over poisson processes

Theorem 3.2. *(*Campbell's theorem for Poisson point process) Assuming a uniform PPP, denoted as Φ with parameter λ on $\mathbb{R}^d$, and the measubale function $g : \mathbb{R}^d \to \mathbb{R}$. The sum of $g(x)$ is presened as:

$$S = \sum_{x \in \Phi} g(x), \tag{3.40}$$

which is absolutely covergent under the conditon $\int_{\mathbb{R}^d} \min(|g(x)|, 1)\mathrm{d}x < \infty$.

If this conditon is satisfied, the momen-geernating function is written as

$$\mathbb{E}(e^{tS}) = \exp(\lambda \int_{\mathbb{R}^d} (e^t g(x) - 1)\mathrm{d}x) \tag{3.41}$$

D. The probability generating and Laplace functionals over poisson processes

Theorem 3.3. *(*Probability generating functional for the Poisson point process) Given a PPP Φ, it is assumed with the measure Λ and the measurable function $v \in V$. Then the PGFL is

$$G[v] \triangleq \mathbb{E}\left(\prod_{x\in\Phi} v(x)\right) = \exp\left(-\int_{\mathbb{R}^d}[1-v(x)]\Lambda(\mathrm{d}x)\right). \tag{3.42}$$

3.4.1 Interference Characterization of PPP Networks

Define a function of path loss $\ell : \mathbb{R}^d \to \mathbb{R}$, all transmitters with unit power are modelled as a point process Φ. For the receiver at position r, the interference power is presented as

$$I(r) = \sum_{x\in\Phi} \ell(r-x), \quad r \in \mathbb{R}^d \tag{3.43}$$

where the channel fading is ignored. According to equation (3.21), the interference $I(r)$ is a shot-noise random field.

By taking the channel fading into account, the received power is obtained by the path loss multiplying attenuation coefficient h_x, hence the interference is

$$I = \sum_{x\in\Phi} \ell(x)h_x, \tag{3.44}$$

where coefficients are assumed independently.

For presenting the statistical characterization of interference, the Laplace transform of interference is operated according to the PGFL of PPP, which is shown as

$$\begin{aligned}\mathscr{L}(s) &= \mathbb{E}\left(e^{-sI}\right) = \mathbb{E}\left(\prod_{x\in\Phi} e^{-sh\ell(x)}\right)\\ &= \exp\left(-\int_0^\infty \mathbb{E}_h[1-e^{-sh\ell(x)}]c_d\lambda d r^{d-1}\mathrm{d}r\right)\\ &= \exp\left(-c_d\lambda\mathbb{E}_h(h^\delta)\Gamma(1-\delta)s^\delta\right)\end{aligned} \tag{3.45}$$

where d, $(d = 1,2,...)$ is the number of dimension, and $\delta = \frac{d}{\alpha}$. If the channel fading is Rayleigh distribution, then the variable h is exponentially distributed. We can obtain $\mathbb{E}_h(h^\delta) = \Gamma(1+\delta)$. Therefore, the interference characterization is finally presented as

$$\begin{aligned}\mathscr{L}(s) &= \exp\left(-c_d\lambda\Gamma(1+\delta)\Gamma(1-\delta)s^\delta\right) \\ &\overset{(a)}{=} \exp\left(-c_d\lambda\frac{\pi\delta}{\sin(\pi\delta)}s^\delta\right) \\ &\overset{(a)}{=} \exp\left(-\frac{c_d\lambda}{\mathrm{sinc}\delta}s^\delta\right)\end{aligned} \tag{3.46}$$

where step (a) follows the fact that $\Gamma(1+\delta)\Gamma(1-\delta) = \frac{\pi\delta}{\sin(\pi\delta)}$, and step (b) follows the fact that $\mathrm{sinc}\delta = \frac{\sin(\pi\delta)}{\pi\delta}$.

3.4.2 Summary

This chapter introduces the basic concepts of stochastic geometry, including the definition and characterization of point processes, and applications in interference analysis of wireless networks. In Chapter 5 and 6, the detailed description that how the stochastic geometry provides the mathematical framework for the analysis of cellular network performance will be presented.

Chapter 4

Exact Line-of-Sight Probability for Channel Modelling in Typical Indoor Environments

Overview

Previous works indicate that the probability of LOS propagation is crucial to model the real signal propagation channels and to evaluate the coverage of SCs. However, existing LOS probability models, such as the exponential model and 3GPP models, are over simplified to provide the exact LOS probability typical indoor scenarios. In this chapter, by taking the realistic layout of building structures into account, an analytical LOS probability model is proposed for downlink radio propagations in typical indoor scenarios, which have rectangular rooms and corridors. The proposed tractable model is validated through Monte Carlo simulations. Numerical results show that the proposed model estimates the network performance accurately and efficiently.

4.1 Introduction

The mobile traffic demand is increasing exponentially with the growing number of mobile devices. The vast majority (80%) of mobile data demand occurs indoors [3]. The ultra-

dense deployment of indoor SC networks has been widely recognized by industry and investigated by academia as a promising solution for increasing spectrum efficiency. In indoor environments, the wireless signals are blocked by building structures [8]. Conventionally, the blockage effect is modeled as a log-normal attenuation of the received signal strength [8–10]. However, LOS links and NLOS links are not distinguished therein, and thus the evaluation might not be accurate enough.

In a NLOS link, the blockage attenuates the wireless signals significantly. Measurement shows that the blockage in the NLOS scenario significantly reduces the bit error rate performance of MIMO systems [12]. Furthermore, the attenuation caused by the blockages has a crucial influence on the estimation of system performance, e.g. coverage probability [8].

Therefore, to efficiently evaluate the performance of indoor wireless networks, an accurate LOS probability model is required. Previous works model the LOS probability as a function with a variable of link length [15–18, 94]. In the 3GPP standards, the LOS probability was modelled as exponential functions against the distance [15]. In [17], the authors further investigated the models proposed in 3GPP by comparing them with the measurement, and determined the best fit LOS model. The authors in [16] improved the original LOS probability model in 3GPP to make it applicable to the 3D channels. The paper [94] employed a LOS probability model obtained through minimizing the error between measurement results and the analytical LOS function to develop a probabilistic omnidirectional path loss model. In [18], an analytical mathematical LOS probability model was derived for randomly located blockages based on the stochastic geometry.

In the moment, the LOS probability is modelled either as an exponential function [15] or a random function [18]. However, in reality the blockages in an indoor environment are fixed when the layout of the building is given. It is predictable that the LOS probability in a building with a fixed layout is neither a simple fixed exponential function nor randomly distributed function. On one hand, the exponential LOS probability function reduces the accuracy of network performance evaluation. On the other hand, the random LOS model sacrifices information of the building layout. A possible pathway to obtain an exact LOS probability function is to randomly generate propagation links in indoor environments and

statistically count the number of LOS ones. However, although the LOS probability can be calculated by the possible pathway, the network evaluation and optimization is still intractable without an analytical LOS probability function.

Therefore, this chapter presents a novel analytical approach to calculate the LOS probability in typical buildings, which consist of multiple rectangular cavities (rooms and corridors). Firstly, we derive the LOS probability function while the BS is assumed to be located in a rectangular cavity. Secondly, a model for computing the LOS probability function under an arbitrary given building layout with multiple rectangular rooms and corridors is proposed. Finally, taking the WINNER II A1 scenario as an example [95], the LOS probability function is computed in a closed form for indoor SC coverage rate evaluation.

Note that for simplicity, the effects of reflection, diffraction and scattering are ignored. Because it is difficult to obtain a tractable model in a complex indoor environment to predict the signal propagation condition while considering propagation phenomena, such as reflection and diffraction. Additionally, the effects of furniture and moving human bodies are also ignored. This chapter will mainly focus on analysing the LOS probability caused by stationary obstacles, e.g., wall blockages as the first milestone. The further physical propagation phenomenon and other obstacles will be considered in our future work.

The remainder of this chapter is summarized as follows: The details of proposed model scheme are described in Section 4.2. The Section 4.3 presents the application of the proposed LOS model by considering the WINNER II A1 scenario. The Section 4.4 provides the validation of proposed model. In Section 4.5, we conclude this chapter and present future works.

4.2 Scheme of the Proposed LOS Probability Model

In this work, we consider the downlink cellular network in typical indoor environments with the BS randomly deployed. Generally, the building structure of typical indoor environments consists of rectangular cavities. Therefore, the derivation of LOS probability is developed in rectangular cavities, and is divided into two steps. In the first step, the LOS probability

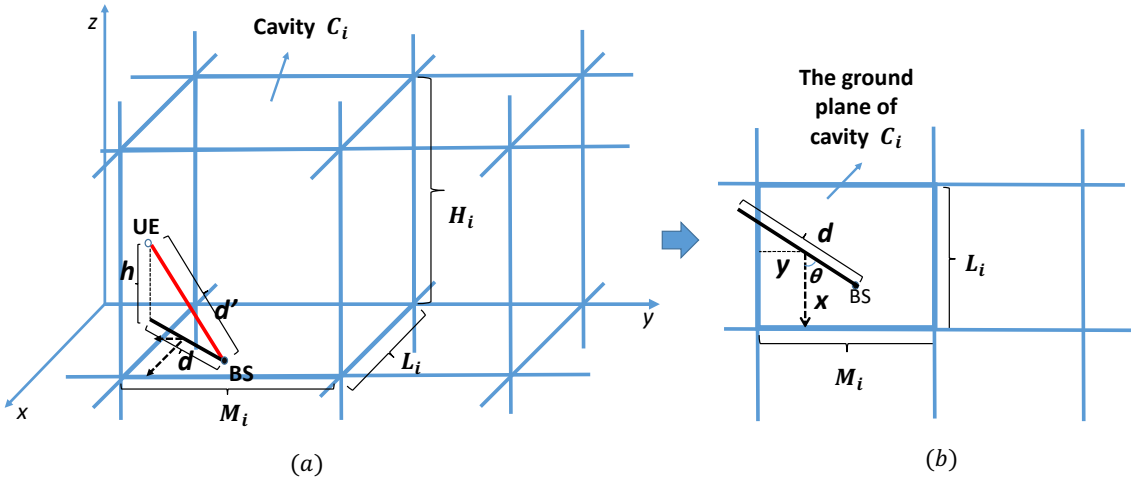

Fig. 4.1 Modelling of a random link that the BS is located in a rectangular cavity (room/corridor) $C_i, (i = 1,2,...)$ with a size of $M_i(\mathrm{m}) \times L_i(\mathrm{m}) \times H_i(\mathrm{m})$. (a) The link in a 3D building; (b) The projection of the link on 2D ground plane

is derived when the BS is randomly located in single rectangular cavity. In the second step, based on the calculated result in single cavity, the LOS probability is derived in the complex building environment. The descriptions of both steps are presented as follows.

4.2.1 Step I: Single Rectangular Cavity Scenario

In this subsection, we will derive the LOS probability for all associated user equipments (UEs) when the BS is located in single rectangular cavity. To present the derivation clearly, we firstly construct a 3D building grid in infinite 3D space. It consists of a collection of planes perpendicular to x, y and z coordinates, as shown in Fig. 4.1(a), which divides the space into many rectangular cavities. This is a generalization of regular buildings consisted of rectangular cavities. For simplicity, we consider a single floor of a building in this work.

Secondly, we assume a link with a given length $d^{'}$, whose ends are respectively the BS and UE, is randomly generated. Both of the link's direction and middle point position are randomly distributed. The transmitter BSs are located on the ground plane (corresponded to the virtual ground plane), and all UEs are at the same height of h. The BS end of the link

is randomly located in a rectangular cavity, which is presented as $\mathrm{C}_i, (i = 1, 2, ...)$ with size $M_i(\mathrm{m}) \times L_i(\mathrm{m}) \times H_i(\mathrm{m})$, as shown in Fig. 4.1. Without loss of generality, we assume $M_i \geq L_i$. If the UE end is also located within $\mathrm{C_i}$, the link is an LOS link and vice versa. Therefore, for cavity $\mathrm{C_i}$, the LOS probability is equal to the probability that the UE is located within it.

Parameters related to the random link $d^{'}$ are also illustrated in Fig. 4.1. The projection of the link $d^{'}$ on ground plane is denoted by d, which is randomly located because of the random generation of link $d^{'}$. Without loss of generality, the research object $d^{'}$ can be transferred to its projection d for simplicity in this context. The angle of d is expressed as θ. The variables x and y are the distances from the middle point of d to the nearest short border and the nearest long border of the rectangular cavity, respectively. Since the values of x, y and θ are independent, and and the their distributions are

$$\begin{cases} x \sim U\left(0, \frac{L_i}{2}\right), \\ y \sim U\left(0, \frac{M_i}{2}\right), \\ \theta \sim U\left(0, \frac{\pi}{2}\right), \end{cases} \tag{4.1}$$

where U denotes the uniform distribution [96, 97].Hence, the joint probability density function $f(x, y, \theta)$:

$$f(x, y, \theta) = \begin{cases} \frac{8}{L_i M_i \pi}, & (x,\ y,\ \theta) \in A, \\ 0, & \text{else}, \end{cases} \tag{4.2}$$

where $A = \left\{ \left(0 \leq x < \frac{L_i}{2}\right) \cap \left(0 \leq y < \frac{M_i}{2}\right) \cap \left(0 \leq \theta < \frac{\pi}{2}\right) \right\}$.

Observing from the projection of the propagation link on ground plane in Fig. 4.1(b), we can obtain the necessary and sufficient condition of LOS link as the following result:

$$\left(x > \frac{d\cos\theta}{2}\right) \cap \left(y > \frac{d\sin\theta}{2}\right), \tag{4.3}$$

where $d = \sqrt{d'^2 - h^2}$. Therefore, the LOS probability $P_{\mathrm{i,LOS}}(d)$ of the cavity C_i can be obtained as in Theorem 4.1.

Theorem 4.1. *The LOS probability $P_{\mathrm{i,LOS}}(d)$ in i-th single cavity scenario can be formulated as in equation* (4.5)*:*

$$P_{\mathrm{i,LOS}}(d) = \begin{cases} P_{\mathrm{i_1,LOS}}(d), & \text{when } 0 \le d < L_i \\ P_{\mathrm{i_2,LOS}}(d), & \text{when } L_i < d \le M_i \\ P_{\mathrm{i_3,LOS}}(d), & \text{when } M_i < d \le \sqrt{{L_i}^2 + {M_i}^2} \\ P_{\mathrm{i_4,LOS}}(d), & \text{when } d > \sqrt{{L_i}^2 + {M_i}^2} \end{cases} \tag{4.4}$$

where $P_{\mathrm{i,LOS}}(d)$ is divided into four pieces when link length d is in different integral range. Each piece is represented as $P_{\mathrm{i_k,LOS}}(d), k = 1,2,3,4$ respectively. $P_{\mathrm{i_k,LOS}}(d)$ is the k-th piece probability function that a BS and a UE separated by a distance d has a LOS link. They are calculated as

$$\begin{aligned} P_{\mathrm{i_1,LOS}}(d) &= \left[d^2 - 2d(L_i + M_i) + L_i M_i \pi\right] \tfrac{1}{L_i M_i \pi}, \\ P_{\mathrm{i_2,LOS}}(d) &= \left[-{L_i}^2 + 2dM_i(\sqrt{1 - \tfrac{{L_i}^2}{d^2}} - 1) + 2L_i M_i \arcsin \tfrac{L_i}{d}\right] \tfrac{1}{L_i M_i \pi}, \\ P_{\mathrm{i_3,LOS}}(d) &= \begin{cases} \Big[d^2 + {L_i}^2 + {M_i}^2 - 2d(M_i\sqrt{1 - \tfrac{{L_i}^2}{d^2}} + L_i\sqrt{1 - \tfrac{{M_i}^2}{d^2}}) \\ \quad + 2L_i M_i(\arccos \tfrac{L_i}{d} + \arccos \tfrac{M_i}{d} - 2\pi)\Big] \tfrac{-1}{L_i M_i \pi}, \end{cases} \\ P_{\mathrm{i_4,LOS}}(d) &= 0, \end{aligned} \tag{4.5}$$

Proof. As can be seen from Fig. 4.1(b), the LOS probability is the probability that the propagation link cannot cross any borders of the cavity. When the link length d is in different range, the value range of the angle θ also changes considering the variables x and y are always conditioned by equation (4.3). Therefore, the k-th piece probability function can be formulated as:

$$P_{\mathrm{i_k,LOS}}(d) = \int_{\frac{d}{2}\cos\theta}^{\frac{L_i}{2}} \int_{\frac{d}{2}\sin\theta}^{\frac{M_i}{2}} \int_{\Theta_k} f(x,y,\theta)\, dx\, dy\, d\theta, \tag{4.6}$$

where Θ_k denotes the integral limit of θ corresponding to the k-th piece in Theorem 4.1. Here $\Theta_1 \in (0, \frac{\pi}{2})$, $\Theta_2 \in (\arccos \frac{L_i}{d}, \frac{\pi}{2})$, $\Theta_3 \in (\arccos \frac{L_i}{d}, \frac{\pi}{2} - \arccos \frac{M_i}{d})$ and $\Theta_4 \in \emptyset$, respectively. □

Theorem 4.1 can be generalised as the LOS probability model of any single rectangular cavity scenario. This will be verified in Section 4.3. On this basis, the LOS probability model in complex building scenario will be obtained, shown as in Corollary 4.1.

4.2.2 Step II: Buildings with Multiple Rectangular Cavities

Generally, a complex scenario is consisted of many rectangular cavities. We assume the entire scenario (denoted by C) is divided by walls into N rectangular cavities with each cavity area of $S_i, i = 1,2,3...N$. Through Theorem 4.1, the LOS probability function in single cavity $\mathrm{C_i}$ has been obtained. Therefore, the LOS probability P_{LOS} in the complex scenario C is presented in Corollary 4.1.

Corollary 4.1. *The LOS probability model in a complex building scenario consisted of rectangular cavities is formulated as*

$$P_{\mathrm{LOS}}(d) = \sum_{i=1}^{N} \frac{S_i}{\sum_{i=1}^{N} S_i} P_{i,\mathrm{LOS}}(d), \tag{4.7}$$

where $P_{i,\mathrm{LOS}}(d)$ denotes the LOS probability function of the i-th rectangular cavity, which can be obtained by Theorem 4.1.

Proof. Since the BS is randomly deployed in the assumed scenario C, the probability that the BS is located within the i-th rectangular cavity can be presented as: $p_i = \frac{S_i}{\sum_{i=1}^{N} S_i}$. Therefore, for the given building structure C, the LOS probability is

$$P_{\mathrm{LOS}}(d) = \sum_{i=1}^{N} P_{\mathrm{LOS}}[P_{i,\mathrm{LOS}}(d) \mid C] = \sum_{i=1}^{N} p_i P_{i,\mathrm{LOS}}(d), \tag{4.8}$$

where $d = \sqrt{d'^2 - h^2}$. Note that the variable h is the height of UEs, which are assumed at the same height in this chapter. □

Thus the mapping from LOS probability to link distance is constructed by Corollary 4.1. In other words, the LOS probability can be directly calculated without any simulation and measurement, only if the layout of the scenario is given. This model is analytically tractable and generally suitable to arbitrary indoor scenarios consisting of rectangular cavities. In

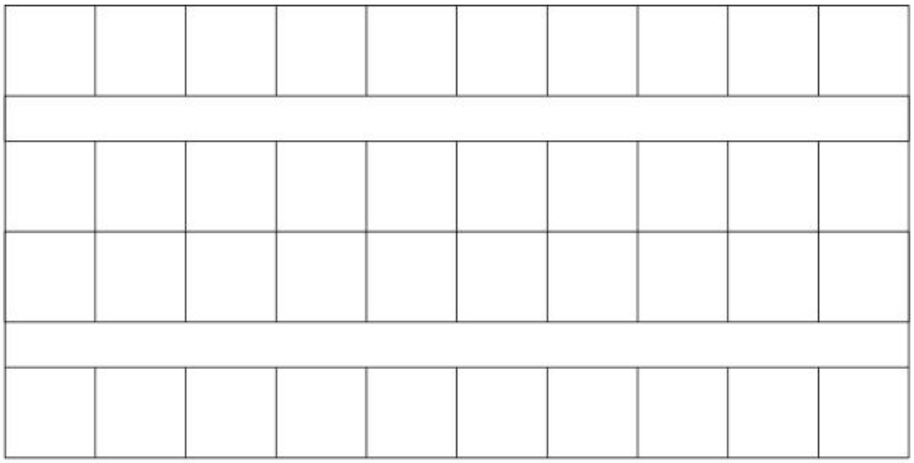

Fig. 4.2 WINNER II A1 model

addition, it is frequency-independent for radio propagation. Its validation will be presented in Section 4.3.

4.3 The Application of Proposed LOS Probability Model

This section will illustrate the application of proposed LOS probability function in WINNER II A1 scenario, which is a building model of typical indoor office cases. The WINNER II A1 scenario is utilized as the bench mark of complex building scenario. It consists of 40 identical rectangular rooms and 2 corridors, of which the layout is as shown in Fig. 4.2. The scenario size is 100m $\times$ 50m $\times$ 3m, of which each room size is 10m $\times$ 10m $\times$ 3m, and the each corridor size is 100m $\times$ 5m $\times$ 3m. The UE is assumed to be located inside the building with a height h being 1.25m.

Now we firstly provide the LOS probability function of WINNER II A1 scenario according to the proposed method. For the ease of illustration, we number all the rooms from 1 to 40, and the corridors from 41 to 42, respectively. The area of entire scenario is S. Due to the identical size of rooms, the area of each room is denoted by S_{R}, and the LOS probability is $P_{\mathrm{LOS}}^{\mathrm{R}}(d)$. Similarly to the rooms, the area of each corridor is denoted by S_{C}, and the LOS probability function is $P_{\mathrm{LOS}}^{\mathrm{C}}(d)$.

According to Theorem 4.1 and Corollary 4.1, the LOS probability model P_{LOS} of WINNER II A1 scenario can be presented as:

$$
\begin{aligned}
P_{\mathrm{LOS}}(d) &= \sum_{i=1}^{N_1+N_2} p_i P_{\mathrm{i,LOS}}(d) = \sum_{i=1}^{N_1} \frac{S_{\mathrm{R}}}{S} P^{\mathrm{R}}_{\mathrm{LOS}}(d) + \sum_{i=1}^{N_2} \frac{S_{\mathrm{C}}}{S} P^{\mathrm{C}}_{\mathrm{LOS}}(d) \\
&= \begin{cases}
\frac{N_1 S_{\mathrm{R}}}{S} P^{R}_{\mathrm{1,LOS}}(d) + \frac{N_2 S_{\mathrm{C}}}{S} P^{C}_{\mathrm{1,LOS}}(d) = f_1(d), & d \in (0, d_1] \\
\frac{N_1 S_{\mathrm{R}}}{S} P^{R}_{\mathrm{1,LOS}}(d) + \frac{N_2 S_{\mathrm{C}}}{S} P^{C}_{\mathrm{2,LOS}}(d) = f_2(d), & d \in (d_1, d_2] \\
\frac{N_1 S_{\mathrm{R}}}{S} P^{R}_{\mathrm{2,LOS}}(d) + \frac{N_2 S_{\mathrm{C}}}{S} P^{C}_{\mathrm{2,LOS}}(d) = f_3(d), & d \in (d_2, d_3] \\
\frac{N_1 S_{\mathrm{R}}}{S} P^{R}_{\mathrm{3,LOS}}(d) + \frac{N_2 S_{\mathrm{C}}}{S} P^{C}_{\mathrm{2,LOS}}(d) = f_4(d), & d \in (d_3, d_4] \\
\frac{N_1 S_{\mathrm{R}}}{S} P^{R}_{\mathrm{3,LOS}}(d) + \frac{N_2 S_{\mathrm{C}}}{S} P^{C}_{\mathrm{3,LOS}}(d) = f_5(d), & d \in (d_4, d_5] \\
\frac{N_1 S_{\mathrm{R}}}{S} P^{R}_{\mathrm{3,LOS}}(d) + \frac{N_2 S_{\mathrm{C}}}{S} P^{C}_{\mathrm{4,LOS}}(d) = f_6(d), & d \in (d_5, \infty)
\end{cases}
\end{aligned}
\tag{4.9}
$$

where the right-hand side functions of equation (4.3) are shown as:

$$
\begin{aligned}
f_1(d) &= \tfrac{4}{5D^2\pi}\left[d^2 - 4dD + D^2\pi\right] + \tfrac{1}{5LM\pi}\left[d^2 - 2d(L+M) + LM\pi\right] \\
f_2(d) &= \tfrac{4}{5D^2\pi}\left[d^2 - 4dD + D^2\right] + \tfrac{1}{5LM\pi}\left[-L^2 + 2dM(\sqrt{1-\tfrac{L^2}{d^2}} - 1) + 2LM\arcsin\tfrac{L}{d}\right] \\
f_3(d) &= \begin{cases}
\tfrac{4}{5D^2\pi}\left[-D^2 + 2dD(\sqrt{1-\tfrac{D^2}{d^2}} - 1) + 2D^2\arcsin\tfrac{D}{d}\right] \\
+\tfrac{1}{5LM\pi}\left[-L^2 + 2dM(\sqrt{1-\tfrac{L^2}{d^2}} - 1) + 2LM\arcsin\tfrac{L}{d}\right]
\end{cases} \\
f_4(d) &= \tfrac{1}{5LM\pi}\left[-L^2 + 2dM(\sqrt{1-\tfrac{L^2}{d^2}} - 1) + 2LM\arcsin\tfrac{L}{d}\right] \\
f_5(d) &= \begin{cases}
\tfrac{1}{5LM\pi}\Big[d^2 + L^2 + M^2 - 2d(M\sqrt{1-\tfrac{L^2}{d^2}} + L\sqrt{1-\tfrac{M^2}{d^2}}) \\
+2LM(\arccos\tfrac{L}{d} + \arccos\tfrac{M}{d} - 2\pi)\Big]\tfrac{-1}{LM\pi}
\end{cases} \\
f_6(d) &= 0
\end{aligned}
$$

where the parameter D denotes the room length room length. The parameters M and L denote the length and width of corridor, respectively. The LOS probability occurring in a corridor is denoted by $P^{\mathrm{C}}_{\mathrm{LOS}}(d)$, which is segmented into four pieces, as shown $P^{\mathrm{C}}_{\mathrm{1,LOS}}(d)$, $P^{\mathrm{C}}_{\mathrm{2,LOS}}(d)$, $P^{\mathrm{C}}_{\mathrm{3,LOS}}(d)$, and $P^{\mathrm{R}}_{\mathrm{3,LOS}}(d)$. The LOS probability $P^{\mathrm{R}}_{\mathrm{LOS}}(d)$ occurring in a corridor is similar to the presentation of LOS probability in a corridor. The difference is that $P^{\mathrm{C}}_{\mathrm{LOS}}(d)$ is divided

into three pieces, since the room length is equal to the width. For each piece of equation (4.3), the lengths are given by $d_1 = M,\ d_2 = D,\ d_3 = D\sqrt{2},\ d_3 = L,$ and $d_5 = \sqrt{L^2 + M^2}$.

Now, the mapping from the LOS probability distribution to the layout of this scenario is constructed. Furthermore, P_{LOS} can be generalized as the LOS probability model for indoor office building cases, since WINNER II A1 is a typical indoor office scenario.

4.4 Performance Evaluation

This section will validate the proposed model in single rectangular cavity scenario and complex building scenario, respectively. Firstly, this model will be verified in single rectangular cavity scenario with various cavity sizes by comparing them with Monte Carlo simulations. Then, in complex building scenario, the WINNER II A1 scenario will be employed as an example, which is a general building model of indoor office building cases [95], to validate the proposed model by the comparison with existing LOS probability models and Monte Carlo simulation.

4.4.1 Single Rectangular Cavity Scenario

Fig. 4.3 illustrates the verification of the proposed model by comparing it with Monte Carlo simulation in terms of different cavity sizes. It is obvious that the proposed model matches the simulations results closely. Moreover, the LOS probability decreases significantly with the distance increasing, and declines slowly with the areas of cavities growing. It can be seen that the LOS probability is not only influenced by the link length, but also by the cavity size. This matches our intuition that a longer link has a higher likelihood of experiencing blockages.

4.4.2 Complex Building

This section illustrates the application of proposed LOS probability function in complex building scenario, and provides the analysis of coverage performance.

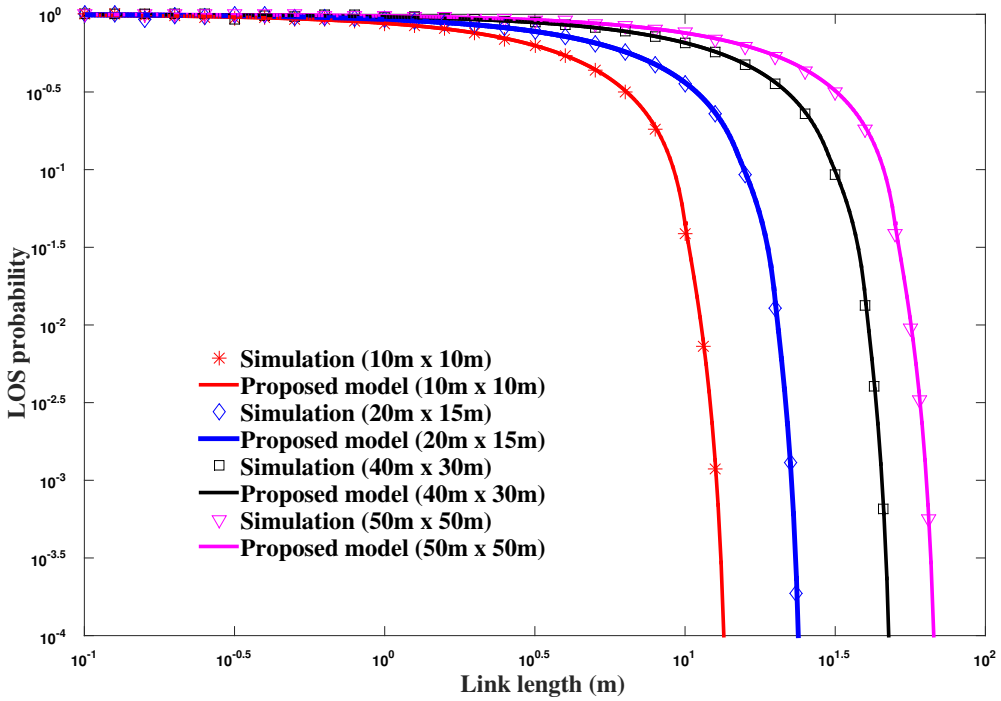

Fig. 4.3 The comparison of proposed model and Monte Carlo simulation in single rectangular cavity. The sizes are 10m $\times$ 10m, 20m $\times$ 15m, 40m $\times$ 30m, and 50m $\times$ 50m separately. The BS and UE are randomly generated within the scenario.

Meanwhile, existing models, such as the exponential LOS probability distribution and the LOS probability in WINNER II A1 scenario [95] (We name them exponential model and WINNER II A1 model, respectively), are used for comparison. The exponential model supposes that the LOS probability decreases exponentially with attenuation coefficients as the distance increases [15]. The attenuation coefficients can be obtained from the best fit for the Monte Carlo simulation by linear least square regression. WINNER II A1 model is specifically designed to describe the LOS probability of this scenario, which is obtained by measurement data. Its expression of LOS probability is presented in [95].

In Fig. 4.4, the comparison of proposed model, exponential model, WINNER II A1 model and Monte Carlo simulation is illustrated. It is shown that our proposed LOS model very closely fits the Monte Carlo simulation, thus the proposed LOS model is validated. According to the proposed model, it is further observed that the trend of LOS probability decreases rapidly at the link distance of around 10 meters, and then moderately decreases

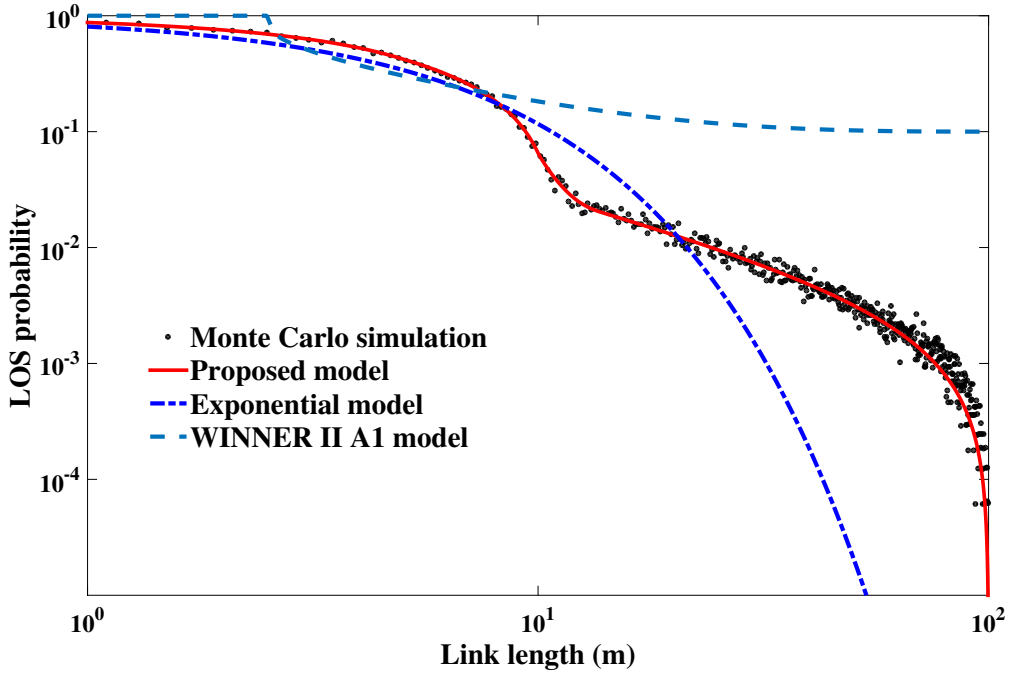

Fig. 4.4 The comparison of the proposed model, Monte Carlo model, Exponential model and WINNER II A1 model in WINNER II A1 scenario.

after that until at around 100 meters. It is because that, in WINNER II A1 scenario, the LOS transmission occurs in both the rooms and corridors when the link length is less than about 10 meters. Otherwise, it only occurs in corridors when the link length is larger than about 10 meters. Additionally, although the exponential model has a higher accuracy than the traditional WINNER II A1 model, it still has a remarkable error compared to the simulation. The deviation is getting worse with the link distance increasing, which will significantly influence the estimation of the performance of edge UEs in SC networks. Our model will improve the accuracy of network performance evaluation (e.g. coverage), especially for the the networks sensitive to LOS and NLOS propagations.

In Fig. 4.5, we present a comparison of coverage probabilities calculated by the aforementioned three LOS models and Monte Carlo simulation, considering BSs are PPP distributed with density λ in WINNER II A1 scenario. It is assumed that the BS with the strongest signal power at UE is the designated server. Signals from other BSs are considered as interferences given the UE located at the central point of building. The coverage probability is expressed

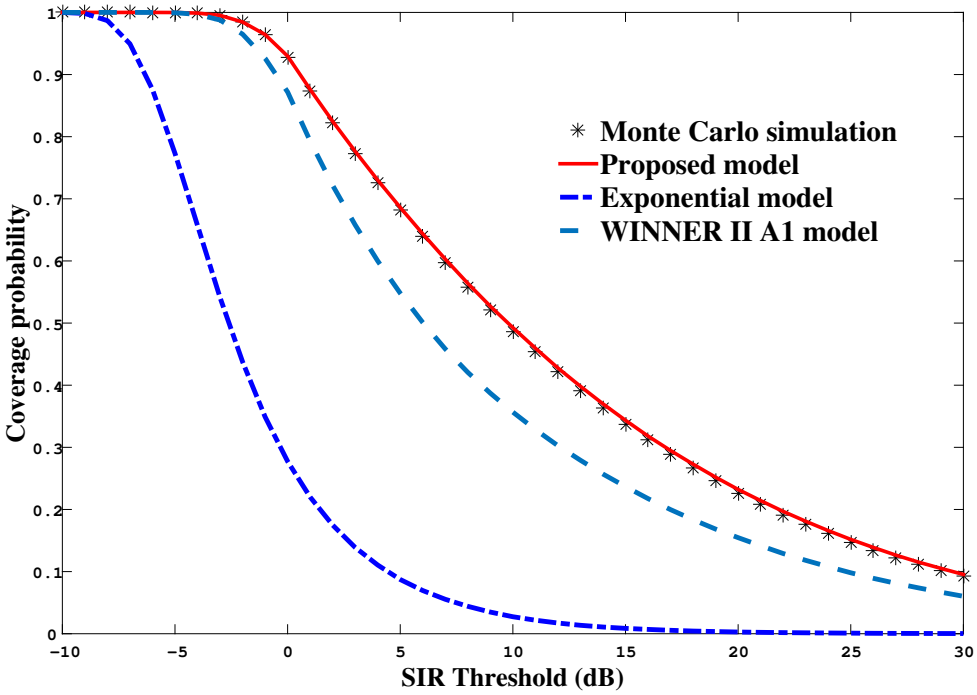

Fig. 4.5 The comparison of coverage probabilities obtained through proposed model, Monte Carlo model, Exponential model and WINNER II A1 model, respectively.

Table 4.1 Simulation parameters

Simulation samples	10^6
Simulation area	$S = 100 \times 50\text{m}^2$
BS density	$\lambda = 0.001\text{m}^{-2}$
Pathloss model	$PL(d) = 38.46 + 20\log d + 0.7d$, [15]
Transmitter power	$P_t = 0\text{dB}$

as: $P_c(T) = P_c\{\text{SIR} > \text{T}\}$, where T is the signal to interference ratio (SIR) threshold. The simulation parameters are summarised in Table 4.1.

Simulation results show that the proposed model agrees to Monte Carlo simulation well, while the exponential and WINNER II A1 models underestimate the coverage probability. In other words, for achieving the same coverage probability, less BSs will be deployed actually. This result will be meaningful to direct the system design of SC networks in indoor environments. Additionally, it only takes several minutes to evaluate the coverage using the

analytical expression, which is much more efficiently than the Monte Carlo simulation (about several hours).

4.5 Conclusions

In this chapter, a novel LOS probability model for radio propagation in typical indoor scenarios has been developed, which analytically constructs the mapping from a building's layout (structure) to the LOS probability distribution. With this model, we can directly obtain the LOS probability of transmission links inside a given building without simulations or measurements. The proposed model also improves the accuracy of obtaining LOS probability because it reduces the randomness of building structure. Numerical results show that traditional LOS probability models underestimate the performance of PPP network.

Further topics for improving the proposed model include the effects of furniture and moving obstacles (e.g. human bodies) on LOS probability distribution, extension to indoor scenarios with rectangular and non-rectangular (other shapes) cavities, and developing the application on cellular network optimization. Regarding of the propagation phenomena, such as reflection, diffraction and scattering, they will also be taken into consideration for more accurately channel modeling.

Chapter 5

Performance Analysis for Indoor Dense Small-Cell Networks with LOS and NLOS Transmissions

Overview

With the rapid development of 5G wireless communication system, the deployment of indoor SCs will become denser, so as to satisfy the higher throughput demand for indoor hotspots. Previous works about the performance analysis for the indoor SC networks are based on the simplified path loss models, which do not distinguish LOS and NLOS transmissions. However, with the network becoming denser, more NLOS transmissions are transformed into LOS transmissions because of the shorter distance between users and BSs. It's certain to make the impact on the indoor network performance. Therefore, this chapter will introduce a practical path loss model including LOS and NLOS propagations, and propose a mathematically tractable approach to analyse their effects on the performance of indoor SC networks. The analytical achievements about three performance metrics, including the coverage probability, SE and ASE, are derived for both a general path loss model and a special linear path loss model. Moreover, analytical achievements are verified by Monte Carlo simulations. The numerical results reveal the effects of BS density and LOS probability

functions on the aforementioned metrics, which has a certain guidance for designing the indoor dense SC networks.

5.1 Introduction

In recent years, the cellular networks in 5G have attracted much attention due to the capability of the higher throughput, the lower latency, and the higher reliability under higher connectivity density and mobility [101]. Herein, for the indoor hotspots, the higher throughput requirement is urgent to be satisfied. Since the applications with the high demand of data transmission rate are still growing, such as ultra high resolution live videos and virtual reality. In this context, the dense SC network, such as picocell and femtocell, has been accepted as an effective solution to improve the throughput for the indoor communication networks [102, 103].

In terms of the performance analysis of SC networks, traditional approaches were based on the simplistic path loss models that fail to differentiate and analyse LOS and NLOS propagations [20–22]. This results in inaccurate analysis of SC networks. The work [20] showed that, when the BS density is large enough, performance metrics of coverage probability and the SE are not sensitive to the BS density, while the ASE is proportional to the BS density. However, these conclusions do no always hold when the path loss model is comprised of the LOS and NLOS transmissions [19, 23–25]. In [23], the authors explored the effects of the multi-slope path loss model, using different path loss exponents according to various distance ranges, on the dense SC networks. In [19, 24, 25], the authors investigated the piece-wise expressions of path loss incorporating both LOS and NLOS transmissions. On this basis, the performance metrics, i.e. the coverage probability and the ASE were derived as functions of the BS density. Moreover, numerical results presented that the coverage probability increases firstly then decreases for the BS density denser than a value of threshold. In addition, different from the conclusion of previous works, the ASE is non-linear with the BS density.

As the aforementioned description, all the works focus on the outdoor SC network. However, there are very limited researches for analysing the indoor dense SC network in

terms of distinguishing LOS from NLOS transmissions. The work [29] presented that the increase of the throughput is non-linear with the BS density, which considered a path loss model with the impact of blockages as an exponential function of distance. Nevertheless, it's based on the scaling law rather than the tractable method.

Motivated by the above fact, this chapter will mainly target to propose a tractable approach to analyse the performance of indoor dense SC networks with differentiating LOS and NLOS propagations. The LOS probability model proposed in Chapter 4 will be adopted, since the LOS model accurately describes the indoor signal propagations. Moreover, the analytical achievements of three performance metrics will be derived.

The remainder of this chapter is organized as follows. The system model is introduced in Section 5.2. The analytical results of performance metrics are derived in Section 5.3. The analytical results are validated in Section 5.4. In the end, this chapter is concluded in Section 5.5.

5.2 System Model

This chapter also focuses on the downlink propagations of indoor SC network. The positions of BSs and users are modelled by two independent 2D homogeneous PPPs Φ_B with density λ_B and Φ_U with density λ_U respectively. Moreover, assume λ_U is much larger than λ_B such that each BS can serve at least one associated users in its coverage and be activated. Each BS transmits with the identical power P_t.

A. Path loss model

In order to practically describe the LOS and NLOS transmissions, the piece-wise path loss model considering the practical LOS and NLOS transmissions, is adopted with respect to the

link distance r between the typical user and the target BS, which is presented as

$$\omega(r)=\begin{cases}\omega_1(r)=\begin{cases}\omega_1^{\mathrm{L}}(r), & \text{with probability } \mathrm{Pr}_1^{\mathrm{L}}(r)\\ \omega_1^{\mathrm{NL}}(r), & \text{with probability } \mathrm{Pr}_1^{\mathrm{NL}}(r)\end{cases}, & \text{when } 0\le r\le d_1\\ \omega_2(r)=\begin{cases}\omega_2^{\mathrm{L}}(r), & \text{with probability } \mathrm{Pr}_2^{\mathrm{L}}(r)\\ \omega_2^{\mathrm{NL}}(r), & \text{with probability } \mathrm{Pr}_2^{\mathrm{NL}}(r)\end{cases}, & \text{when } d_1<r\le d_2\\ \vdots & \vdots\\ \omega_N(r)=\begin{cases}\omega_N^{\mathrm{L}}(r), & \text{with probability } \mathrm{Pr}_N^{\mathrm{L}}(r)\\ \omega_N^{\mathrm{NL}}(r), & \text{with probability } \mathrm{Pr}_N^{\mathrm{NL}}(r)\end{cases}, & \text{when } r>d_{N-1}\end{cases} \tag{5.1}$$

where the function of path loss $\omega(r)$ is divided into N pieces, represented by $\omega_n(r)$, $n\in\{1,2,3,\cdots,N\}$. In addition, the variables $\omega_n^{\mathrm{L}}(r)$ and $\omega_n^{\mathrm{NL}}(r)$ denote the n-th piece path loss function for the LOS and NLOS propagation, respectively. Similarly, the variables $\mathrm{Pr}_n^{\mathrm{L}}(r)$ and $\mathrm{Pr}_n^{\mathrm{NL}}(r)$ represent the n-th segment of the LOS and NLOS probability function, respectively. Note that, for each piece n, $\mathrm{Pr}_n^{\mathrm{L}}(r)+\mathrm{Pr}_n^{\mathrm{NL}}(r)=1$.

Moreover, for each piece $\omega_n(r)$, it is modeled as

$$\omega_n(r)=\begin{cases}\omega_n^{\mathrm{L}}(r)=K_n^{\mathrm{L}}r^{-\alpha_n^{\mathrm{L}}}, & \text{for LOS transmission}\\ \omega_n^{\mathrm{NL}}(r)=K_n^{\mathrm{NL}}r^{-\alpha_n^{\mathrm{NL}}}, & \text{for NLOS transmission}\end{cases} \tag{5.2}$$

where the path loss exponents are denoted by α_n^{L} and α_n^{NL} for the LOS and NLOS path, separately. The variables K_n^{L} and K_n^{NL} are the reference path loss at a unit distance (1m), for the LOS and NLOS path, respectively. In general, the value of α_n^{L} is smaller than that of α_n^{NL}, since the negative effects of the obstacles (e.g. buildings, walls and corridors) will cause a higher attenuation of NLOS transmissions compared with the LOS cases. In reality, the above four important path loss parameters are constants, attained by the complicated and actual channel environments measuring.

As shown in (5.1), $\mathrm{Pr}_n^{\mathrm{L}}(r)$ is the n-th piece LOS probability function, which monotonically decreases with distance r. Therefore, it can be also modeled as a piece-wise function, which

is given by

$$\Pr^{\mathrm{L}}(r) = \begin{cases} \Pr_1^{\mathrm{L}}(r), & \text{when } 0 \le r \le d_1 \\ \Pr_2^{\mathrm{L}}(r), & \text{when } d_1 < r \le d_2 \\ \vdots & \vdots \\ \Pr_N^{\mathrm{L}}(r), & \text{when } r > d_{N-1} \end{cases} \tag{5.3}$$

Combining (5.1), (5.2) and (5.3), the proposed path loss model can be obtained completely. It is line with the proposed path loss model by the 3GPP standards [104]. Furthermore, the path loss model with single slope (i.e., $\omega(r) = Kr^{-\alpha}$), widely used in the current communication networks, can be easily derived with the following parameters: $N = 1, K_1^{\mathrm{L}} = K_1^{\mathrm{NL}} = K, \alpha_1^{\mathrm{L}} = \alpha_1^{\mathrm{NL}} = \alpha, \Pr^{\mathrm{L}}(r) = 1, \Pr^{\mathrm{NL}}(r) = 0$. Remarkably, our developed path loss model will be more complex to derive the analytical results than the simplistic ones. But its results are more practical and accurate, especially in the denser SC networks, since the transition of transmissions from the NLOS to LOS seems to experience more likelihood with the link distance being closer.

Finally, in this chapter, the user association strategy (UAS) is determined as the smallest path loss. This is more practical than the nearest distance UAS. Assume both the LOS and NLOS transmission experience the Rayleigh fading, which is a variable of the exponential distribution with a unit mean, $h \sim \exp(1)$.

B. Line-of-Sight probability function

As stated in chapter 4, the existing LOS probability functions for indoor wireless communications are already complicated, such as exponential functions or random functions against the distance r. Note that if we consider the layout of the building, the LOS probability function is going to be more accurate but more sophisticated than the former two functions. Therefore, in order to derive the tractable expression of the performance for indoor dense SC network, it's expected to use some elementary functions (e.g., linear functions) to approximate the sophisticated LOS probability function with minor errors. For tractability, a two-piece

approximation function is adopted [19], which is given by

$$\Pr^{\mathrm{L}}(r) = \begin{cases} 1 - \frac{r}{L_1}, & 0 < r \leq L_1 \\ 0, & r > L_1 \end{cases} \tag{5.4}$$

Herein, L_1 is an important parameter which can be explained as the LOS possibility of a given transmission environment. In other word, the larger L_1 is, the less obstacles the propagating environment contains, and then the higher the LOS probability is at a provided link distance. Moreover, L_1 can be adjusted to match the complicated LOS probability function, which will be shown at Section 5.4.

Moreover, for verifying the the approximation method's generality and practicability in this study, the LOS probability model proposed in Chapter 4 is adopted for the performance analysis in indoor dense SC networks regarding of LOS and NLOS transmission. It is given by

$$\Pr^{\mathrm{L}}(r) = \begin{cases} \frac{4}{5D^2\pi}\left[r^2 - 4rD + D^2\right] + \frac{1}{5LM\pi}\left[r^2 - 2r(L+M) + LM\pi\right], & 0 < r \leq d_1 \\ \frac{4}{5D^2\pi}\left[-L^2 + 2rM(\sqrt{1-\frac{L^2}{r^2}} - 1) + 2LM\arcsin\frac{L}{r}\right] & \\ + \left[r^2 - 4rD + D^2\right] + \frac{1}{5LM\pi}, & d_1 < r \leq d_2 \\ \frac{4}{5D^2\pi}\left[-D^2 + 2rD(\sqrt{1-\frac{D^2}{r^2}} - 1) + 2D^2\arcsin\frac{D}{r}\right] & \\ + \frac{1}{5LM\pi}\left[-L^2 + 2rM(\sqrt{1-\frac{L^2}{r^2}} - 1) + 2LM\arcsin\frac{L}{r}\right], & d_2 < r \leq d_3 \\ \frac{1}{5LM\pi}\left[-L^2 + 2rM(\sqrt{1-\frac{L^2}{r^2}} - 1) + 2LM\arcsin\frac{L}{r}\right], & d_3 < r \leq d_4 \\ \frac{1}{5LM\pi}\Big[r^2 + L^2 + M^2 - 2r(M\sqrt{1-\frac{L^2}{r^2}} + L\sqrt{1-\frac{M^2}{r^2}}) & \\ +2LM(\arccos\frac{L}{r} + \arccos\frac{M}{r} - 2\pi)\Big] + \frac{-1}{LM\pi}, & d_4 < r \leq d_5 \\ 0, & r > d_5 \end{cases} \tag{5.5}$$

where the parameters from d_1 to d_5 are link distances, and the parameters $D, L,$ and M present the layout of the building. The details can be referred to Chapter 4.

C. Performance metrics

The main purpose of the indoor dense SC network is to improve the coverage probability for the downlink, and enhance the SE and the ASE for the overall network. Therefore, the following three performance metrics are of great importance.

1) The *coverage probability*, which is defined as the probability that the received signal to interference plus noise ratio (SINR) is larger than the threshold T:

$$p_c(\lambda_B, T) = \mathbb{P}[\text{SINR} > T] \tag{5.6}$$

The elaborate expression of SINR will be given in the next section.

2) The *SE* in bps/Hz, which is represented as

$$\varepsilon_{SE}(\lambda_B, T_0) = \int_{T_0}^{\infty} \log_2(1+T) f_t(\lambda_B, T) \mathrm{d}T \tag{5.7}$$

where T_0 is the minimum SINR to make sure the indoor dense SC network working, and $f_t(\lambda_B, T)$ denotes the probability density function (PDF) of the received SINR with regard to the defined threshold T and the BS density λ_B. Moreover, $f_t(\lambda_B, T)$ can be calculated by

$$f_t(\lambda_B, T) = \frac{\partial(1 - p_c(\lambda_B, T))}{\partial T} \tag{5.8}$$

3) The *ASE* in bps/Hz/km^2, which is shown as

$$\varepsilon_{ASE}(\lambda_B, T_0) = \frac{\lambda_B \cdot S \cdot B \cdot \varepsilon_{SE}}{S \cdot B} = \lambda_B \cdot \varepsilon_{SE} \tag{5.9}$$

where S is the area size, and B is the system bandwidth. Obviously, ε_{ASE} is more influenced by the denser SC network than ε_{SE}.

5.3 Performance Analysis

On the basis of the theory from stochastic geometry, this section derives the analytical and tractable expressions of the above three performance metrics in the system model of Section 5.2. Firstly, a general but abstract LOS probability function (5.3) is considered, such that the corresponding results are also universal and portable. Then, we investigate a two-piece linear LOS probability function (5.4) as a special case in our study, following the main results obtained from the former general case. Thereafter, in the next section, we will use the tractable results from the above special case to approximate the practical LOS probability function (5.5). The numerical results show that the approximation error is trivial.

5.3.1 General Case and Main Results

Without any loss of generality, assume that a typical user locates at the point of origin o. At first, the coverage probability is investigated according to the equation (5.6) for the user, where the SINR is denoted as

$$\text{SINR} = \frac{P_t \omega(r) h}{\sigma^2 + I_r} \tag{5.10}$$

where σ^2 denotes the power of the additive white Gaussian noise (AWGN), and I_r represents the interference by the sum of interfering BSs, as shown

$$I_r = \sum_{i:\, b_i \in \Phi_B \setminus b_0} P_t \varphi_i g_i \tag{5.11}$$

Herein, b_i is the i-th interfering BS, φ_i and g_i are the path loss and power gain of Rayleigh fading between the i-th interfering BS b_i and the typical user, respectively.

Therefore, the coverage probability is obtained as shown the followed.

Theorem 5.1. *For the typical user in the indoor dense SC network, considering the general LOS probability function in (5.3) , the coverage probability $p_c(\lambda_B, T)$ defined in (5.6) is given by*

$$p_c(\lambda_B, T) = \sum_{n=1}^{N} (C_n^L + C_n^{NL}) \tag{5.12}$$

where C_n^L and C_n^{NL} are the n-th piece coverage probability for the situation that the typical user is connected to a BS with a LOS link and with a NLOS link, respectively.

Moreover,

$$C_n^L = \int_{d_{n-1}}^{d_n} \mathbb{P}\left[\frac{P_t \omega_n^{\mathrm{L}}(r)h}{\sigma^2 + I_r} > T\right] f_{R,n}^{\mathrm{L}}(r)\mathrm{d}r \tag{5.13}$$

$$C_n^{NL} = \int_{d_{n-1}}^{d_n} \mathbb{P}\left[\frac{P_t \omega_n^{\mathrm{NL}}(r)h}{\sigma^2 + I_r} > T\right] f_{R,n}^{\mathrm{NL}}(r)\mathrm{d}r \tag{5.14}$$

where $f_{R,n}^{\mathrm{L}}(r)$ and $f_{R,n}^{\mathrm{NL}}(r)$ denote the n-th piece PDF of the distances R_n^{L} and R_n^{NL} from the BS and user. R_n^{L} and R_n^{NL} are the distances under the situation that the typical user is connected to a LOS BS and a NLOS BS, respectively.

Proof. According to (5.6) and (5.10), $p_c(\lambda_B, T)$ can be presented as

$$\begin{aligned}
p_c(\lambda_B, T) &= \mathbb{P}[\mathrm{SINR} > T] \\
&= \mathbb{E}_r[\mathbb{P}[\mathrm{SINR} > T|r]] \\
&= \int_{r>0} \mathbb{P}[\mathrm{SINR} > T|r] f_R(r)\mathrm{d}r \\
&= \int_{r>0} \mathbb{P}[\frac{P_t \omega(r)h}{\sigma^2 + I_r} > T] f_R(r)\mathrm{d}r \\
&\overset{(a)}{=} \int_0^{d_1} \mathbb{P}[\frac{P_t \omega_1^{\mathrm{L}}(r)h}{\sigma^2 + I_r} > T] f_{R,1}^{\mathrm{L}}(r)\mathrm{d}r + \int_0^{d_1} \mathbb{P}[\frac{P_t \omega_1^{\mathrm{NL}}(r)h}{\sigma^2 + I_r} > T] f_{R,1}^{\mathrm{NL}}(r)\mathrm{d}r \\
&\quad + \cdots \\
&\quad + \int_{d_{N-1}}^{\infty} \mathbb{P}[\frac{P_t \omega_N^{\mathrm{L}}(r)h}{\sigma^2 + I_r} > T] f_{R,N}^{\mathrm{L}}(r)\mathrm{d}r + \int_{d_{N-1}}^{\infty} \mathbb{P}[\frac{P_t \omega_N^{\mathrm{NL}}(r)h}{\sigma^2 + I_r} > T] f_{R,N}^{\mathrm{NL}}(r)\mathrm{d}r \\
&= \sum_{n=1}^{N} (C_n^L + C_n^{NL})
\end{aligned} \tag{5.15}$$

where (a) follows from the definition of $f_R(r)$, which is the PDF of the distance between the typical user and its serving BS, given by

$$f_R(r)=\begin{cases} f_{R,1}(r)=\begin{cases} f_{R,1}^{\mathrm{L}}(r), & \text{with LOS connection} \\ f_{R,1}^{\mathrm{NL}}(r), & \text{with NLOS connection} \end{cases}, & 0\le r\le d_1 \\ f_{R,2}(r)=\begin{cases} f_{R,2}^{\mathrm{L}}(r), & \text{with LOS connection} \\ f_{R,2}^{\mathrm{NL}}(r), & \text{with NLOS connection} \end{cases}, & d_1<r\le d_2 \\ \vdots & \vdots \\ f_{R,N}(r)=\begin{cases} f_{R,N}^{\mathrm{L}}(r), & \text{with LOS connection} \\ f_{R,N}^{\mathrm{NL}}(r), & \text{with NLOS connection} \end{cases}, & r>d_{N-1} \end{cases} \tag{5.16}$$

Obviously, $f_R(r)$ has a similar formalization as (5.1). Besides, we have $f_{R,n}(r)=f_{R,n}^{\mathrm{L}}(r)+f_{R,n}^{\mathrm{NL}}(r)$, because the two conditions that the typical user is connected to a LOS BS or a NLOS BS are disjoint events. □

As can be seen from Theorem 5.1,if we want to derive the coverage probability, the key point is to obtain functions $f_{R,n}^{\mathrm{L}}(r)$, $f_{R,n}^{\mathrm{NL}}(r)$, and the probability $\mathbb{P}\left[\frac{P_t\omega_n^{\mathrm{L}}(r)h}{\sigma^2+I_r}>T\right]$,$\mathbb{P}\left[\frac{P_t\omega_n^{\mathrm{NL}}(r)h}{\sigma^2+I_r}>T\right]$.

Hence, the results of them are presented in Lemma 1 and Lemma 2, respectively.

Lemma 1. *In Theorem 5.1, considering the smallest-path-loss user association strategy,* $f_{R,n}^{\mathrm{L}}(r)$ *and* $f_{R,n}^{\mathrm{NL}}(r)$ *are given by*

$$\begin{aligned} f_{R,n}^{\mathrm{L}}(r)=2\pi r\lambda_B\times \mathrm{Pr}_n^{\mathrm{L}}(r)\times\exp\left(-2\pi\lambda_B\int_0^r \mathrm{Pr}^{\mathrm{L}}(t)t\mathrm{d}t\right) \\ \times\exp\left(-2\pi\lambda_B\int_0^{r_1}\left(1-\mathrm{Pr}^{\mathrm{L}}(t)\right)t\mathrm{d}t\right) \end{aligned} \tag{5.17}$$

and

$$\begin{aligned} f_{R,n}^{\mathrm{NL}}(r)=2\pi r\lambda_B\times\left(1-\mathrm{Pr}_n^{\mathrm{L}}(r)\right)\times\exp\left(-2\pi\lambda_B\int_0^r\left(1-\mathrm{Pr}^{\mathrm{L}}(t)\right)t\mathrm{d}t\right) \\ \times\exp\left(-2\pi\lambda_B\int_0^{r_2}\mathrm{Pr}^{\mathrm{L}}(t)t\mathrm{d}t\right) \end{aligned} \tag{5.18}$$

respectively, where the variables r_1 and r_2 can be calculated by,

$$r_1 = \arg_{r_1} \left\{ \omega^{NL}(r_1) = \omega_n^L(r) \right\} \tag{5.19}$$

and

$$r_2 = \arg_{r_2} \left\{ \omega^{L}(r_2) = \omega_n^{NL}(r) \right\} \tag{5.20}$$

Proof. Firstly, we give a demonstration to $f_{R,n}^{\mathrm{L}}(r)$ as follows.

As mentioned before, $f_{R,n}^{\mathrm{L}}(r)$ is the n-th piece PDF of the variable of distance R_n^{L}, under the situation that the typical user is connected to the serving BS with a LOS path. Thus, under the smallest-path-loss UAS, the following two conditions should be satisfied,

1) Condition A1 : For the typical user, the serving BS is with a nearest LOS path.

2) Condition A2 : For the typical user, the serving BS goes through a smaller path loss than the nearest BS with a NLOS path.

In order to formulate the above two conditions, the distance between the typical user and the nearest BS with a LOS path is denoted as X^{L}. Then, for condition A1, no other BSs with the LOS paths can be closer than X^{L}. So,the cumulative distribution function (CDF) of X^{L} is formulated as

$$F_{X^{\mathrm{L}}}(x) = 1 - \exp\left(-\lambda_B \int_0^x \mathrm{Pr}^{\mathrm{L}}(t) 2\pi t \mathrm{d}t \right) \tag{5.21}$$

Therefore, the PDF of X^{L} can be found as

$$\begin{aligned} f_{X^{\mathrm{L}}}(x) &= \frac{\partial F_{X^{\mathrm{L}}}(x)}{\partial x} \\ &= 2\pi x \lambda_B \mathrm{Pr}^{\mathrm{L}}(x) \times \exp\left(-\lambda_B \int_0^x \mathrm{Pr}^{\mathrm{L}}(t) 2\pi t \mathrm{d}t \right) \end{aligned} \tag{5.22}$$

For condition A2, there should be no NLOS BS for the user within a circle with a radius $x_1 < x$, which has the smaller path loss than the nearest LOS BS at the distance $X^{\mathrm{L}} = x$. Moreover, $x_1 = \arg_{x_1} \left\{ \omega^{NL}(x_1) = \omega_n^L(x) \right\}$. So, the conditional probability of A2 can be derived as

$$\mathbb{P}[\mathrm{A2} | X^{\mathrm{L}} = x] = \exp\left(-\lambda_B \int_0^{x1} \left(1 - \mathrm{Pr}^{\mathrm{L}}(t) \right) 2\pi t \mathrm{d}t \right) \tag{5.23}$$

Next step calculates the PDF of R^{L}, which is the distance from the user to its designated BS. At first step, we derive the CCDF of R^{L} as

$$\begin{aligned} F_{R^{\mathrm{L}}}(r) &= \mathbb{E}_{X^{\mathrm{L}}}\left\{\mathbb{P}[R^{\mathrm{L}} > r | X^{\mathrm{L}}]\right\} \\ &= \int_0^{\infty} \mathbb{P}[R^{\mathrm{L}} > r | X^{\mathrm{L}} = x] f_{X^{\mathrm{L}}}(x)\mathrm{d}x \\ &\overset{(a)}{=} \int_0^{r} 0 \times f_{X^{\mathrm{L}}}(x)\mathrm{d}x + \int_r^{\infty} \mathbb{P}[A2 | X^{\mathrm{L}} = x] f_{X^{\mathrm{L}}}(x)\mathrm{d}x \\ &= \int_r^{\infty} \mathbb{P}[A2 | X^{\mathrm{L}} = x] f_{X^{\mathrm{L}}}(x)\mathrm{d}x \end{aligned} \tag{5.24}$$

where the step (a) is according to that, when $0 < x \leq r$, then $\mathbb{P}[R^{\mathrm{L}} > r | X^{\mathrm{L}} = x] = 0$; and when $x > r$, then $\mathbb{P}[R^{\mathrm{L}} > r | X^{\mathrm{L}} = x] = \mathbb{P}[A2 | X^{\mathrm{L}} = x]$.

Therefore, the PDF of R^{L} is formulated as

$$f_{R^{\mathrm{L}}}(r) = \mathbb{P}[A2 | X^{\mathrm{L}} = r] f_{X^{\mathrm{L}}}(r) \tag{5.25}$$

For the n-th piece $d_{n-1} < x \leq d_n$, we can have

$$\begin{aligned} f_{R,n}^{\mathrm{L}}(r) = 2\pi r \lambda_B \times \mathrm{Pr}_n^{\mathrm{L}}(r) \times \exp\left(-2\pi\lambda_B \int_0^{r} \mathrm{Pr}^{\mathrm{L}}(t) t \mathrm{d}t\right) \\ \times \exp\left(-2\pi\lambda_B \int_0^{r_1} \left(1 - \mathrm{Pr}^{\mathrm{L}}(t)\right) t \mathrm{d}t\right) \end{aligned} \tag{5.26}$$

Similarly, $f_{R,n}^{\mathrm{NL}}(r)$ can also be derived. So the proof is omitted here. □

Lemma 2. *In Theorem 5.1,* $\mathbb{P}\left[\frac{P_t \omega_n^{\mathrm{L}}(r) h}{\sigma^2 + I_r} > T\right]$ *and* $\mathbb{P}\left[\frac{P_t \omega_n^{\mathrm{NL}}(r) h}{\sigma^2 + I_r} > T\right]$ *are given by*

$$\mathbb{P}\left[\frac{P_t \omega_n^{\mathrm{L}}(r) h}{\sigma^2 + I_r} > T\right] = \exp\left(-\frac{T\sigma^2}{P_t \omega_n^{\mathrm{L}}(r)}\right) \times \mathscr{L}_{I_r}^{\mathrm{L}}\left(\frac{T}{P_t \omega_n^{\mathrm{L}}(r)}\right) \tag{5.27}$$

and

$$\mathbb{P}\left[\frac{P_t \omega_n^{\mathrm{NL}}(r) h}{\sigma^2 + I_r} > T\right] = \exp\left(-\frac{T\sigma^2}{P_t \omega_n^{\mathrm{NL}}(r)}\right) \times \mathscr{L}_{I_r}^{\mathrm{NL}}\left(\frac{T}{P_t \omega_n^{\mathrm{NL}}(r)}\right) \tag{5.28}$$

respectively. Herein, $\mathscr{L}_{I_r}^{\mathrm{L}}(s)$ and $\mathscr{L}_{I_r}^{\mathrm{NL}}$ denote the Laplace transform of I_r for the LOS and NLOS propagation, respectively. They can be computed by the following equations,

$$\begin{aligned}\mathscr{L}_{I_r}^{\mathrm{L}}(s) = \exp\left(-2\pi\lambda_B \int_r^{\infty} \frac{\mathrm{Pr}^{\mathrm{L}}(t)t}{1+(sP_t\omega^{\mathrm{L}}(t))^{-1}}\mathrm{d}t\right) \\ \times \exp\left(-2\pi\lambda_B \int_{r1}^{\infty} \frac{[1-\mathrm{Pr}^{\mathrm{L}}(t)]t}{1+(sP_t\omega^{\mathrm{NL}}(t))^{-1}}\mathrm{d}t\right)\end{aligned} \tag{5.29}$$

$$\begin{aligned}\mathscr{L}_{I_r}^{\mathrm{NL}}(s) = \exp\left(-2\pi\lambda_B \int_{r_2}^{\infty} \frac{\mathrm{Pr}^{\mathrm{L}}(t)t}{1+(sP_t\omega^{\mathrm{L}}(t))^{-1}}\mathrm{d}t\right) \\ \times \exp\left(-2\pi\lambda_B \int_{r}^{\infty} \frac{[1-\mathrm{Pr}^{\mathrm{L}}(t)]t}{1+(sP_t\omega^{\mathrm{NL}}(t))^{-1}}\mathrm{d}t\right)\end{aligned} \tag{5.30}$$

Proof.

$$\begin{aligned}\mathbb{P}\left[\frac{P_t\omega_n^{\mathrm{L}}(r)h}{\sigma^2+I_r} > T\right] &= \mathbb{E}_{I_r}\left\{\mathbb{P}\left[h > \frac{T(\sigma^2+I_r)}{P_t\omega_n^{\mathrm{L}}(r)}\right]\right\} \\ &\overset{(a)}{=} \mathbb{E}_{I_r}\left\{\exp\left(-\frac{T(\sigma^2+I_r)}{P_t\omega_n^{\mathrm{L}}(r)}\right)\right\} \\ &= \exp\left(-\frac{T\sigma^2}{P_t\omega_n^{\mathrm{L}}(r)}\right)\mathbb{E}_{I_r}\left\{\exp\left(-\frac{TI_r}{P_t\omega_n^{\mathrm{L}}(r)}\right)\right\} \\ &= \exp\left(-\frac{T\sigma^2}{P_t\omega_n^{\mathrm{L}}(r)}\right)\mathscr{L}_{I_r}^{\mathrm{L}}\left(\frac{T}{P_t\omega_n^{\mathrm{L}}(r)}\right)\end{aligned} \tag{5.31}$$

where the step (a) is obtained by the assumption of fading h, presented as $h \sim \exp(1)$.

In addition, based on the smallest-path-loss user association strategy, $\mathscr{L}_{I_r}^{\mathrm{L}}(s)$ is derived as

$$\begin{aligned}\mathscr{L}_{I_r}^{\mathrm{L}}(s) &= \mathbb{E}_{I_r}\left\{\exp(-sI_r)|\text{ LOS connection for the typical user}\right\} \\ &= \mathbb{E}_{[\Phi_B,\varphi_i,g_i]}\left\{\exp\left(-s\sum_{i:\, b_i\in\Phi_B\setminus b_0} P_t\varphi_i g_i\right)\right\} \\ &\overset{(b)}{=} \exp\left(-2\pi\lambda_B\int_r^{\infty}\mathrm{Pr}^{\mathrm{L}}(t)\times\left[1-\mathbb{E}_g[\exp(-sP_t\omega^{\mathrm{L}}(t)g)]\right]t\mathrm{d}t\right) \\ &\quad\times\exp\left(-2\pi\lambda_B\int_{r_1}^{\infty}\left[1-\mathrm{Pr}^{\mathrm{L}}(t)\right]\times\left[1-\mathbb{E}_g[\exp(-sP_t\omega^{\mathrm{NL}}(t)g)]\right]t\mathrm{d}t\right) \\ &\overset{(c)}{=} \exp\left(-2\pi\lambda_B\int_r^{\infty}\frac{\mathrm{Pr}^{\mathrm{L}}(t)t}{1+(sP_t\omega^{\mathrm{L}}(t))^{-1}}\mathrm{d}t\right) \\ &\quad\times\exp\left(-2\pi\lambda_B\int_{r1}^{\infty}\frac{[1-\mathrm{Pr}^{\mathrm{L}}(t)]t}{1+(sP_t\omega^{\mathrm{NL}}(t))^{-1}}\mathrm{d}t\right)\end{aligned} \tag{5.32}$$

where the step (b) is obtained from the PGFL. The step (c) is calculated from $g \sim \exp(1)$.

Note that the former exponential function represents the aggregate interference from the LOS paths, and the latter represents the aggregate interference from the NLOS paths.

Similarly, $\mathbb{P}\left[\frac{P_t \omega_n^{\mathrm{NL}}(r)h}{\sigma^2+I_r} > T\right]$ and $\mathscr{L}_{I_r}^{\mathrm{NL}}(s)$ can also be derived. The proof of them is omitted here. □

From Theorem 5.1, Lemma 1 and Lemma 2, it is observed that the coverage probability $p_c(\lambda_B, T)$ is determined by the three important functions: piece-wise LOS and NLOS path loss function $\omega_N^{\mathrm{L}}(r)$ and $\omega_N^{\mathrm{NL}}(r)$, as well as the piece-wise LOS probability function $\mathrm{Pr}_n^{\mathrm{L}}(r)$. Therefore, next section will numerically evaluate their impacts on the indoor dense SC network.

Corollary 5.1. *For computing the SE, the simple step is to substitute (5.12) into (5.8), and then get the result using (5.7). Similarly, for computing the ASE, we can substitute the result obtained from (5.7) into (5.9).*

Note that, the SE and the ASE are affected differently by the density of BSs, which will be shown in the next section as well.

5.3.2 Special Case and Main Results

As previously mentioned, in this subsection, the two-piece linear LOS probability function shown as in(5.4) is applied as a special case for Theorem 5.1. That is explained as the followed for doing that : (1) using the linear LOS probability function can lead to more tractable and analytical results for the system model with LOS and NLOS transmission; (2) using the linear LOS probability function can easily approximate the practical but more complex LOS probability function, e.g. (5.5).

Owing to the current cellular frequency band lower than 6GHz, the path loss exponent α^{NL} for LOS path is assumed to be same for all segments of path loss model. The variable α^{NL} is in a similar way.

According to Theorem 5.1, the coverage probability (5.6) is provided by

$$p_c(\lambda_B, T) = \sum_{n=1}^{2} (C_n^L + C_n^{NL}) \tag{5.33}$$

where C_1^L, C_1^{NL}, C_2^L and C_2^{NL} are derived in the following parts.

A. The derivation of C_1^L

Based on (5.13) and (5.27), C_1^L can be computed by

$$\begin{aligned} C_1^L &= \int_0^{L_1} \mathbb{P}\left[\frac{P_t \omega_1^{\mathrm{L}}(r) h}{\sigma^2 + I_r} > T\right] f_{R,1}^{\mathrm{L}}(r)\mathrm{d}r \\ &= \int_0^{L_1} \exp\left(-\frac{T\sigma^2}{P_t \omega_1^{\mathrm{L}}(r)}\right) \times \mathscr{L}_{I_r}^{\mathrm{L}}\left(\frac{T}{P_t \omega_1^{\mathrm{L}}(r)}\right) f_{R,1}^{\mathrm{L}}(r)\mathrm{d}r \\ &= \int_0^{L_1} \exp\left(-\frac{T\sigma^2 r^{\alpha^{\mathrm{L}}}}{P_t K^{\mathrm{L}}}\right) \times \mathscr{L}_{I_r}^{\mathrm{L}}\left(\frac{T r^{\alpha^{\mathrm{L}}}}{P_t K^{\mathrm{L}}}\right) f_{R,1}^{\mathrm{L}}(r)\mathrm{d}r \end{aligned} \tag{5.34}$$

Intuitively, in order to compute C_1^L, the variables $f_{R,1}^{\mathrm{L}}(r)$ and $\mathscr{L}_{I_r}^{\mathrm{L}}(s)$ should be obtained firstly. From lemma 1 and (5.17),

$$\begin{aligned} f_{R,1}^{\mathrm{L}}(r) &= 2\pi r \lambda_B \times (1 - \frac{r}{L_1}) \times \exp\left(-2\pi\lambda_B \int_0^r (1 - \frac{t}{L_1}) t \mathrm{d}t\right) \\ &\quad \times \exp\left(-2\pi\lambda_B \int_0^{r_1} \frac{t}{L_1} t \mathrm{d}t\right) \\ &= 2\pi r \lambda_B \times (1 - \frac{r}{L_1}) \times \exp\left(-\pi\lambda_B r^2 + \frac{2\pi\lambda_B}{3L_1}(r^3 - r_1^3)\right) \end{aligned} \tag{5.35}$$

when $0 < r \leq L_1$. Moreover, according to (5.19), the variable r_1 is

$$r_1 = \left(\frac{K^{\mathrm{NL}}}{K^{\mathrm{L}}}\right)^{\frac{1}{\alpha^{\mathrm{NL}}}} r^{\frac{\alpha^{\mathrm{L}}}{\alpha^{\mathrm{NL}}}} \tag{5.36}$$

According to lemma 2 and (5.29), the Laplace transform of the aggregate interference for the LOS transmission is represented as

$$\begin{aligned}\mathscr{L}_{I_r}^{\mathrm{L}}(s) = &\exp\left(-2\pi\lambda_B \int_r^{L_1}\left(1-\frac{t}{L_1}\right)\times\frac{t}{1+(sP_tK^{\mathrm{L}}t^{-\alpha^{\mathrm{L}}})^{-1}}\mathrm{d}t\right)\\ &\times\exp\left(-2\pi\lambda_B \int_{r_1}^{L_1}\left(\frac{t}{L_1}\right)\times\frac{t}{1+(sP_tK^{\mathrm{NL}}t^{-\alpha^{\mathrm{NL}}})^{-1}}\mathrm{d}t\right)\\ &\times\exp\left(-2\pi\lambda_B \int_{L_1}^{\infty}1\times\frac{t}{1+(sP_tK^{\mathrm{NL}}t^{-\alpha^{\mathrm{NL}}})^{-1}}\mathrm{d}t\right)\end{aligned} \tag{5.37}$$

Note that, due to $0 < r \leq L_1$, the aggregate interference comes from both LOS and NLOS paths. Seen from the above equation (5.37), the first item denotes the aggregate interference from LOS paths, but the second and third items are the aggregate interference from NLOS paths.

Finally, substituting (5.35) and (5.37) into (5.34), the detailed expression of C_1^L can be obtained.

B. The derivation of C_1^{NL}

Based on (5.14) and (5.28), C_1^{NL} is computed by

$$\begin{aligned}C_1^{NL} &= \int_0^{L_1}\mathbb{P}\left[\frac{P_t\omega_1^{\mathrm{NL}}(r)h}{\sigma^2+I_r} > T\right] f_{R,1}^{\mathrm{NL}}(r)\mathrm{d}r\\ &= \int_0^{L_1}\exp\left(-\frac{T\sigma^2}{P_t\omega_1^{\mathrm{NL}}(r)}\right)\times\mathscr{L}_{I_r}^{\mathrm{NL}}\left(\frac{T}{P_t\omega_1^{\mathrm{NL}}(r)}\right) f_{R,1}^{\mathrm{NL}}(r)\mathrm{d}r\\ &= \int_0^{L_1}\exp\left(-\frac{T\sigma^2 r^{\alpha^{\mathrm{NL}}}}{P_tK^{\mathrm{NL}}}\right)\times\mathscr{L}_{I_r}^{\mathrm{NL}}\left(\frac{Tr^{\alpha^{\mathrm{NL}}}}{P_tK^{\mathrm{NL}}}\right) f_{R,1}^{\mathrm{NL}}(r)\mathrm{d}r\end{aligned} \tag{5.38}$$

Intuitively, in order to compute C_1^{NL}, the variables $f_{R,1}^{\mathrm{NL}}(r)$ and $\mathscr{L}_{I_r}^{\mathrm{NL}}(s)$ should be obtained firstly. From Lemma 1 and (5.18),

$$\begin{aligned}f_{R,1}^{\mathrm{NL}}(r) = &2\pi r\lambda_B\times(\frac{r}{L_1})\times\exp\left(-2\pi\lambda_B\int_0^{r}(\frac{t}{L_1})t\mathrm{d}t\right)\\ &\times\exp\left(-2\pi\lambda_B\int_0^{r_2}(1-\frac{t}{L_1})t\mathrm{d}t\right),\end{aligned} \tag{5.39}$$

for $0 < r \leq L_1$. Moreover, according to (5.20), the variable r_2 is

$$r_2 = \left(\frac{K^{\mathrm{L}}}{K^{\mathrm{NL}}}\right)^{\frac{1}{\alpha^{\mathrm{L}}}} r^{\frac{\alpha^{\mathrm{NL}}}{\alpha^{\mathrm{L}}}} \tag{5.40}$$

Note that, different from only one condition $r_1 < L_1$ for computing $f_{R,1}^{\mathrm{L}}(r)$, there are two conditions for computing $f_{R,1}^{\mathrm{NL}}(r)$: $r_2 > L_1$ and $r_2 \leq L_1$.

Condition (1): When $0 < r_2 \leq L_1$, namely, $0 < r \leq u_1 = L_1^{\frac{\alpha^{\mathrm{L}}}{\alpha^{\mathrm{NL}}}} \left(\frac{K^{\mathrm{NL}}}{K^{\mathrm{L}}}\right)^{\frac{1}{\alpha^{\mathrm{L}}}}$, the expression of $f_{R,1}^{\mathrm{NL}}(r)$ is derived as

$$\begin{aligned} f_{R,1}^{\mathrm{NL}}(r) &= 2\pi r\lambda_B \times (\frac{r}{L_1}) \times \exp\left(-2\pi\lambda_B \int_0^r (\frac{t}{L_1}) t \mathrm{d}t\right) \\ &\quad \times \exp\left(-2\pi\lambda_B \int_0^{r_2} (1 - \frac{t}{L_1}) t \mathrm{d}t\right) \\ &= 2\pi r\lambda_B \times (\frac{r}{L_1}) \times \exp\left(-\pi\lambda_B r_2^2 + \frac{2\pi\lambda_B}{3L_1}(r_2^3 - r^3)\right), \end{aligned} \tag{5.41}$$

when $0 < r \leq u_1$.

Condition(2): When $r_2 > L_1$, namely, the expression of $u_1 < r \leq L_1$, $f_{R,1}^{\mathrm{NL}}(r)$ is

$$\begin{aligned} f_{R,1}^{\mathrm{NL}}(r) &= 2\pi r\lambda_B \times (\frac{r}{L_1}) \times \exp\left(-2\pi\lambda_B \int_0^r (\frac{t}{L_1}) t \mathrm{d}t\right) \\ &\quad \times \exp\left(-2\pi\lambda_B \int_0^{L_1} (1 - \frac{t}{L_1}) t \mathrm{d}t\right) \\ &= 2\pi r\lambda_B \times (\frac{r}{L_1}) \times \exp\left(-\pi\lambda_B \left(\frac{L_1^2}{3} + \frac{2r^3}{3L_1}\right)\right) \end{aligned} \tag{5.42}$$

when $u_1 < r \leq L_1$.

Correspondingly, there are two different expressions of the aggregate interference for the above two conditions.

Condition (1): when $0 < r \leq u_1$, according to lemma 2 and (5.30), the Laplace transform of the aggregate interference for the NLOS transmission is expressed as

$$\begin{aligned}\mathscr{L}_{I_r}^{\mathrm{NL}}(s) = &\exp\left(-2\pi\lambda_B \int_{r_2}^{L_1}\left(1-\frac{t}{L_1}\right)\times\frac{t}{1+(sP_tK^{\mathrm{L}}t^{-\alpha^{\mathrm{L}}})^{-1}}\mathrm{d}t\right)\\ &\times\exp\left(-2\pi\lambda_B \int_{r}^{L_1}\left(\frac{t}{L_1}\right)\times\frac{t}{1+(sP_tK^{\mathrm{NL}}t^{-\alpha^{\mathrm{NL}}})^{-1}}\mathrm{d}t\right)\\ &\times\exp\left(-2\pi\lambda_B \int_{L_1}^{\infty}1\times\frac{t}{1+(sP_tK^{\mathrm{NL}}t^{-\alpha^{\mathrm{NL}}})^{-1}}\mathrm{d}t\right)\end{aligned} \tag{5.43}$$

when $0 < r \leq u_1$.

Condition (2): when $u_1 < r \leq L_1$, according to lemma 2 and (5.30), the Laplace transform of the aggregate interference for the NLOS transmission is represented as

$$\begin{aligned}\mathscr{L}_{I_r}^{\mathrm{NL}}(s) = &\exp\left(-2\pi\lambda_B \int_{r}^{L_1}\left(\frac{t}{L_1}\right)\times\frac{t}{1+(sP_tK^{\mathrm{NL}}t^{-\alpha^{\mathrm{NL}}})^{-1}}\mathrm{d}t\right)\\ &\times\exp\left(-2\pi\lambda_B \int_{L_1}^{\infty}1\times\frac{t}{1+(sP_tK^{\mathrm{NL}}t^{-\alpha^{\mathrm{NL}}})^{-1}}\mathrm{d}t\right)\end{aligned} \tag{5.44}$$

when $u_1 < r \leq L_1$.

Note that, the aggregate interference in condition (1) comes from both LOS and NLOS paths. However, the aggregate interference in condition (2) comes from NLOS paths only.

Finally, C_1^{NL} is computed as

$$\begin{aligned}C_1^{NL} = &\int_0^{u_1}\exp\left(-\frac{T\sigma^2 r^{\alpha^{\mathrm{NL}}}}{P_tK^{\mathrm{NL}}}\right)\times\left(\mathscr{L}_{I_r}^{\mathrm{NL}}\left(\frac{Tr^{\alpha^{\mathrm{NL}}}}{P_tK^{\mathrm{NL}}}\right)f_{R,1}^{\mathrm{NL}}(r)\middle|0<r\leq u_1\right)\mathrm{d}r\\ &+\int_{u_1}^{L_1}\exp\left(-\frac{T\sigma^2 r^{\alpha^{\mathrm{NL}}}}{P_tK^{\mathrm{NL}}}\right)\times\left(\mathscr{L}_{I_r}^{\mathrm{NL}}\left(\frac{Tr^{\alpha^{\mathrm{NL}}}}{P_tK^{\mathrm{NL}}}\right)f_{R,1}^{\mathrm{NL}}(r)\middle|u_1<r\leq L_1\right)\mathrm{d}r\end{aligned} \tag{5.45}$$

where (5.41), (5.42), (5.43) and (5.44) are substituted into (5.45).

C. The derivation of C_2^L

Based on (5.13) and (5.27), C_2^L can be obtained by

$$\begin{aligned} C_2^L &= \int_{L_1}^{\infty} \mathbb{P}\left[\frac{P_t \omega_2^{\mathrm{L}}(r) h}{\sigma^2 + I_r} > T\right] f_{R,2}^{\mathrm{L}}(r)\mathrm{d}r \\ &= \int_{L_1}^{\infty} \exp\left(-\frac{T\sigma^2}{P_t \omega_2^{\mathrm{L}}(r)}\right) \times \mathscr{L}_{I_r}^{\mathrm{L}}\left(\frac{T}{P_t \omega_2^{\mathrm{L}}(r)}\right) f_{R,2}^{\mathrm{L}}(r)\mathrm{d}r \\ &= \int_{L_1}^{\infty} \exp\left(-\frac{T\sigma^2 r^{\alpha^{\mathrm{L}}}}{P_t K^{\mathrm{L}}}\right) \times \mathscr{L}_{I_r}^{\mathrm{L}}\left(\frac{T r^{\alpha^{\mathrm{L}}}}{P_t K^{\mathrm{L}}}\right) f_{R,2}^{\mathrm{L}}(r)\mathrm{d}r \end{aligned} \tag{5.46}$$

Intuitively, in order to compute C_2^L, the expressions of $f_{R,2}^{\mathrm{L}}(r)$ and $\mathscr{L}_{I_r}^{\mathrm{L}}(s)$ should be obtained firstly. From Lemma 1 and (5.17),

$$\begin{aligned} f_{R,1}^{\mathrm{L}}(r) &= 2\pi r \lambda_B \times 0 \times \exp\left(-2\pi\lambda_B \int_0^r \Pr^{\mathrm{L}}(t) t \mathrm{d}t\right) \\ &\quad \times \exp\left(-2\pi\lambda_B \int_0^{r_1} \left(1 - \Pr^{\mathrm{L}}(t)\right) t \mathrm{d}t\right) \\ &= 0 \end{aligned} \tag{5.47}$$

Therefore, we have $C_2^L = 0$.

D. The derivation of C_2^{NL}

Based on (5.14) and (5.28), C_2^{NL} can be computed by

$$\begin{aligned} C_2^{NL} &= \int_{L_1}^{\infty} \mathbb{P}\left[\frac{P_t \omega_2^{\mathrm{NL}}(r) h}{\sigma^2 + I_r} > T\right] f_{R,2}^{\mathrm{NL}}(r)\mathrm{d}r \\ &= \int_{L_1}^{\infty} \exp\left(-\frac{T\sigma^2}{P_t \omega_2^{\mathrm{NL}}(r)}\right) \times \mathscr{L}_{I_r}^{\mathrm{NL}}\left(\frac{T}{P_t \omega_2^{\mathrm{NL}}(r)}\right) f_{R,2}^{\mathrm{NL}}(r)\mathrm{d}r \\ &= \int_{L_1}^{\infty} \exp\left(-\frac{T\sigma^2 r^{\alpha^{\mathrm{NL}}}}{P_t K^{\mathrm{NL}}}\right) \times \mathscr{L}_{I_r}^{\mathrm{NL}}\left(\frac{T r^{\alpha^{\mathrm{NL}}}}{P_t K^{\mathrm{NL}}}\right) f_{R,2}^{\mathrm{NL}}(r)\mathrm{d}r \end{aligned} \tag{5.48}$$

The functions of $f_{R,2}^{\mathrm{NL}}(r)$ and $\mathscr{L}_{I_r}^{\mathrm{NL}}(s)$ are calculated firstly. From lemma 1 and (5.18),

$$\begin{aligned} f_{R,2}^{\mathrm{NL}}(r) &= 2\pi r\lambda_B \times \exp\left(-2\pi\lambda_B\left(\int_0^{L_1}(\frac{t}{L_1})t\mathrm{d}t + \int_{L_1}^{r} t\mathrm{d}t\right)\right) \\ &\quad \times \exp\left(-2\pi\lambda_B\int_0^{L_1}(1-\frac{t}{L_1})t\mathrm{d}t\right) \\ &= \exp(-\pi\lambda_B r^2)2\pi\lambda_B r \end{aligned} \tag{5.49}$$

when $r > L_1$.

Through lemma 2 and (5.30), the Laplace transform of the aggregate interference for NLOS transmissions is calculated as

$$\mathscr{L}_{I_r}^{\mathrm{NL}}(s) = \exp\left(-2\pi\lambda_B\int_r^{\infty} 1 \times \frac{t}{1+(sP_tK^{\mathrm{NL}}t^{-\alpha^{\mathrm{NL}}})^{-1}}\mathrm{d}t\right) \tag{5.50}$$

when $r > L_1$.

Here, the aggregate interference only comes from NLOS paths.

Finally, substituting (5.49) and (5.50) into (5.48), the detailed expression of C_2^{NL} can be obtained.

E. The main results of performance metrics

Based on (5.33) and the results from the subsections A-D, the coverage probability is given by

$$p_c(\lambda_B, T) = C_1^L + C_1^{NL} + C_2^{NL} \tag{5.51}$$

where C_1^L, C_1^{NL} and C_2^{NL} are shown as (5.34), (5.45) and (5.48), respectively.

Straightforwardly, according to Corollary 5.1, substitute the equation 5.51 into equations 5.7, 5.8 and 5.9 to derive the expressions of SE and ASE, respectively. Now, the analytical results of coverage probability, SE and ASE have been obtained for the special case considering a two-piece linear LOS probability model.

5.4 Numerical Results and Discussion

This section numerically evaluates the analytical results of performance metrics obtained in Section 5.3. Firstly, the approximated results of the LOS probability function (5.5) by the linear function (5.4) are presented. The validation of the approximation method is shown through numerical results and Monte Carlo simulations. Then, the impact of different LOS functions on performance metrics is illustrated. Moreover, the differences of the network performance are demonstrated based on two types of path loss model: the simplistic path loss model with single slope and the practical piece-wise path loss model with LOS/NLOS transmissions.

Unless otherwise stated, the following parameters are set for the channel model:

$\alpha_1^{\mathrm{L}} = \alpha_2^{\mathrm{L}} = 1.69, \alpha_1^{\mathrm{NL}} = \alpha_2^{\mathrm{NL}} = 4.33, K_1^{\mathrm{L}} = K_2^{\mathrm{L}} = 10^{-3.28}, K_1^{\mathrm{NL}} = K_2^{\mathrm{NL}} = 10^{-1.15}, P_t = 24dBm, \sigma^2 = -95dBm$, according to the indoor SC channel of 3GPP standard [104].

A. Validation of the approximated LOS probability functions

This subsection chooses the practical LOS probability function (5.5) for the performance analysis in the indoor SC network. Its related parameters are referred to Section 4.3 in Chapter 4. In order to match this practical model well by using the approximated method, L_1 is set to 8.4m so that (5.4) can intersect with (5.5) at the point with LOS probability 0.5 . The results are shown in Fig. 5.1. In addition, the approximated LOS probability functions with other different parameters of $L_1 = 48.4m$ and $L_1 = 88.4m$ are also shown in Fig.5.1, which are only for the subsequent researches, e.g. the influence of various propagation environments on the indoor dense SC network.

In order to demonstrate the validation of the approximated LOS probability model, we present the comparison between the Monte Carlo simulations of coverage probability based on (5.5) and the numerical results of coverage probability based on (5.4) with $L_1 = 8.4m$. The results are shown in Fig. 5.2. It is observed that the analytical results present a good match for the simulation results when the density of BS is large. In terms of the relatively small BS density, only very small gaps exist, which is caused by the approximation of the

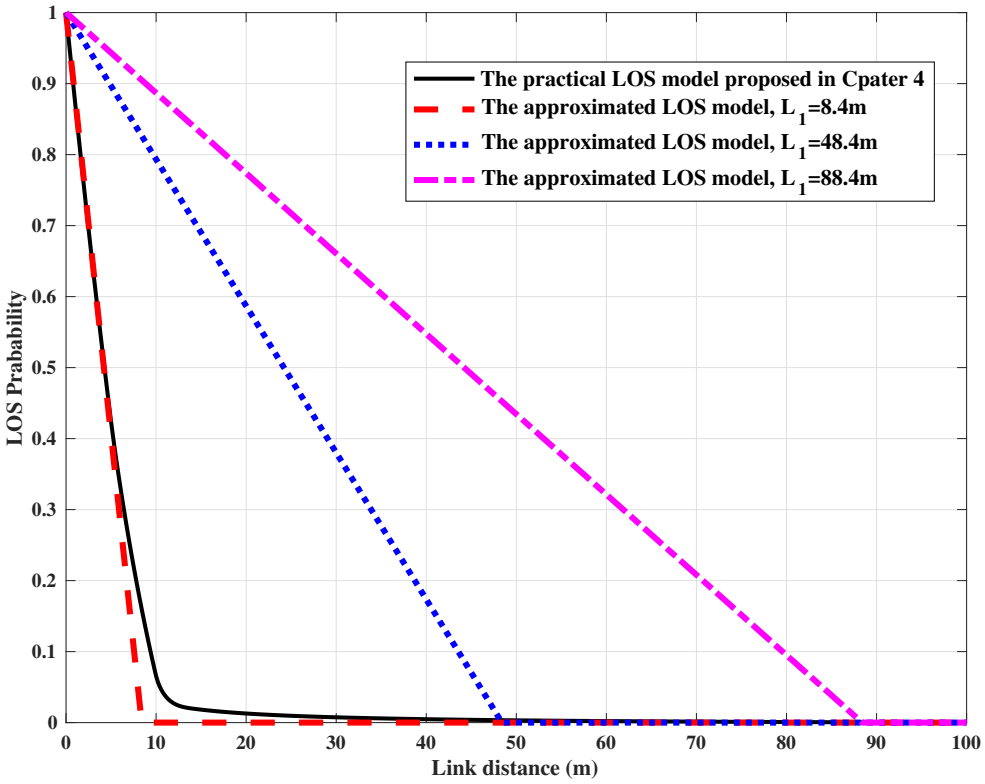

Fig. 5.1 The approximated LOS probability function vs. the practical LOS probability function

LOS probability. But its effects are trivial. Therefore, we will directly use numerical results of the approximated LOS model to analyse the indoor network performance later.

B. Discussion about three performance metrics

Now, we discuss the relationship between the BS density and the three critical performance metrics shown as in Section 5.2. Moreover, the effects of the different propagation environments, i.e., different LOS probability functions, on the network performance are also uncovered. In order to highlight the characteristics of the indoor dense network with LOS and NLOS transmission, the traditional single-slope path loss model is adopted [20]. Following the reference, its path loss exponent is set as $\alpha = \alpha^{\mathrm{NL}} = 4.33$.

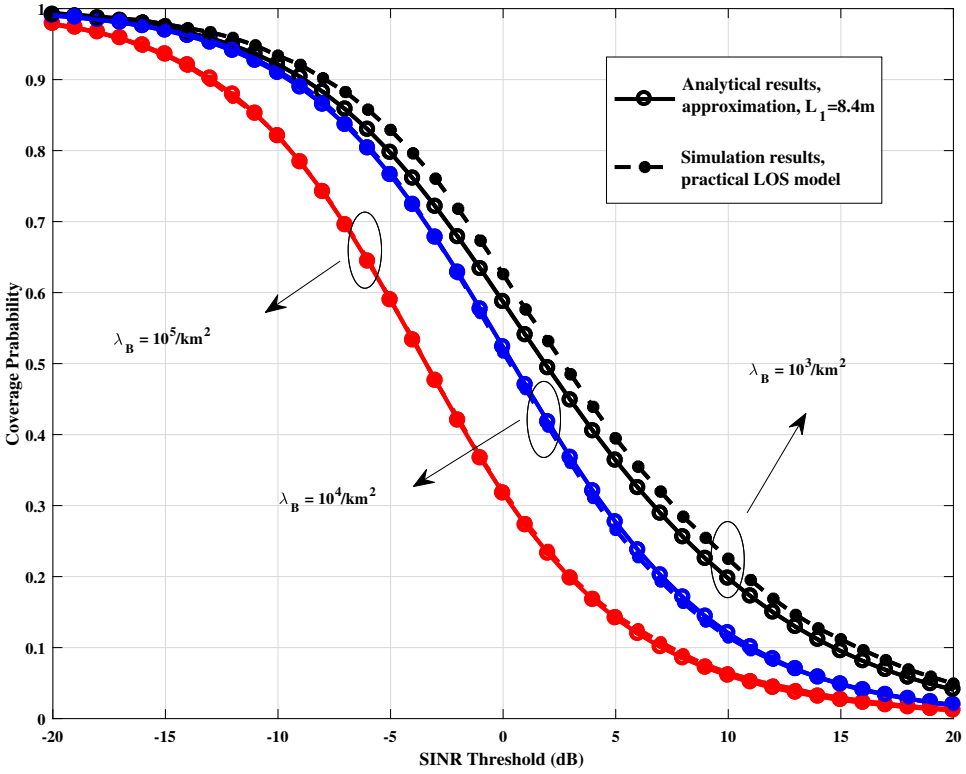

Fig. 5.2 The coverage probability vs. the SINR threshold

In Fig. 5.3, it's clearly seen that the significant differences exist between the coverage probability analysis of the proposed model in this chapter and the analysis of [20]. In the work [20], the coverage probability increases with the BS density λ_B firstly since the distance is being closer between the user and the designated BS. Then, the coverage probability keeps constant and becomes irrelevant of λ_B, when the BS density λ_B is large enough. This is because more interference is introduced by the dense network at the same time. However, for the analysis through the proposed model with $L_1 = 8.4m$, the coverage probability increases at first then reaches the peak value when λ_B is around $10^3 BSs/km^2$, while decreases after that. The reason for this trend is that with the denser deployment of BSs, the more NLOS transmissions between the interfering BSs and the typical users are transformed into LOS transmissions due to the closer transmission distance.

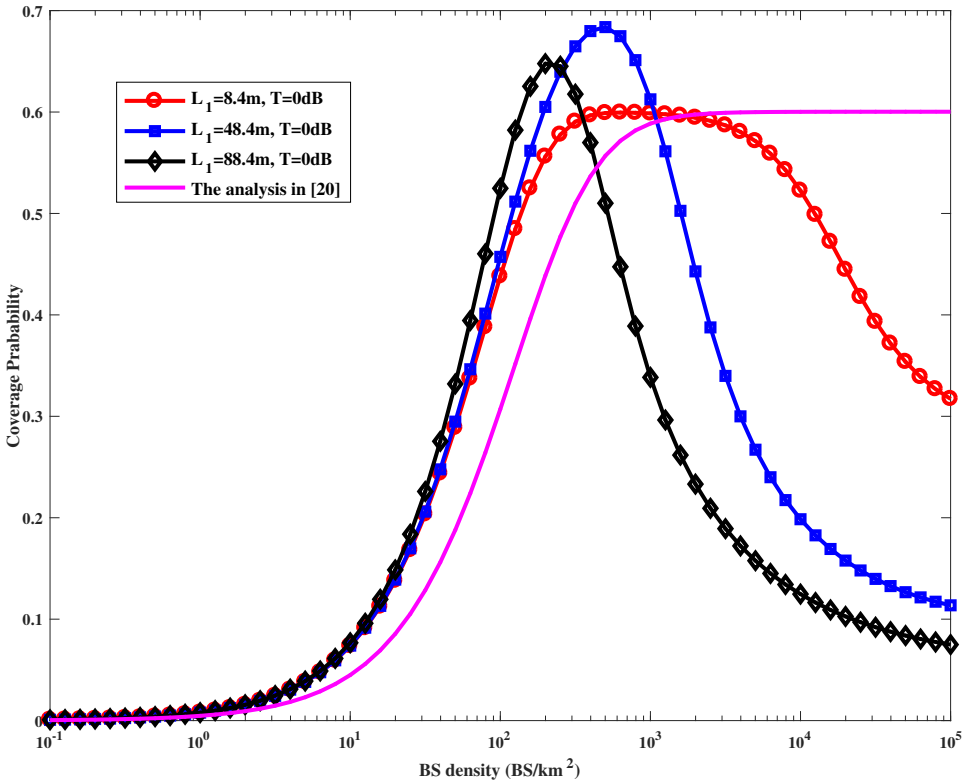

Fig. 5.3 The coverage probability vs. the BS density (the threshold of SINR T = 0 dB)

Meantime, Fig. 5.3 demonstrates the coverage probability performance is also affected by the LOS probability functions. It's clear that the peak value of the coverage probability becomes more sharp and moves towards left, with the parameter L_1 increasing (from 8.4m to 48.4m to 88.4m). It means that the optimal density of BSs density for the coverage probability is related to the parameter L_1, which decreases with the increase of L_1. It's reasonable because the propagation environment becomes sparser with the larger L_1, which leads to the faster transformation from NLOS to LOS.

In order to demonstrate the generality of the above conclusions, we also give the coverage probability performance analysis with the SINR threshold different from the Fig. 5.3. The conclusions obtained from Fig. 5.4 are similar to Fig. 5.3, although their values of the SINR threshold are different.

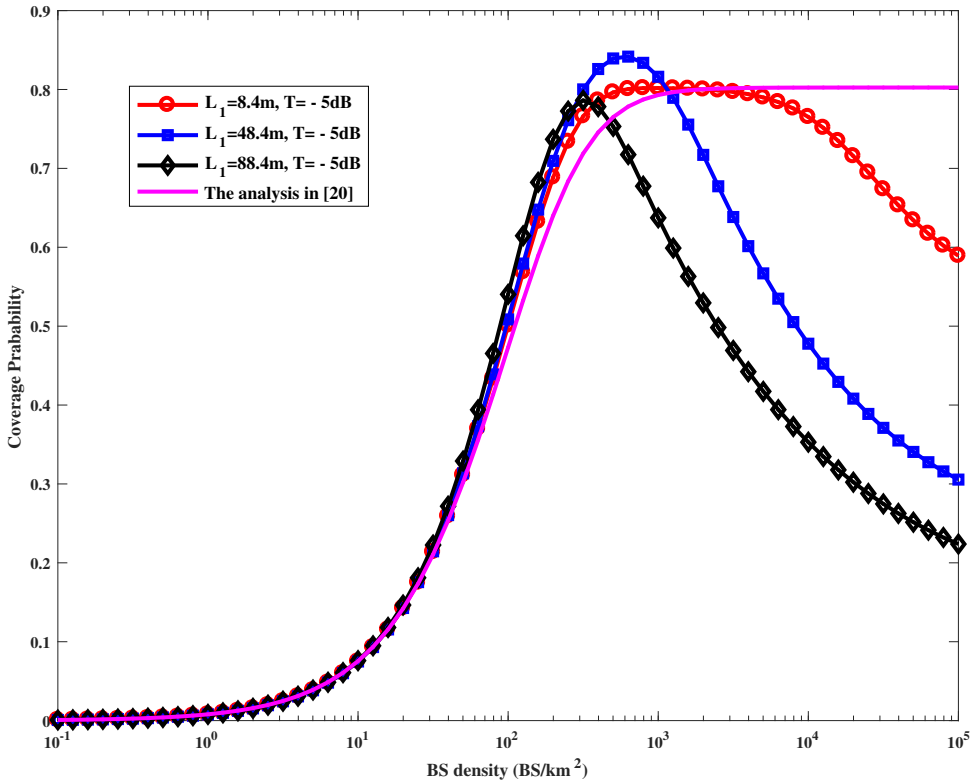

Fig. 5.4 The coverage probability vs. the BS density (the threshold of SINR T = -5 dB)

Fig. 5.5 shows the SE analysis with the BS density, which is similar to the trend of curves in Fig. 5.3. Because it is mainly decided by the coverage probability according to the equation (5.7).

Fig. 5.6 demonstrates the ASE performance analysis with the BS density. Compared with the SE, the ASE performance is more dependent on the BS density as shown in Fig. 5.6. Based on the analysis in [20], the ASE increases linearly with λ_B when the BSs are enough dense. It's reasonable because the coverage probability is constant and independent of λ_B under such ultra-dense transmission environments. However, in terms of the analysis with our proposed model, the ASE increases super-linearly with λ_B for the low-density indoor network, but increases sub-linearly with λ_B for the high-density indoor network. The reason is that the ASE is affected by both the SE and the densification of BSs.

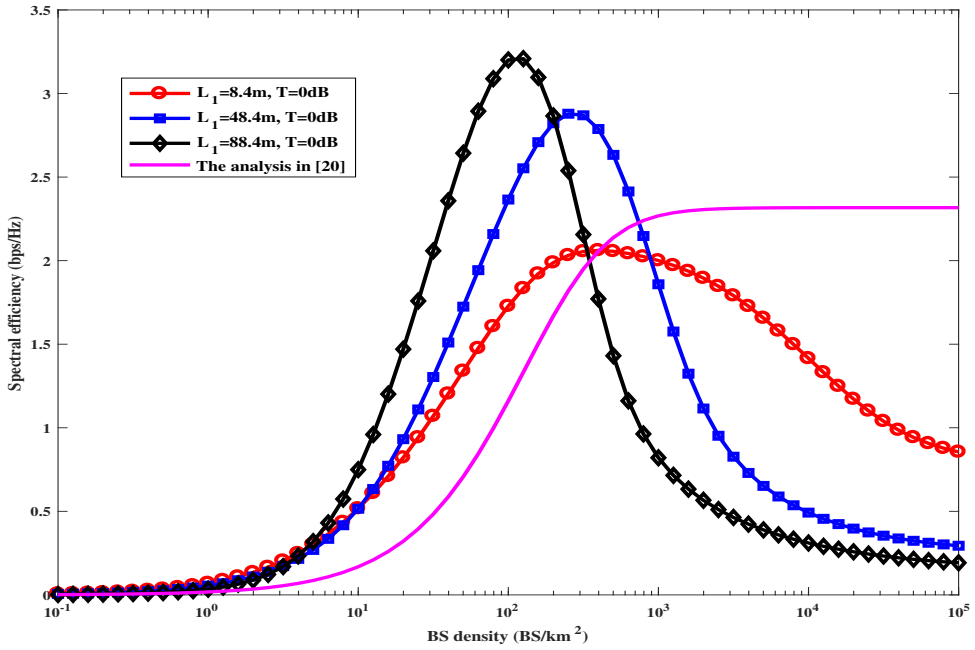

Fig. 5.5 The SE vs. the BS density (the threshold of SINR T = 0 dB)

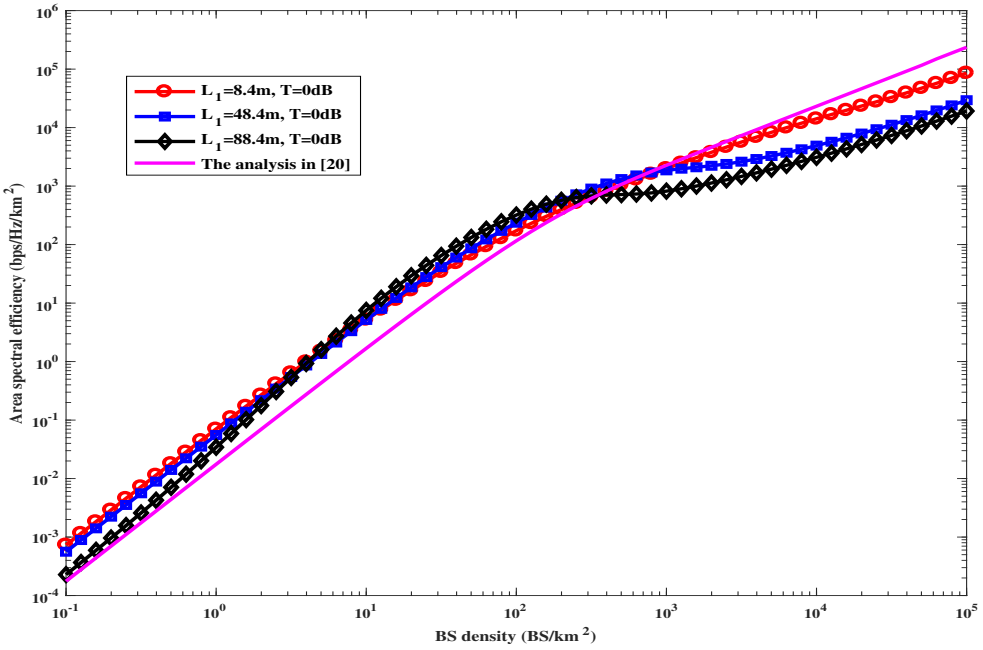

Fig. 5.6 The ASE vs. the BS density (the threshold of SINR T = 0 dB)

5.5 Conclusions

This chapter has developed a tractable path loss model by distinguishing between LOS and NLOS transmission from LOS and NLOS path and has proposed a novel LOS prob- ability function in indoor 3D scenarios. The path loss model and the LOS probability function are then utilized to analyse the performance metrics of indoor dense SC networks. On the basis of stochastic geometry, three performance metrics, including coverage probability, SE and ASE, are derived analytically. The analytical results are validated by comparing with Monte Carlo simulations. Simulations results reveal that the above performance metrics are affected by both the BS density and LOS probability function. Specifically, the influence of LOS and NLOS propagations is notable. As a consequence, the results obtained in this chapter provide insights on the design of future dense SC networks. For future work, more typical indoor scenarios, i.e., airport and stadium, will be discussed. The impact of different types of fading, such as Rician fading and the shadow fading introduced by the blockage of indoor walls, will also be in the consideration.

Chapter 6

Analysis of Indoor Wireless Communications by A Blockage Model

Overview

In indoor environments, the performance of ultra-dense cellular networks is significantly affected by blockages, especially for ultra-high frequencies. However, previous works either ignore or simplify such effects for analysing the networks. On the basis of stochastic geometry, this chapter proposes a mathematically tractable approach to analyse ultra-dense networks in indoors, which considers both the effects of wall blockages and the distance-based path loss. The effect of wall blockages is firstly investigated by modelling the walls as a Boolean scheme of straight lines on a finite plane. Then a path loss model incorporating both the distance-based and blockage-based path loss is applied to derive the performance expressions of indoor wireless networks. Finally, analytical results are validated by comparing it with Monte Carlo simulations. Moreover, simulation results reveal the optimal transmitter density is finite for indoor ultra-dense networks with blockages, although the coverage probability benefits from the increase of transmitter density.

6.1 Introduction

This not only limits its general applicability but also ignores the specific characteristics of scenarios, including the various lengths and densities of interior walls [36]. Secondly, the distance dependency of wall-blockage effects is not captured by the measurement based approach. Indeed, the longer link length is likely blocked by more interior wall blockages, resulting in severer shadowing fading experienced by the indoor transmission [18]. Recently, the concepts and tools from random shape theory have been utilized to generate blockage models without the need of environmental specific data [35]. As a branch of stochastic geometry, random shape theory models the blockages in wireless cellular networks as random processes. [98, 99]. In [18], the authors investigated the effects of outdoor blockages by further modelling the buildings as a random project process. The buildings were assumed as rectangles with random positions and orientations. Although it established a theory to model blockages aiming for the accurate performance estimation of networks, it was developed for urban outdoor environments only. Additionally, the assumption of random blockage orientations sacrifices the characteristics of realistic layout of interior wall blockages, which are usually vertical (e.g., ceilings and floors) and horizontal in reality. Hence, the blockage model proposed in [18] is not particularly suitable for analysing indoor wireless communications.

Furthermore, in [36, 37, 39], the authors extended the stochastic outdoor blockage model to indoor environments. The authors in [36, 37] established the indoor wall blockage model by randomly generating the walls as straight lines in a plane, of which the orientations of wall blockages are assumed in the horizontal or vertical direction in a 2D plane. However, the authors only applied the proposed model on networks with a specific arrangement of transmitters, in which there are four transmitters located at the four corners of the considered rectangular indoor scenario, respectively. This is a very limited utilization for indoor SC networks. The work in [39] presented a wall blockage model based on Poisson line process, through which a building was randomly divided into rectangular rooms. Although the authors investigated the general application of their wall blockage model on the analysis of indoor networks, they ignored the effects of distance-dependent path loss. This may result in an inaccurate estimation of network performance.

we present a novel approach to accurately model the aggregated interference in indoor dense SC networks and analyse indoor network performance by considering both the effects of wall blockages and distance-dependent path loss. Firstly, by using tools from random shape theory, we model the interior wall blockages as straight lines whose centers form a PPP. In terms of the wall orientation, a 2D coordinate system is defined with the vertical and horizontal axis in this work. By taking realistic layouts of interior walls into account, the wall orientation is assumed to be facing the horizontal or vertical axis with an equal probability. Based on the proposed interior wall blockage model, the distribution of penetration loss caused by walls on a link is derived. Then, a path loss model incorporating both the blockage-based and distance-dependent path loss is established. Finally, the composite path loss model is applied to investigate the coverage probability of a typical user in indoor dense SC networks. The results indicate that there exits an optimal SC-BS density for maximizing the coverage probability of the typical user, and this optimal SC-BS density is dependent on the interior blockage density.

This chapter is organised as follows. In Section 5.2, the system model is firstly illustrated. Then, the blockage model is presented in Section 5.3. Then the wall blockage model is presented and its analytical tractability is demonstrated, and the coverage probability for the indoor scenario with impenetrable blockages is also derived in Section 5.4. The simulation and numerical results are presented to validate our proposed indoor blockage modelling approach and to analyse the coverage probability of indoor dense SC networks in Section 5.5. At last, the chapter is concluded in Section 5.6.

6.2 Downlink System Model

Firstly, the system model is introduced in detail for the performance analysis of indoor dense SC networks. The downlink communication is our focus for an indoor typical user. Assume the typical user is only served by indoor transmitters. Some key assumptions are presented as follows.

A. Transmitter and receiver

This chapter considers a random indoor cellular network, whose transmitters are arranged as the HPPP $\{\Phi_B\}$ with the density μ. In addition, the transmitters are assumed to be set with the fixed transmitter power P_T. The typical user is set at the central point of an indoor scenario. The transmission path between the transmitter $B_i, (i = 0, 1, 2, ...)$ and the typical user is the i-th link, denoted by OB_i.

B. Wall blockages

In this chapter, we employ a tractable Boolean scheme of straight lines to generate wall blockages within an indoor scenario. The length l of each wall is assumed to be an arbitrary distribution $f_L(l)$ with the average length $E[L]$. The centres of wall blockages form a PPP with λ. The orientation of each line is assumed to be a binary choice in $\left\{0, \frac{\pi}{2}\right\}$ with equal probability. The width is ignored here due to the width is much smaller compared with the wall length. Note that, we only consider single floor of an indoor scenario, hence the height of walls is not taken into account.

C. Path loss model

This chapter employs the path loss model incorporating the distance-based and blockage-based propagation loss. Moreover, Rayleigh fading is considered as the small-scale fading. The received power of i-th link is

$$P_i = \frac{P_T h_i S_i}{d_i^{\alpha}}, \tag{6.1}$$

where P_i is the useful signal power for the receiver of i-th link. P_T is assumed as a constant transmitted power for each transmitter. The variable h_i is power gain of Rayleigh fading, which accords with an exponential distribution with a unit mean, denoted as $h \sim \exp(1)$. The variable d_i^{α} is the path loss of i-th link. The variable α is the path loss exponent. S_i is the blockage-based path loss caused by wall blockages on the i-th link.

D. Coverage probability

For the indoor wireless networks, the coverage probability is an important metric for analysing network performance. In this chapter, it is defined as the probability that the received SIR at typical user is stronger than the SIR threshold T. The SIR is presented as

$$\mathrm{SIR} = \frac{h_0 S_0 d_0^{-\alpha}}{\sum\limits_{i>0, i\in\Phi_B} h_i S_i d_i^{-\alpha}} \tag{6.2}$$

where $h_0,\ S_0$ and d_0 are the Rayleigh fading, blockage-based path loss and the distance of the link from the designated server to typical user, respectively. Except for the designated server, other transmitters are considered as interferences. The variables of $h_i,\ S_i$ and d_0 characterize the i-th transmission link. Without loss of accuracy, the noise is neglected in this chapter.

Therefore, the SIR coverage probability is formulated by

$$P_c(T) = P(SIR > T) = P\left(\frac{h_0 S_0 d_0^{-\alpha}}{\sum\limits_{i>0, i\in\Phi_B} h_i S_i d_i^{-\alpha}} > T\right) \tag{6.3}$$

6.3 Blockage Model

A. Average number of walls

The signal power attenuation ratio caused by wall blockages of the i-th link is presented as $S_i = \prod_{k=0}^{K_i} \omega_{i_k}$. where the variable K_i denotes the number of interior wall that the i-th link intersects, and ω_{i_k} denotes the caused by the k-th ($0 < k \leq K_i$) wall of the i-th link. Note that the value range of the variable $\omega_{i,k}$ is $[0,1]$. For simplicity, we assume that all the interior walls have the same attenuation, i.e., $\omega_{i_k} = \omega$, hence $S_i = \prod_{k=0}^{K_i} \omega$. Therefore, it is necessary to identify statistical distribution for the number of interior walls first.

As aforementioned in Section 6.2, we assume that the orientation angles of wall blockages are binary random variables taking values in the set $\left\{0, \frac{\pi}{2}\right\}$ with equal probabilities. Based on the system model defined the assumptions of walls in Section 6.2, the average number of interior walls that each link intersects can be calculated following Theorem 6.1.

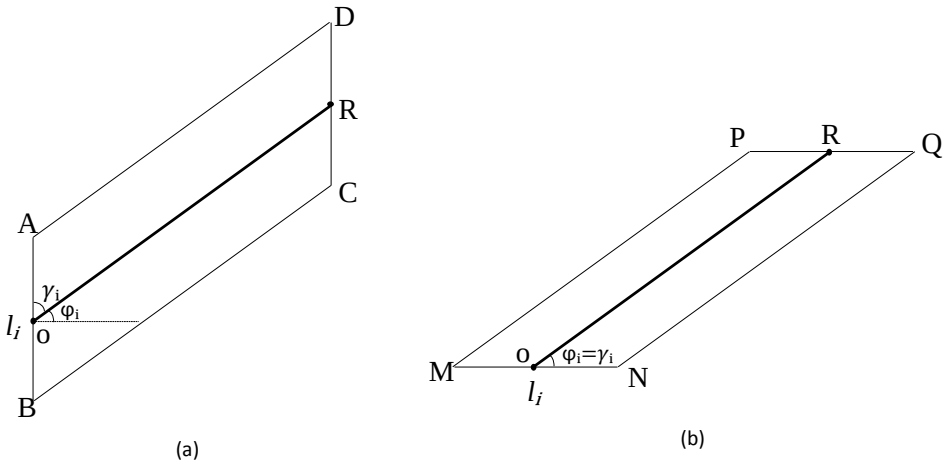

Fig. 6.1 *OR* represents the *i*-th link with length d_i. $|AB|$ and $|CD|$ are two examples of walls each with the vertical orientation angle, denoted by $\theta = \frac{\pi}{2}$. $|MN|$ and $|PQ|$ are two examples of walls each with an horizontal orientation angle, denoted by $\theta = 0$. The variable γ_i is the angle between a wall and the *i*-th link, and the variable ϕ_i denotes the angle between the horizontal axis and the *i*-th link. The points *O* and *R* represent the positions of the typical user and the BS, respectively. (a) An example with the wall orientation angle $\theta = \frac{\pi}{2}$. (b) An example with the wall orientation angle $\theta = 0$.

In this section, we focus on modelling the wall blockages. The wall blockages are generated as a Boolean scheme. Assuming the angles of wall blockages as the set of $\left\{0, \frac{\pi}{2}\right\}$ with equal probability, it resembles the angles of realistic wall blockages. With the assumptions of walls in Section 6.2, the average wall number that each link intersects is developed as Theorem 6.1.

Theorem 6.1. *By considering the wall orientation angle θ as the set of $\left\{0, \frac{\pi}{2}\right\}$ with equal probability, the average wall number that the i-th link intersects can be formulated as in equation* (6.4)*:*

$$E[K_i] = \frac{1}{2}\left(|\sin(\varphi_i)| + |\cos(\varphi_i)|\right)\lambda E\left[L\right] d_i \tag{6.4}$$

where φ_i is the link angle between the i-th link and the horizontal axis. It accords with an uniform distribution in $(0, 2\pi]$. d_i denotes the i-th link length.

Proof. As shown in Fig. 6.1, the i-th link is intersected by the wall if and only if its center falls into the parallelogram region $ABCD$ (or $MNQP$). The number of walls that the i-th link intersects is equal to the number of centre points falling into the region, which is given by $K_i = \lambda l_i d_i |\sin\gamma_i|$. We define the variable γ_i as the acute angle between a wall and the i-th link, which is uniformly distributed in $[0, \pi/2]$.

Under the assumption of wall orientation in Section 6.2, the orientation angle of the wall blockage is denoted by $\theta = 0$ or $\frac{\pi}{2}$. For $\varphi_i \in \left(0, \frac{\pi}{2}\right]$, we can obtain the relationship between γ_i and φ_i from Fig. 6.1, given by

$$\gamma_i = \begin{cases} \frac{\pi}{2} - \varphi_i, & when\ \theta = \frac{\pi}{2}, \\ \varphi_i, & when\ \theta = 0. \end{cases} \tag{6.5}$$

Therefore, the PDF $f_\Gamma(\gamma_i)$ of γ_i is calculated by the equation (6.6)

$$f_\Gamma(\gamma_i) = \frac{1}{2}\delta[\gamma_i - (\frac{\pi}{2} - \varphi_i)] + \frac{1}{2}\delta[\gamma_i - \varphi_i] \tag{6.6}$$

where δ is Dirac function. When φ_i is in $\left(\frac{\pi}{2}, 2\pi\right]$, the function $f_\Gamma(\gamma_i)$ is the same as in equation (6.6). The derivation is omitted here for brevity.

Following Theorem 1 of the work [18], the expected value of K_i can be calculated

$$\begin{aligned} E[K_i] &= \int_L \int_\Gamma \lambda l_i d_i |\sin\gamma_i| f_L(l_i) f_\Gamma(\gamma_i) dl\ d\gamma \\ &= \frac{1}{2}\left(|\sin(\varphi_i)| + |\cos(\varphi_i)|\right) \lambda E[L] d_i, \end{aligned} \tag{6.7}$$

where $f_L(l_i)$ is the probability density function of the length of an interior wall. □

The average number of walls intersected by each link is influenced by characteristics of both the link and the wall blockage. It will be verified in Section 6.5.

B. Effects of wall blockages

According to the independent thinning, the number of points falling into the region $ABCD$ (or $MNQP$) is still a PPP [100]. Moreover, Theorem 6.1 provides the average number of wall

blockages on each link. Therefore, we can obtain that the number K_i of walls intersected by the i-link is a Poisson random variable with a mean $E[K_i]$. Hence, the PDF of K_i is directly written as $f_K(k_i) = \frac{e^{-E[k_i]}(E[k_i])^{k_i}}{k_i!}$.

As aforementioned above, the attenuation is expressed as $S_i = \prod_{k=0}^{K_i} \omega$, where K_i is the wall number on the i-th link. Now with the distribution of the number of interior walls intersected by the i-th link, the signal attenuation caused by wall blockages to the i-th link can be investigated. The average signal attenuation caused by wall blockages of the i-th link , which is presented as

$$\begin{aligned} E[S_i] &= E[\omega^{K_i}] = \int_0^{\infty} \omega^{k_i} f_K(k_i) \mathrm{d}k_i \\ &= e^{-E[K_i](1-\omega)} \\ &= e^{-\frac{1}{2}(|\sin(\varphi_i)|+|\cos(\varphi_i)|)\lambda E[L] d_i (1-\omega)}. \end{aligned} \tag{6.8}$$

The average signal attenuation $E[S_i]$ caused by interior wall blockages is influenced by the characteristics of both links and wall blockages based on the equation (6.8). This analytical result will be verified in Section 6.5.

Based on the signal attenuation S_i caused by interior wall blockages, we analyse the performance of indoor wireless networks. In the following, we will investigate the case of mmWave networks, since wireless transmissions in this frequency range are particularly sensitive to blockages. For the simplicity of analysis, we assume that the wall blockages are impenetrable, i.e., the worst case scenario for wireless signal propagation. In this case, a user is only connected to the SC BSs with LOS links (namely visible transmitters). With impenetrable wall blockages, the signal attenuation ratio caused by wall blockages can be modeled as a Bernoulli random variable according to whether the link is blocked or not.

Corollary 6.1. *For millimetre wave signals, in indoor environments, the wall blockages are assumed as impenetrable. The signal attenuation ratio S_i is a Bernoulli random variable. The conditional probability of $S_i = 1$ is presented as $P\{S_i = 1|\varphi_i\} = e^{-\lambda E[L] d_i \beta(\varphi_i)}$, where $\beta(\varphi_i) = \frac{1}{2}(|\sin(\varphi_i)| + |\cos(\varphi_i)|)$.*

The proof is straightforward and omitted here. According to Corollary 6.1, it is conveniently to obtain the conditional probability of a wireless link experiencing LOS propagation in indoor environments with interior wall blockages.

Corollary 6.2. *Indoor indoor environments with impenetrable wall blockages, the conditional probability that the i-th link is LOS is given by* $P_{LOS} = e^{-\lambda E[L] d_i \beta(\varphi_i)}$.

Through Corollary 6.2, the conditional probability that a link is LOS decreases exponentially with the increase of link length, which matches the models in 3GPP [15]. The validation of Corollary 6.2 will be presented in Section 6.5.

6.4 Analytical Scheme

This section will present the analysis of network performance under the system model with the provided connectivity policy.

6.4.1 Connectivity

In this subsection, we will investigate the link connectivity between the user and the transmitter. We assume the user is only connected to the nearest LOS transmitter. The distance from the user to the closest LOS transmitter is denoted as R. If there are more than one nearest visible transmitters with a distance R the user, then the user randomly selects one of them to connect. An example of the successful link is shown as the Fig. 6.2.

Now, we define a ball zone $B(O,r)$, where the radius r is less than R. The center O is the typical user's position. Within the ball zone, the transmitters are distributed following a PPP with the mean of $\pi r^2 \mu$ [100], where μ denotes the density of the transmitters. We define the event $E_1 = \{\text{There are } n \text{ transmitters within the ball zone } B(\mathrm{O},\mathrm{r})\,.\}$, where $n = \{0,1,2,...\}$, then the probability of event E_1 is given by $P(E_1) = \frac{e^{-\pi r^2 \mu}(\pi r^2 \mu)^n}{n!}$.

The necessary and sufficient condition of a successful connectivity for the typical user is that all the n transmitters within the above defined ball zone are not visible to the typical user. The event $E_2 = \{\text{All the } n \text{ transmitters inside the zone } \mathrm{B}(\mathrm{O},\mathrm{r}) \text{ are invisible to the typical user.}\}$

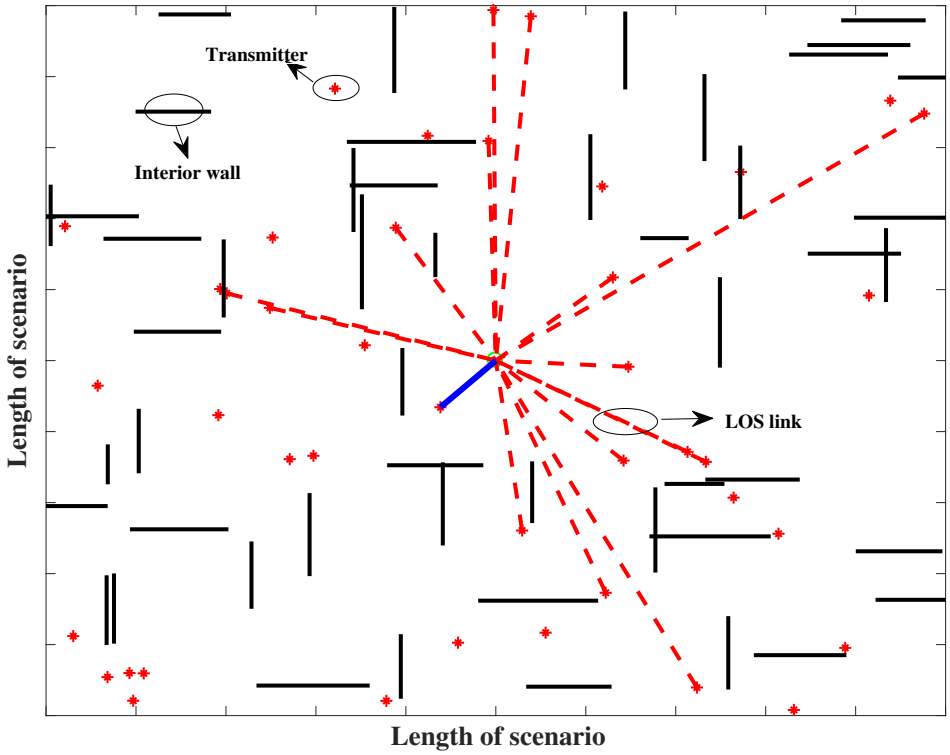

Fig. 6.2 The wall blockages are generated as the black straight lines. All the transmitters are presented by the red points. The typical user is seated at the central position of the scenario. For the typical user, all the LOS links are shown as the red dotted lines. Assume the user is only covered by the nearest LOS transmitter, as shown the blue solid line.

is defined. The conditional probability of event E_2 is the probability that all the n transmitters are NLOS links to the typical user under the condition of event E_1. The conditional probability $P(E_2)$ of event E_2 is given by

$$\begin{aligned} P(E_2|E_1) &= \left[\int_0^{2\pi}\int_0^r (1-P_{LOS})\frac{2t}{r^2}\frac{1}{2\pi}\mathrm{d}t\mathrm{d}\varphi_i\right]^n \\ &= \left[1-\frac{2}{r^2}\int_0^{2\pi} M[\beta(\varphi_i)]\frac{1}{2\pi}\mathrm{d}\varphi_i\right]^n. \end{aligned} \tag{6.9}$$

where $M[\beta(\varphi_i)] = \frac{1-\{\beta(\varphi_i)E[L]\lambda r+1\}e^{-\beta(\varphi_i)E[L]\lambda r}}{\{\beta(\varphi_i)E[L]\lambda\}^2}$, and P_{LOS} is obtained from Corollary 6.2. The equation (6.9) follows the fact that all points in the ball are independent and uniformly

distributed according to a PPP. The link angle φ_i is uniformly distributed in $(0, 2\pi]$. The blockages that intersect each individual are assumed independently.

Following Theorem 8 of the work in [18], the distribution of the distance from the typical user to the nearest visible transmitter is presented as

$$\begin{aligned} P(R>r) &= P(E_2) = \sum_{n=0}^{\infty} P(E_2|E_1)P(E_1) \\ &= \sum_{n=0}^{\infty} \left[1 - \frac{2}{r^2}\int_0^{2\pi} M[\beta(\varphi_i)]\frac{1}{2\pi}\mathrm{d}\varphi_i\right]^n \frac{e^{-\pi r^2\mu}(\pi r^2\mu)^n}{n!}, \\ &= e^{-2\pi\mu\left[\int_0^{2\pi} M[\beta(\varphi_i)]\frac{1}{2\pi}\mathrm{d}\varphi_i\right]} \\ &\overset{(a)}{\approx} e^{-2\pi\mu M\left[\mathbb{E}_{\varphi_i}[\beta(\varphi_i)]\right]} = e^{-2\pi\mu M\left[\widetilde{\beta}\right]}, \end{aligned} \tag{6.10}$$

where the step (a) takes an approximation in order to obtain the closed form of equation (6.10), here

$$M[\widetilde{\beta}] = \frac{1 - \left\{\widetilde{\beta}E[L]\lambda r + 1\right\}e^{-\widetilde{\beta}E[L]\lambda r}}{\left\{\widetilde{\beta}E[L]\lambda\right\}^2},$$

and

$$\mathbb{E}_{\varphi_i}[\beta(\varphi_i)] = \widetilde{\beta} = \int_0^{2\pi} \beta(\varphi_i)\frac{1}{2\pi}\mathrm{d}\varphi_i = \frac{2}{\pi}.$$

The approximation brings minor error, which will be verified in chapter 6.5. Following equation (6.10), the PDF of R can be calculated directly by differentiation, as presented in Theorem 6.2.

Theorem 6.2. *The typical user is connected to one of the nearest visible SC BSs at a distance R away from the typical user. The probability density function of R is given by*

$$f_R(r) = 2\pi\mu r e^{-[2\pi\mu M[\widetilde{\beta}] + E[L]\lambda r\widetilde{\beta}]} \tag{6.11}$$

The derivation is straightforwardly by differentiating $1 - P(R > r)$ and is omitted here for brevity.

6.4.2 Coverage probability

Now we have investigated the effects of wall blockages, and the connectivity between the transmitter and typical user for the case of impenetrable wall blockages. This section will demonstrate the analysis of cellular network performance, i.e. coverage probability. In chapter 6.2, the coverage probability $P_c(T)$ is defined as the probability that the SIR received at the typical user is larger than the threshold T, i.e.,

$$P_c(T) = P(\text{SIR} > T).$$

The coverage probability is an important metric for the analysis of network performance, which is influenced by the density of SC BSs, and the density and topology of interior walls. Moreover, another influential factor is the user-cell association strategy for a user to select a SC BS to connect to. Usually a user is connected to the SC BS with the strongest downlink received power or the maximum received SIR. We assume that the typical user is served by the nearest visible SC BS, which is referred to as the serving BS. The downlink transmissions from other BSs are considered as interference to the typical user. If there is no visible SC BS to the user, then the user is not covered, i.e., without a successful connectivity. For analytical simplicity, we assume that the number of wall blockages on each individual link is independent. The coverage probability is given in Theorem 6.3.

Theorem 6.3. *The typical user selects the nearest visible SC BS as its serving BS. Assuming that the number of wall blockages on each link is independent and the SIR threshold is T, then the coverage probability $P_c(T)$ is given by*

$$P_c(T) = \int_0^D \exp\left(-2\pi\mu \int_r^\infty \left[\frac{Tr^\alpha e^{-\lambda E[L] t\widetilde{\beta}}}{t^\alpha + Tr^\alpha}\right] t\mathrm{d}t\right) f_R(r)\mathrm{d}r, \tag{6.12}$$

where $\widetilde{\beta} = \frac{2}{\pi}$, and the parameter D is the maximum link length within an indoor scenario.

Proof. According to the pathloss model described in chapter 6.2, the downlink SIR of the typical user can be presented as

$$\mathrm{SIR} = \frac{h_0 S_0 r^{-a}}{\sum\limits_{i:d_i \in (r,D)} h_i S_i d_i^{-\alpha}}, \tag{6.13}$$

where the 0-th link is the successful connectivity from the nearest visible transmitter to the typical user given that the distance from the typical user to the closest visible transmitter is $R = r$. The variable d_i is the length of i-th link, where $r < d_i < D$. The variable D denotes the maximum length of links within the indoor scenario, and it is defined as $D = \frac{\sqrt{{L_s}^2 + {W_s}^2}}{2}$, in which the parameters of L_s and W_s are the length and width of the indoor scenario, respectively. For improving the accuracy of analysis, the value of link length d_i is taken according to the specific indoor scenario size. The variable S_i is the wall attenuation ratio of i-th link, where $S_0 = 1$. The fading loss denoted by h_i (and h_0) is following a unit-mean exponential distribution.

Therefore, the coverage probability conditioned on the distance from the typical user to the closest transmitter is computed as

$$\begin{aligned}
&P\{\mathrm{SIR} > T \mid R = r\} = P\left\{ h_0 > \left(\sum_{i:d_i \in (r,D)} h_i S_i d_i^{-\alpha} \right) T r^{\alpha} \right\} \\
&= E\left[\exp\left(-\Big(\sum_{i:d_i \in (r,D)} h_i S_i d_i^{-\alpha} \Big) T r^{\alpha} \right) \right] \\
&= E\left[\prod_{i:d_i \in (r,D)} E_{S_i,h_i}\left[\exp\left(-h_i S_i d_i^{-\alpha} T r^{\alpha} \right) \right] \right] \\
&\overset{(a)}{=} E\left(\prod_{i:d_i \in (r,D)} E_{h_i}\left[\exp\left(-h_i d_i^{-\alpha} T r^{\alpha} \right) \right] P(S_i = 1) + 1 - P(S_i = 1) \right) \\
&\overset{(b)}{=} E\left(\prod_{i:d_i \in (r,D)} E_{h_i}\left[\exp\left(-h_i d_i^{-\alpha} T r^{\alpha} \right) \right] \int_0^{2\pi} P(S_i = 1|\varphi_i) \frac{1}{2\pi} \mathrm{d}\varphi_i + 1 - \int_0^{2\pi} P(S_i = 1|\varphi_i) \frac{1}{2\pi} \mathrm{d}\varphi_i \right) \\
&\overset{(c)}{=} E\left(\prod_{i:d_i \in (r,D)} 1 - \frac{T r^{\alpha} \int_0^{2\pi} e^{-\lambda E[L] d_i \beta(\varphi_i)} \frac{1}{2\pi} \mathrm{d}\varphi_i}{d_i^{\alpha} + T r^{\alpha}} \right) \\
&\overset{(d)}{=} \exp\left(-2\pi\mu \int_r^{\infty} \left[\frac{T r^{\alpha} \int_0^{2\pi} e^{-\lambda E[L] d_i \beta(\varphi_i)} \frac{1}{2\pi} \mathrm{d}\varphi_i}{t^{\alpha} + T r^{\alpha}} \right] t \mathrm{d}t \right),
\end{aligned} \tag{6.14}$$

where step (a) follows Corollary 6.1, S_i follows the Bernoulli distribution with the conditional probability of $P(S_i = 1|\varphi_i)$, step (b) takes an approximation for reducing the computing complexity, which is shown as

$$\int_0^{2\pi} P(S_i = 1|\varphi_i)\frac{1}{2\pi}\mathrm{d}\varphi_i \approx e^{-\lambda E[L] r E_{\varphi_i}[\beta(\varphi_i)]} = e^{-\lambda E[L] r \widetilde{\beta}}.$$

Step (c) is obtained from the probability generating functional (PGFL) of the PPP that models the spatial distribution of transmitters.

Based on equation (6.14) and Theorem 6.2, the unconditional coverage probability is formulated by deconditioning the variable r as follows.

$$P\{\mathrm{SIR} > T\} = \int_0^D P\{\mathrm{SIR} > T \mid R = r\} f_R(r)\mathrm{d}r, \tag{6.15}$$

where the parameter D is the maximum link length within the considered indoor scenario, given that the typical user is located at the centre of the considered network area as shown in Fig. 6.2. □

According to Theorem 6.3, although it s difficult to obtain the closed form of coverage probability, the coverage probability expression in equation (6.12) can be used to numerically investigate the distribution of coverage. In the next section, Theorem 6.3 will be employed to analyse the performance of indoor cellular networks with impenetrable wall blockages.

6.5 Numerical Simulations

In this section, we present the numerical performance-evaluation results of dense cellular networks in indoor environments. Firstly, the analytical results obtained will be validated by comparing with Monte Carlo simulation results. Then the coverage performance of indoor dense SC networks will be analysed based on both numerical and simulation results.

We validate the average number of obtained in Theorem 6.1 by comparing with Monte Carlo simulations as shown in Fig. 6.3. The analytical average number of walls that each link intersects is obtained from Theorem 6.1. In the comparisons, we fix the link length at 20

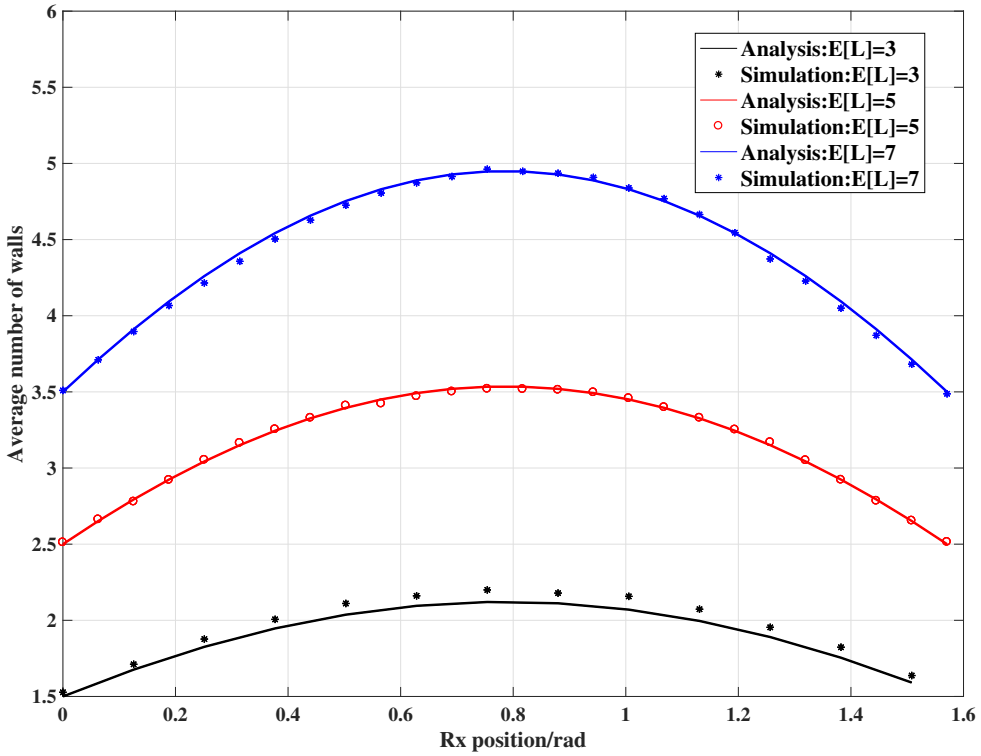

Fig. 6.3 The validation of average wall number intersected by links. We simulate a square area of 40×40 m^2. The wall density is assumed as $\lambda = 0.05$ m^{-2}. The average wall length takes $E[L] = 3, 5, 7$ m respectively. The link length is assumed as half of the square length $d_0 = 20$ m for both the analysis and simulation. The position of typical user is located at the centre of the scenario as shown in Fig. 6.2. The position of the server BS is located at the circle with the centre of the user's position and the radius of link length.

meters and consider three different values of the average wall length $E[L]$: 3 meters, 5 meters and 7 meters. Considering that the considered network scenario is symmetric with respect to its central point (the position that the typical user is located) as shown in Fig. 6.2, only the results in the interval $(0, \pi/2]$ of the angles between the links and the horizontal axis are presented here. The Monte Carlo simulation results are averaged over 10,000 samples. From Fig. 6.3, it is observed that the analytical results fit simulation results closely. The links with angle $\phi = 0$ or $\pi/2$ intersect the smallest number of interior walls on average. The reason is the links with angle $\phi = 0$ or $\pi/2$ are only blocked by the horizontal or vertical walls at this time, where the density of walls is only half of λ.

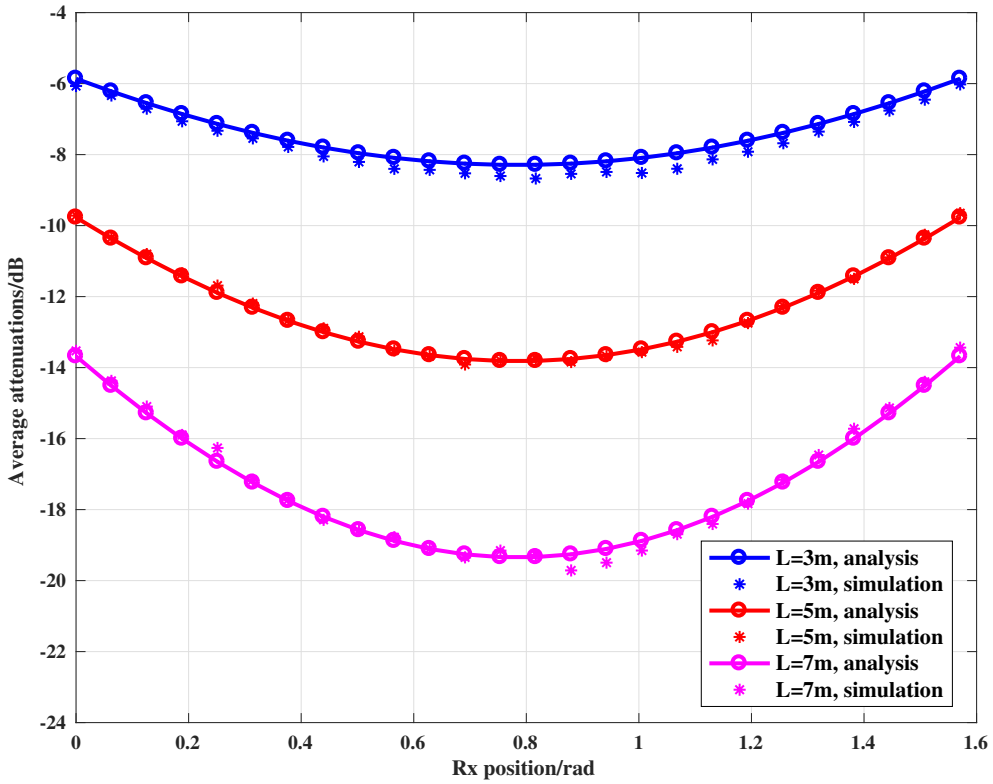

Fig. 6.4 Average wall attenuation. Given $\lambda = 0.05$ m^{-2} and $E[L] = 3, 5, 7$ m respectively. The link length is assumed as half of the square length $d_0 = 20$ m for both the analysis and simulation.

Fig. 6.4 presents the average signal attenuation $E[S_i]$ caused by blockages. The analytical result is obtained by equation 6.8. The Monte Carlo simulation is operated within a square with the area 40×40 m^2. From Fig. 6.4, it is observed that the analytical results fit Monte Carlo simulations closely. The evaluated average attenuation of the i-th link is a dependency of the link angle, link length and wall density. The most attenuation occurs at the angle of $\pi/4$, due to the link at this direction experiences the most walls (as shown in Fig. 6.3).

The comparison of LOS probability conditioned on the link angle is presented, as shown in Fig. 6.5. The analytical result is obtained from Corollary 6.2. As can be seen, the link with the angle 0 or $\frac{\pi}{2}$ has a higher LOS probability than with the angle $\frac{\pi}{4}$. The reason is that the wall density is only half of λ at the orientations of 0 and $\frac{\pi}{2}$. Moreover, the LOS

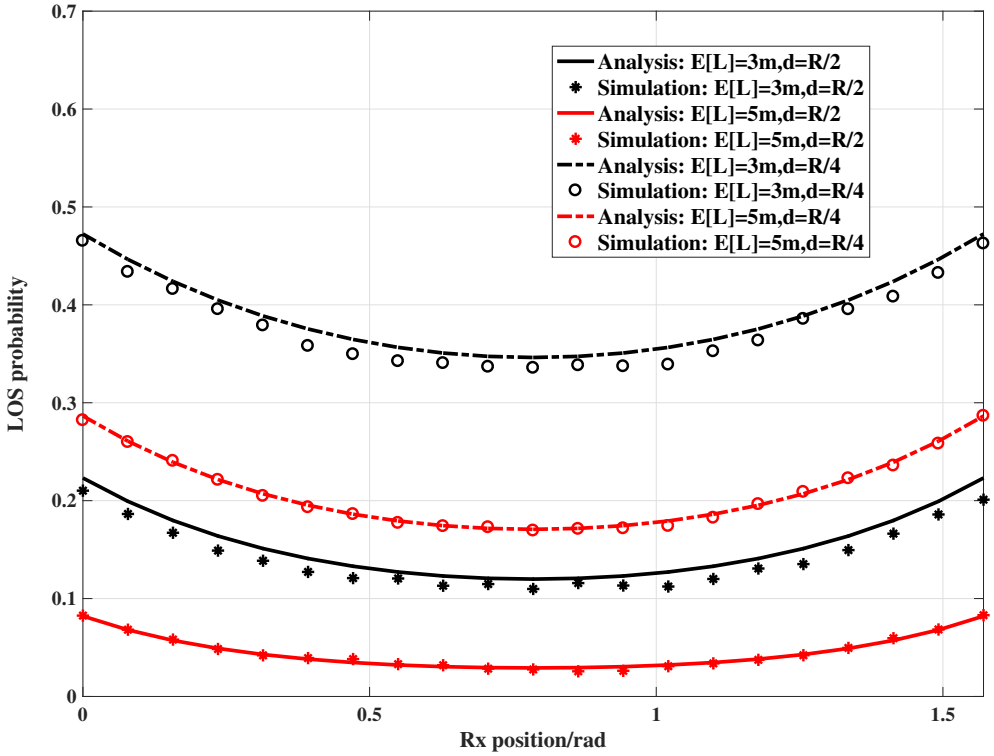

Fig. 6.5 The LOS probability conditioned on links angle. Given $\lambda = 0.05$ m^{-2} and $E[L] = 3,5$ m respectively. The LOS probability is investigated when the link length takes $d_0 = 20,10$ m.

probability decreases with the link length arising, since the longer link has a higher likelihood of experiencing walls. This also matches our intuition.

Fig. 6.6 verifies the approximation in equation (6.10), which gives the distribution of the distance R. It is observed that the approximated results present an accurate match to the analytical results without approximation. Thus, the approximation in equation (6.10) is acceptable with a very minor error. The probability of $P(R > r)$ is distance-dependency, and reduces with the increase of link length.

The Fig. 6.7 presents a comparison of coverage probability between analytical results and Monte Carlo simulation results, under impenetrable wall blockages. The analytical results are obtained from Theorem 6.3. The parameter T denotes the SIR threshold. The values of the main parameters are summarised in Table 6.1. From Fig. 6.7, we can observe that the curves of analytical results match Monte Carlo simulation results closely with only

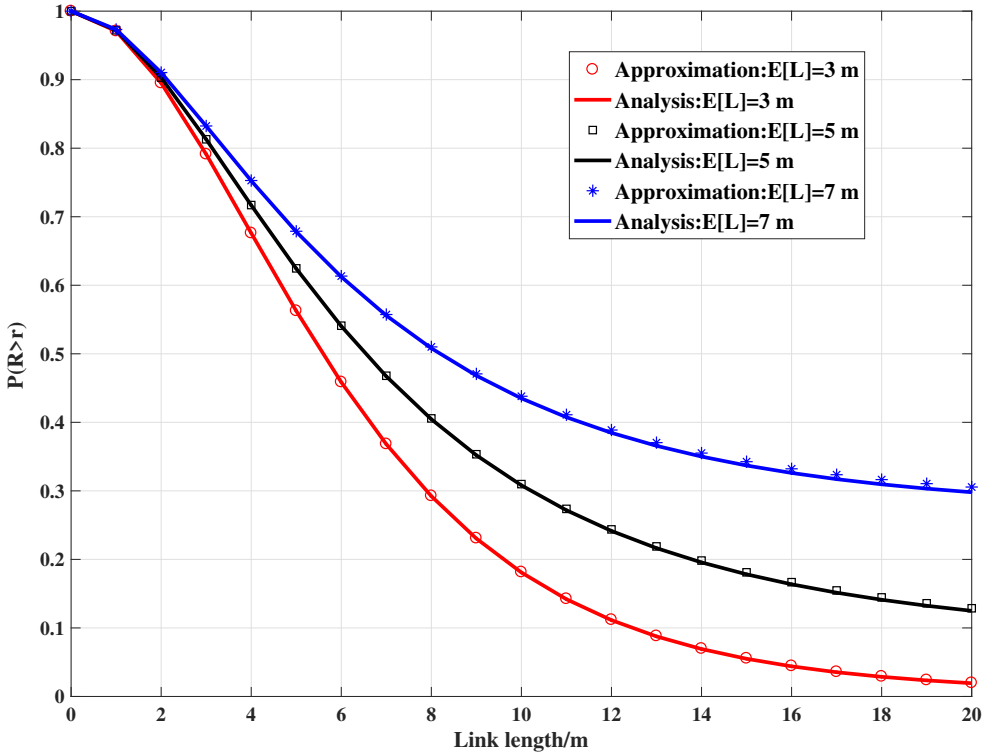

Fig. 6.6 The verification of approximation in equation (6.10) which gives the distribution of the distance from the typical user to the nearest visible transmitter.

a small gap between them. The small gap is caused by the correlations of wall blockage effects on different links, which are captured in the Monte Carlo simulation but ignored in the analytical result in Theorem 6.3. Additionally, in stochastic geometry, the average coverage probability is derived by aggregating SIR over the infinite 2D plane. However, the considered indoor scenario is of a finite area. We adjust the integral limits in equation 6.12 according to the specific indoor scenario size, which contributes to the difference between the analytical coverage probability and the simulation result. The reasonably good accuracy of the analytical coverage probability expression in Theorem 6.3 (as compared with the Monte Carlo simulation result) indicates that Theorem 6.3 offers a good trade-off between performance evaluation (or prediction) accuracy and the computational complexity. The Monte Carlo simulation took several hours to complete all the calculations for 10,000 samples.

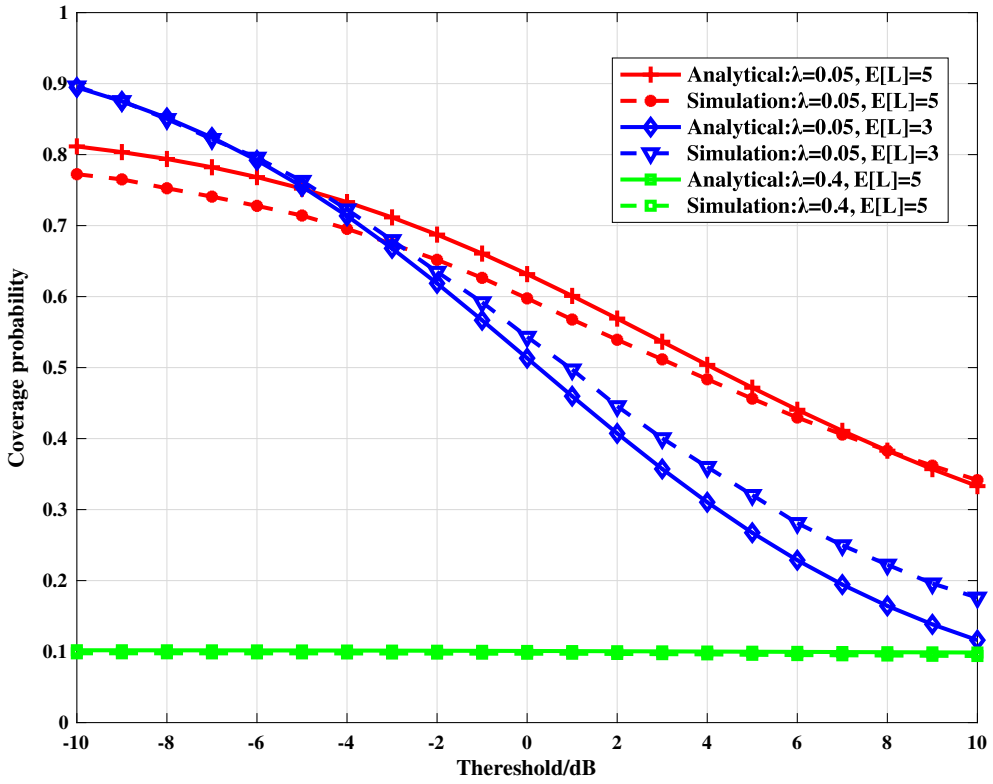

Fig. 6.7 The verification of the coverage probability expression in 6.14 by comparing it with Monte Carlo simulation results. Assume the indoor scenario as a square of 40×40 m^2. Given the distribution of transmitters with a density $\beta = 0.01$ m^{-2}, the values of wall density are taken as $\lambda = 0.01, 0.4$ m^{-2}, and average wall length are taken as $E[L] = 3, 5$ m, respectively. The typical user is located at the center of the considered network scenario.

Table 6.1 Simulation parameters

Pathloss exponent	$\alpha = 2$
Transmit power	$P = 1$W
Wall loss	$\omega = 10$dB
Simulation realizations	10^4

Fig. 6.8 presents the coverage probability calculated using equation (6.12) in Theorem 6.3 versus the SIR threshold for different values of transmitter density. With a minor error, the noise power is ignored here. An apparent observation is that the coverage probability does not always to benefit from the increasing transmitter density, given the distribution of wall blockages in an indoor environment. In other words, for indoor dense cellular networks

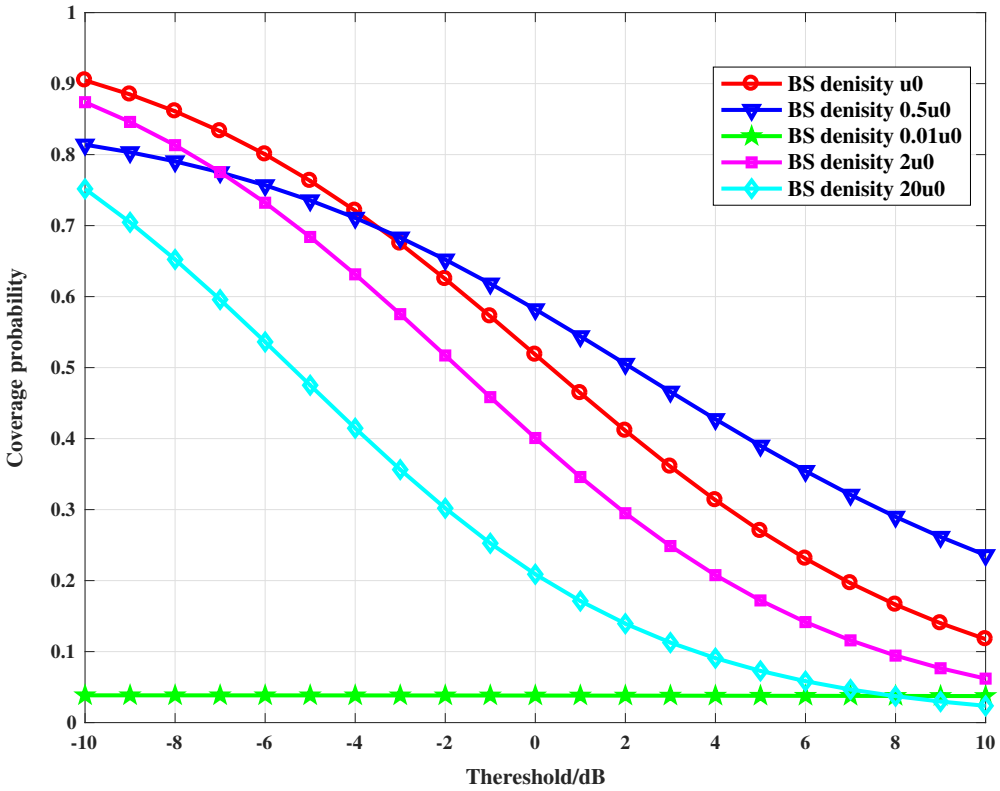

Fig. 6.8 The comparison of coverage probability obtained as a function of transmitter density in Theorem 6.3 versus the SIR threshold for different values of transmitter density, given the wall density $\lambda = 0.05$ m^{-2}. The average wall length is $E[L] = 3$ m. The transmitter density is $\mu_0 = 0.01$ m^{-2}. The typical user is located at the center of the considered indoor network scenario.

with interior wall blockages, there is a finite optimum density of transmitters that maximizes the coverage probability. This is because increasing the density of transmitters will also increase the number and density of interfering links, making the coverage probability limited by the interference. In addition, the coverage is very poor when the transmitter density is relatively low compared to the wall blockage density. This is because the typical user can hardly find any LOS transmitter to connect to when the wall blockage density is much larger than that of transmitter density.

6.6 Conclusions

In this chapter,we have investigated the interior wall blockages and the associated analysis of interference effects and coverage performance of indoor dense SC networks. The wall blockage model is developed on the basis of stochastic geometry. The key idea is that the interior walls are stochastically modelled as straight lines. Then the effects of wall blockages on signal transmissions are investigated for indoor SC networks. Finally, the analytical coverage probability is obtained in the case of impenetrable wall blockages. Numerical results show that the performance, e.g. coverage probability is sensitive to wall blockage density. Although the coverage probability can benefit from the increasing of transmitter density, the optimal transmitter density is a finite value given the distribution of walls. For the next step, an interesting topic that the correlation between wall blockages is taken into consideration. Since in a finite indoor environment, the correlation between wall blockages is higher than in urban environments. Another interesting topic includes the refinement of blockage model by considering the reflection, which is an influential factor for indoor densely SC networks.

Chapter 7

Conclusions and Future Work

7.1 Conclusions

This thesis mainly investigates the indoor wireless communications in the background of dense cellular networks. For satisfying the exponential increase of indoor traffic-data demand, the indoor wireless communications are evolving from outdoor macrocells to indoor-deployment dense SC networks. In the meantime, challenges are also brought for evaluating the performance of indoor communications. Firstly, the unique features of indoor environments, such as complex obstacles and various building layouts, significantly influence the signal propagating channels. Moreover, with the higher density of in-building SC networks, the link distances between users and transmitters become much shorter. It is certain that the characterizations of LOS and NLOS propagations are different from the previous observation. Finally, the impact of blockages on signals becomes dominant in indoor environments because of the more complex and dense obstacles and the shorter link distances. The traditional path loss models can not exactly capture the blockage effects.

Focusing on the channel modelling, previous works demonstrate that the distribution of LOS probability is crucial to capture the characterizations of propagating environments. Whereas, existing LOS probability models, such as the exponential model and 3GPP models, are too simplified to describe the exact LOS and NLOS transmissions in typical indoor scenarios. By considering the realistic structures of buildings, an analytical method is pro-

posed to build a novel LOS probability model for downlink radio propagations in typical indoor scenarios, which are consisted of rectangular grids. The proposed model analytically constructs the mapping from a building's layout (structure) to the LOS probability distribution. With this model, we can directly obtain the LOS probability of transmission links inside a given building without simulations or measurements. The proposed model also improves the accuracy of the LOS probability because it reduces the randomness of building structure. Numerical results show that traditional LOS probability models underestimate the performance of PPP network.

In terms of the performance of LOS and NLOS transmissions, traditional works do not distinguish them. However, it is not practical for indoor dense cellular networks. Thus, a tractable and analytical path loss model with LOS and NLOS propagations is proposed for the performance analysis in indoor dense SC networks. On the basis of stochastic geometry, the performance metrics, such as coverage probability, SE and ASE are analytically derived. Monte Carlo simulations validate its correctness of derivation. Moreover, numerical results demonstrate that the above three performance metrics are influenced by the BS density and LOS probability functions. The effects of LOS and NLOS transmissions are notably different from the traditional channel transmission with the single-slope path loss model. As a consequence, the obtained results provide insights on the deployment of future indoor dense SC networks.

Targeting to the dominant effects of indoor blockages, conventional works can not describe it accurately since it is incorporated into the log-normal shadowing. Therefore, a wall blockage model is developed based on the stochastic geometry theory. By modelling wall blockages as a random process of PPP, the effects of wall blockages on signal transmission are mathematically investigated for indoor dense SC networks. Finally, the mathematical framework of coverage probability is obtained for the case of impenetrable wall blockages. Simulation results demonstrate that the performance, e.g. coverage probability is sensitive to wall blockage density. On one hand, the coverage probability can benefit from the increasing of transmitter density. On the other hand, the optimal density of transmitters is a finite value given the distribution of walls.

7.2 Future work

This thesis has investigated the performance analysis of indoor wireless communications in dense SC networks. A novel and analytical LOS probability model has been established for typical indoor scenarios. The effects caused by indoor wall blockages have been evaluated by the random shape theory for network performance analysis. The impact of LOS/NLOS propagations on indoor dense SC networks has been investigated on the basis of the stochastic geometry theory.

As presented in Chapter 4, an analytical and novel model of LOS probability is proposed by considering the effects of the building structure in typical indoor scenario, which is consisted of rectangular grids. In reality, buildings usually have various and more complex structures. The obstacles also include moving human bodies and furniture. In future work, more complex building models will be given a consideration, such as multi-floors and buildings with irregular shapes. Moreover, the effects of other obstacles on LOS probability will be included in future work.

As presented in Chapter 5, the influence of LOS/NLOS transmissions on the performance of indoor dense networks is presented by considering Rayleigh fading for both LOS and NLOS paths. Actually, the model of channel fading is more complex, and has different impact on signal transmissions. Future work will investigate the more practical model of path loss by considering different types of fading, e.g. Rician fading or shadow fading caused by wall blockages. The development of corresponding analytical methods should be a meaningful challenge.

As presented in Chapter 6, the effects of blockages are analytically illustrated for performance analysis by a random theory. The expression of coverage probability is obtained for the case of impenetrable walls. However, the random theory assumes that its objects are independently distributed, which is not practical for realistic walls. In future work, the correlation between wall blockages will be considered for modelling blockages. Another meaningful topic is that the mathematical expressions of performance metrics will be investigated for more general wall-attenuation cases.

Apart from the extensions related to this thesis, there are still a lot of challenges and opportunities for analysing and improving indoor wireless communications, which will continue to be the important role for the forthcoming information era.

References

[1] "Cisco visual networking index: Global mobile data traffic forecast update, 2016–2021," Cisco, USA, White Paper, Mar. 2017.

[2] N. Bhushan, *et al.*, "Network densification: The dominant theme for wireless evolution into 5G," *IEEE Commun. Mag.*, vol. 52, no. 2, pp. 82–89, Feb. 2014.

[3] J. Zhang, *et al.*, *Femtocells: Technologies and Deployment*, Wiley, 2010.

[4] A. K. Gupta, X. Zhang, and J. G. Andrews, "SINR and throughput scaling in ultradense urban cellular networks," *IEEE Wireless Commun. Lett.*, vol. 4, no. 6, pp. 605–608, Dec. 2015.

[5] C. Galiotto, N. K. Pratas, L. Doyle, and N. Marchetti, "Effect of LOS/NLOS propagation on 5G ultra-dense networks," *Computer Networks*, vol. 120, pp. 126-140, Jun. 2017.

[6] W. C. Jakes, and D. C. Cox, *Microwave mobile communications*. Wily-IEEE Press, 1994.

[7] A. Goldsmith, *Wireless communications*. Cambridge, U.K.: Cambridge Univ. Press, 2005.

[8] R. Mathur, M. Klepal, A. McGibney, and D. Pesch, "Influence of people shadowing on bit error rate of IEEE 802.11 2.4 GHz channel," in *Proc. 1st Int. Symp. of Wireless Communication Systems (ISWCS)*, pp. 448-452, Sep. 2004.

[9] J. Salo, L. Vuokko, H. M. El-Sallabi, and P. Vainikainen, “An additive model as a physical basis for shadow fading,” *IEEE Trans. on Veh. Technol.*, vol. 56, no.1, pp. 13-26, Jan. 2007.

[10] T. Chrysikos and S. Kotsopoulos, “Characterization of large-scale fading for the 2.4 GHz channel in obstacle-dense indoor propagation topologies,” in *Proc. IEEE Veh. Tech. Conf. (VTC)*, Sep. 2012.

[11] Z. Pi and K. Farooq, ”An introduction to millimeter-wave mobile broadband systems,” *IEEE Commun. Mag.*, vol. 49, no. 6, pp. 101–107, 2011.

[12] J. Zhang, Y. Wang, J. Zhang, and L. Ding, “Performance of spatial modulation with constant transmitted power under LOS and NLOS scenarios,” in *Proc. IEEE Int. Conf. on Commun. (ICC)*, pp. 2750-2755, 2015.

[13] C.R. Anderson and T.S. Rappaport, “In-building wideband partition loss measurements ar 2.5 and 60Ghz,” *IEEE Trans. Wireless Commu.*, vol. 3, no. 3, pp. 922-928, Mar. 2004.

[14] M. P. M. Hall, L. W. Barclay, and M. T. Hewitt, “Propagation of radiowaves,” Institution of Electrical Engineers, 1996.

[15] 3GPP, “TR 36.814 (v9.0.0) : Evolved universal terrestrial radio access (E-UTRA): Further advancements for E-UTRA physical layer aspects,” 2010.

[16] B. Mondal, T. Thomas, *et al.*, “3D channel model in 3GPP," *IEEE Commun. Mag.*, vol. 53, no. 3, pp. 16-23, Mar. 2015.

[17] S. Sun, T. A. Thomas, T. S. Rappaport, H. Nguyen, I. Z. Kovács, and I. Rodriguez, “Path loss, shadow fading, and line-of-sight probability models for 5G urban macro-cellular scenarios," in *Proc. IEEE Global Commun. Conf. Workshop (Globecom Workshop)*, pp. 1-7, Dec. 2015.

[18] T. Bai, R. Vaze, and R. W. Heath, “Analysis of blockage effects on urban cellular networks," *IEEE Trans. on Wireless Commun.*, vol. 13, no. 9, pp. 5070-5083, Sep. 2014.

[19] M. Ding, P. Wang, D. López-Pérez, G. Mao, and Z. Lin, “Performance impact of LoS and NLoS transmissions in dense cellular networks,” *IEEE Trans. on Wireless Commun.*, vol.15, no.3, pp. 2365–2380, Mar. 2016.

[20] J. G. Andrews, F. Baccelli, and R. K. Ganti,“A tractable approach to coverage and rate in cellular networks,” *IEEE Trans. Commun.*, vol. 59, no. 11, pp. 3122–3134, Nov. 2011.

[21] H. S. Dhillon, R.K. Ganti, F. Baccelli, and J.G. Andrews, “Modeling and analysis of K-tier downlink heterogeneous cellular networks,” *IEEE J. Sel. Areas Commun.*, vol.30, no.3, pp. 550–560, Apr. 2012.

[22] S. Singh, H. S. Dhillon, and J. G. Andrews, “Offloading in heterogeneous networks: Modeling, analysis, and design insights,” *IEEE Trans. Wireless Commun.*, vol. 12, no. 5, pp. 2484–2497, May 2013.

[23] X. Zhang and J. G. Andrews, “Downlink cellular network analysis with multi-slope path loss models,” *IEEE Trans. Commun.*, vol.63, no.5, pp. 1881–1894, Mar 2015.

[24] C. Galiotto, N. K. Pratas, N. Marchetti, and L. Doyle, “A stochastic geometry framework for LOS/NLOS propagation in dense small cell networks,” in *Proc IEEE Int. Conf. on Commun. (ICC)*, pp. 2851–2856, 2015.

[25] T Ding, M. Ding, G. Mao, Z. Lin, D. López-Pérez, and Y. Albert, “Uplink Performance Analysis of Dense Cellular Networks With LoS and NLoS Transmissions,” *IEEE Trans. on Wireless Commun.*, vol.16, no.4, pp. 2601–2613, Apr. 2017.

[26] J. Arnau, I. Atzeni, and M. Kountouris, “Impact of LOS/NLOS propagation and path loss in ultra-dense cellular networks,” in *Proc. IEEE Int. Conf. on Commun. (ICC)*, pp. 1–6, 2016.

[27] M. Ding and D. López-Pérez, *et al.*, "Performance impact of base station antenna heights in dense cellular networks," *IEEE Trans. on Wireless Commun.*, vol.16, no.12, pp. 8147–8161, Dec. 2017.

[28] M. Ding, D. López-Pérez, G. Mao, and Z. Lin, "Performance impact of idle mode capability on dense small cell networks," *IEEE Trans. Veh. Technol.*, vol.66, no.11, pp. 10446–10460, Nov. 2017.

[29] J. Ling and D. Chizhik, "Capacity scaling of indoor pico-cellular networks via reuse," *IEEE Commun. Lett.*, vol.16, no.2, pp. 231–233, Feb. 2012.

[30] K. Schaubach, N. Davis, and T. Rappaport,"A ray tracing method for predicting path loss and delay spread in microcellular environments," in *Proc. IEEE Veh. Tech. Conf. (VTC)*, vol. 2, pp. 932–935, May 1992.

[31] K. Rizk, J. F. Wagen, and F. Gardiol, "Two-dimensional ray-tracing modeling for propagation prediction in microcellular environments," *IEEE Trans. Veh. Technol.*, vol. 46, no. 2, pp. 508–518, May 1997.

[32] K. Haneda, J. Jarvelainen, *et al.*, "Spatial coexistence of millimeter-wave distributed indoor channels," in *Proc. IEEE Veh. Tech. Conf. (VTC)*, pp. 1–5, May 2015.

[33] T. Hashimoto, Y. Nishioka, Y. Inasawa, and H. Miyashita, "Indoor propagation estimation combining statistical models with ray-tracing," in *Proc. Int. Symp. Antennas Propag. (ISAP)*, pp. 1–3, Nov. 2015.

[34] S. R. Lamas, D. Gonzalez G, and J. Hamalainen, "Indoor planning optimization of ultra-dense cellular networks at high carrier frequencies," in *Proc. IEEE Wireless Commun. Netw. Conf. Workshops (WCNCW)*, pp. 23–28, Mar. 2015.

[35] T. Bai , R. Vaze , and RW. Heath, "Using random shape theory to model blockage in random cellular networks", in *Proc. IEEE Signal Processing and Commun. (SPCOM)*, pp. 1-5, Jul. 2012.

[36] M. K. Müller, M. Taranetz, and M. Rupp, “Effects of wall-angle distributions in indoor wireless communication,” in *Proc. Int. Workshop on Signal Process. Adv. in Wireless Commun. (SPAWC)*, pp. 1-5, Jul. 2016.

[37] M.K. Müller, M. Taranetz, and M. Rupp, “Analyzing wireless indoor communications by blockage models,” *IEEE Access*, vol.5, pp. 2172-2186, 2017.

[38] F. Baccelli and X. Zhang, “A Correlated Shadowing Model for Urban Wireless Networks,” in *Proc. IEEE IEEE Int. Conf. on Computer Commun. (INFOCOM)*, pp. 801 - 809, Aug. 2015

[39] J. Lee, X. Chen, and F. Baccelli, “A 3-D spatial model for in-building wireless networks with correlated shadowing,” *IEEE Trans. on Wireless Commun.*, vol. 15, no. 11, pp. 7778-7793, 2016

[40] M. Z. Win, “A mathematical model for network interference," in *Proc. IEEE Commun. Theory Workshop,* Sedona, AZ, USA, May 2007.

[41] M. Z. Win, P. C. Pinto, and L. A. Shepp,“A mathematical theory of network interference and its applications,” *Proceedings of the IEEE*, vol. 97, no. 2, pp. 205–230, Feb. 2009.

[42] M. Haenggi, J. G. Andrews, F. Baccelli, O. Dousse, and M. Franceschetti, “Stochastic geometry and random graphs for the analysis and design of wireless networks," *IEEE J. Sel. Areas Commun.*, vol. 27, no. 7, pp. 1029–1046, Sep. 2009.

[43] M. Haengg, *Stochastic geometry for wireless networks*. Cambridge Uni. Press, 2012.

[44] H. ElSawy, E. Hossain, and M. Haenggi, “Stochastic geometry for modeling, analysis, and design of multi-tier and cognitive cellular wireless networks: A survey,” *IEEE Commun. Surveys Tuts.*, vol. 15, no. 3, pp. 996–1019, 3rd Quart., 2013.

[45] H. ElSawy, A. Sultan-Salem, and M. Alouini, “Modelling and analysis of cellular networks using stochastic geometry: A tutorial,” *IEEE Commun. Surveys Tuts.*, vol, 19, no. 1, 2017.

[46] S. N. Chiu, D. Stoyan, W. S. Kendall, and J. Mecke, *Stochastic geometry and its applications*, John Wiley & Sons, 1996.

[47] F. Baccelli, M. Klein, M. Lebourges, and S. Zuyev, "Stochastic geometry and architecture of communication networks," *J. Telecommun. Syst.*, vol. 7, no. 1, pp. 209–227, Jun. 1997.

[48] T. X. Brown, "Cellular performance bounds via shotgun cellular systems," *IEEE J. Sel. Areas Commun.*, vol. 18, no. 11, pp. 2443–2455, Nov. 2000.

[49] A. Guo and M. Haenggi,"Spatial stochastic models and metrics for the structure of base stations in cellular networks," *IEEE Trans. Wireless Commun.*, vol. 12, no. 11, pp. 5800–5812, Nov. 2013.

[50] B. Blaszczyszyn, M. K. Karray, and H. P. Keeler, "Using Poisson processes to model lattice cellular networks," *in Proc. 32th Annu. IEEE Int. Conf. Comput. Commun. (INFOCOM)*, pp. 773–781, Apr. 2013.

[51] M. D. Renzo and P. Guan, "Stochastic geometry modeling of coverage and rate of cellular networks using the Gil-Pelaez inversion theorem," *IEEE Commun. Lett.*, vol. 18, no. 9, pp. 1575–1578, Sep. 2014.

[52] H. S. Dhillon, R. K. Ganti, F. Baccelli, and J.G. Andrews, "Coverage and ergodic rate in K-tier downlink heterogeneous cellular networks," in *Proc. 49th Annu. Allerton Conf. Commun. Control Comput. (Allerton)*, pp. 1627–1632, Sep. 2011.

[53] M. D. Renzo, A. Guidotti, and G. E. Corazza, "Average rate of downlink heterogeneous cellular networks over generalized fading channels: A stochastic geometry approach," *IEEE Trans. Commun.*, vol. 61, no. 7, pp. 3050–3071, Jul. 2013.

[54] H. S. Dhillon and J. G. Andrews, "Downlink rate distribution in heterogeneous cellular networks under generalized cell selection," *IEEE Wireless Commun. Lett.*, vol. 3, no. 1, pp. 42–45, Feb. 2014.

[55] X. Yu, Q. Cui, and M. Haenggi, "Coherent joint transmission in downlink heterogeneous cellular networks," *IEEE Wireless Commun. Lett.*, vol. 7, no. 2, pp. 274–277, Apr. 2017.

[56] J. Zhang and J. G. Andrews, "Distributed antenna systems with randomness," *IEEE Trans. Wireless Commun.*, vol. 7, no. 9, pp. 3636–3646, Sep. 2008.

[57] H. S. Dhillon, M. Kountouris, and J. G. Andrews, "Downlink MIMO HetNets: Modeling, ordering results and performance analysis," *IEEE Trans. Wireless Commun.*, vol. 12, no. 10, pp. 5208–5222, Oct. 2013.

[58] A. K. Gupta, H. S. Dhillon, S. Vishwanath, and J.G. Andrews, "Downlink multi-antenna heterogeneous cellular network with load balancing," *IEEE Trans. Commun.*, vol. 62, no. 11, pp. 4052–4067, Nov. 2014.

[59] R. Tanbourgi, H. S. Dhillon, and F. K. Jondral, "Analysis of joint transmit–receive diversity in downlink MIMO heterogeneous cellular networks," *IEEE Trans. Wireless Commun.*, vol. 14, no. 12, pp. 6695–6709, Dec. 2015.

[60] M. Di Renzo and W. Lu, "Stochastic geometry modeling and performance evaluation of MIMO cellular networks using the equivalent-in-distribution (EiD)-based approach," *IEEE Trans.Commun.*, vol. 63, no. 3, pp. 977–996, Mar. 2015.

[61] A. Adhikary, H. S. Dhillon, and G. Caire, "Massive-MIMO meets HetNet: Interference coordination through spatial blanking," *IEEE J. Sel. Areas Commun.*, vol. 33, no. 6, pp. 1171–1186, Jun. 2015.

[62] Q. Zhang, H. Yang, T. Q. Quek, and J. Lee, "Heterogeneous cellular networks with LoS and NLoS transmissions-the role of massive MIMO and small cells," *IEEE Trans. Wireless Commun.*, vol. 16, no. 12, pp. 7996–8010, Dec. 2017

[63] M. D. Renzo, "Stochastic geometry modeling and analysis of multi-tier millimeter wave cellular networks," *IEEE Trans. Wireless Commun.*, vol. 14, no. 9, pp. 5038–5057, Sep. 2015.

[64] N. Muhammad, P. Wang, Y. Li, and B. Vucetic, "Analytical model for outdoor millimeter wave channels using geometry-based stochastic approach," *IEEE Trans. Veh. Technol.*, vol. 66, no. 2, pp. 912–926, Jun. 2017.

[65] M. Rebato, J. Park, P. Popovski, E. De Carvalho, and M. Zorzi, "Stochastic geometric coverage analysis in mmWave cellular networks with a realistic channel model," in *Proc. IEEE Global Commun. Conf. (GLOBECOM)*, pp. 1–6, Dec. 2017.

[66] G. Nigam, P. Minero, and M. Haenggi, "Coordinated multipoint joint transmission in heterogeneous networks," *IEEE Trans. Commun.*, vol. 62, no. 11, pp. 4134–4146, Nov. 2014.

[67] A. Omri and M. Hasna, "Modeling and performance analysis of 3-D heterogeneous networks with interference management," *IEEE Commun. Lett.*, vol. 21, no. 8, pp. 1787–1790, Aug. 2017.

[68] J. Yoon and G. Hwang, "Distance-based inter-cell interference coordination in small cell networks: stochastic geometry modeling and analysis," *IEEE Trans. Wireless Commun.*, vol. 17, no. 6, pp. 4089–4103, Apr. 2018.

[69] G. Nigam, P. Minero, and M. Haenggi, "Spatiotemporal cooperation in heterogeneous cellular networks," *IEEE J. Sel. Areas Commun.*, vol. 33, no. 6, pp. 1253–1265, Jun. 2015.

[70] F. Baccelli and A. Giovanidis, "A stochastic geometry framework for analyzing pairwise-cooperative cellular networks," *IEEE Trans. Wireless Commun.*, vol. 14, no. 2, pp. 794–808, Feb. 2015.

[71] R. K. Ganti and M. Haenggi, "Spatial analysis of opportunistic downlink relaying in a two-hop cellular system," *IEEE Trans. Commun.*, vol. 60, no. 5, pp. 1443–1450, May 2012.

[72] S. Wu, R. Atat, N. Mastronarde, and L. Liu, "Improving the coverage and spectral efficiency of millimeter-wave cellular networks using device-to-device Rrelays," *IEEE Trans. Commun.*, vol. 66, no. 5, pp. 2251–2265, May. 2018.

[73] M. Di Renzo and W. Lu, "On the diversity order of selection combining dual-branch dual-hop AF relaying in a Poisson field of interferers at the destination," *IEEE Trans. Veh. Technol.*, vol. 64, no. 4, pp. 1620–1628, Apr. 2015.

[74] K. Belbase, Z. Zhang, H. Jiang, and C. Tellambura, "Coverage analysis of millimeter wave decode-and-forward networks with best relay selection," *IEEE Access.*, vol. 6, pp. 22670–22683, Apr. 2018.

[75] H. ElSawy, E. Hossain, and D. I. Kim, "HetNets with cognitive small cells: User offloading and distributed channel access techniques," *IEEE Commun. Mag.*, vol. 51, no. 6, pp. 28–36, Jun. 2013.

[76] Z. Yan, W. Zhou, S. Chen, and H. Liu, "Modeling and analysis of two-tier HetNets with cognitive small cells," *IEEE Access.*, vol. 5, pp. 2904–2912, Dec. 2016.

[77] S. Kusaladharma and C. Tellambura, "Performance analysis of co-operative beacon sensing strategies for spatially random cognitive users," *IEEE Trans.Cognit Commun Network.*, vol. 3, no. 4, pp. 585–598, Aug. 2017.

[78] Y. S. Soh, T. Q. Quek, M. Kountouris, and G. Caire, "Cognitive hybrid division duplex for two-tier femtocell networks," *IEEE Trans. Wireless Commun.*, vol. 12, no. 10, pp. 4852–4865, Oct. 2013.

[79] O. Kolawole, S. Vuppala, M. Sellathurai, and T. Ratnarajah, "On the performance of cognitive satellite-terrestrial networks," *IEEE Trans.Cognit Commun Network.*, vol. 3, no. 4, pp. 668–683, 2017.

[80] Y. S. Soh, T. Q. Quek, M. Kountouris, and H. Shin, "Energy efficient heterogeneous cellular networks," *IEEE J. Sel. Areas Commun.*, vol. 31, no. 5, pp. 840–850, May 2013.

[81] H. Jin, X. Wu, H. Kim, and B. C. Jung, "Energy efficiency of ultra-dense small-cell downlink networks with adaptive cell breathing," *IET. Commun.*, vol. 12, no. 3, pp. 367–372, Mar. 2018.

[82] C. Li, J. Zhang, and K. B. Letaief, "Throughput and energy efficiency analysis of small cell networks with multi-antenna base stations," *IEEE Trans. Wireless Commun.*, vol. 13, no. 5, pp. 2505–2517, May 2014.

[83] Z. Chen, L. Qiu, and X. Liang, "Area spectral efficiency analysis and energy consumption minimization in multiantenna Poisson distributed networks," *IEEE Trans. Wireless Commun.*, vol. 15, no. 7, pp. 4862–4874, Jul. 2016.

[84] M. Di Renzo, A. Zappone, T. T. Lan, and M. Dehhah, "System-level modeling and optimization of the energy efficiency in cellular networks-a stochastic geometry framework," *IEEE Trans. Wireless Commun.*, vol. 17, no. 4, pp. 2539–2556, Apr. 2018.

[85] H. S. Dhillon, Y. Li, P. Nuggehalli, Z. Pi, and J. G. Andrews, "Fundamentals of heterogeneous cellular networks with energy harvesting," *IEEE Trans. Wireless Commun.*, vol. 13, no. 5, pp. 2782–2797, May. 2014.

[86] T. Khan, P. Orlik, K. J. Kim, R. W. Heath, and K. Sawa, "A stochastic geometry analysis of large-scale cooperative wireless networks powered by energy harvesting," *IEEE Trans. Commun.*, vol. 65, no. 8, pp. 3343-3358, Aug. 2017.

[87] J. Ye, H. Lei, Y. Liu, G. Pan, D. B. da Costa, Q. Ni, and Z. Ding, "Cooperative communications with wireless energy harvesting over Nakagami- m fading channels," *IEEE Trans. Commun.*, vol. 65, no. 12, pp. 5149–5164, Dec. 2017.

[88] H. ElSawy and E. Hossain, "On stochastic geometry modeling of cellular uplink transmission with truncated channel inversion power control," *IEEE Trans. Wireless Commun.*, vol. 13, no. 8, pp. 4454–4469, Aug. 2014.

[89] P. Guan and M. Renzo, “Stochastic geometry analysis and optimization of uplink cellular networks with fractional power control and optimum combining,” in *Proc. IEEE Int. Conf. on Commun. (ICC)*, pp. 1-6, 2016.

[90] H. Wang, S. Leung, and R. Song, “Uplink area spectral efficiency analysis for multichannel heterogeneous cellular networks with interference coordination,” *IEEE Access.*, vol. 6, pp. 14485–14497, Mar. 2018.

[91] X. Lin, J. G. Andrews, and A. Ghosh, “Spectrum sharing for device-to- device communication in cellular networks,” *IEEE Trans. Wireless Commun.*, vol. 13, no. 12, pp. 6727–6740, Dec. 2014.

[92] S. Joshi and R. Mallik, “Coverage and interference in D2D networks with Poisson cluster process,” *IEEE Commun. Lett.*, vol. 22, no. 5, pp. 1098–1101, May. 2018.

[93] Y. J. Chun, S. L. Cotton, H. S. Dhillon, A. Ghrayeb, and M. O. Hasna, “A stochastic geometric analysis of device-to-device communications operating over generalized fading channels,” *IEEE Trans. Wireless Commun.*, vol. 16, no. 7, pp. 4151–4165, Jul. 2017.

[94] M. Samimi, T. S. Rappaport, and G. MacCartney, “Probabilistic omnidirectional path loss models for millimeter-wave outdoor communications," *IEEE Wireless Commu. Lett.*, vol. 4, no. 4, pp. 357-360, Aug. 2015.

[95] J. Meinilä, P. Kyösti, T. Jämsä, *et al.*, *WINNER II channel models*. 2009.

[96] “Random: Probability, mathematical statistics, stochastic process.” Internet: http://www.randomservices.org/random/index.html [Assessed 15 Jan. 2018]

[97] R. Fakler, “Buffon’s needle problem for a rectangular grid,” *National Council of Teachers of Mathematics*, vol. 88, no. 3, pp. 205-208, Mar. 1995.

[98] M. Berman, “Distance distributions associated with poisson processes of geometric figure”, *Journal of Applied Probability*, vol. 14, no. 1, pp. 195–199, Mar. 1977.

[99] R. Cowan, “Objects arranged randomly in space: an accessible theory”, *Advances in Applied Probability*, vol. 21, no. 3, pp. 543-569, Sep. 1989.

[100] F. Baccelli and B. Blaszczyszyn, *Stochastic geometry and wireless networks, Volume I-Theory.* NoW PublishersBreda, 2009.

[101] J. G. Andrews, S. Buzzi, W. Choi, S. V. Hanly, A. Lozano, A. C. Soong, and J. C. Zhang“What will 5G be?”, *IEEE J. Sel. Areas Commun.*, vol.32, no.6, pp. 1065-1082, Jun. 2014.

[102] M. Kamel, W. Hamouda, and A. Youssef, “Ultra-dense networks: A survey”, *IEEE Commun. Surveys Tuts.*, vol.18, no.4, pp. 2522-2545, May. 2016.

[103] D. Lopez-Perez and M. Ding, “Towards 1 Gbps/UE in cellular systems: Understanding ultra-dense small cell deployments”, *IEEE Commun. Surveys Tuts.*, vol.17, no.4, pp. 2078-2101, Jun. 2015.

[104] 3GPP, “TR 36.873 (V12.7.0) : Study on 3D channel model for LTE,” Dec. 2017.